5-2017

Exploring Thermoresponsive Affinity Agents to Enhance Microdialysis Sampling Efficiency of Proteins

Thaddeus Vasicek
University of Arkansas, Fayetteville

Exploring Thermoresponsive Affinity Agents to Enhance Microdialysis Sampling Efficiency of Proteins

A dissertation submitted in partial fulfillment
of the requirements for the degree of
Doctor of Philosophy in Chemistry

by

Thaddeus Vasicek
University of Arkansas
Bachelor of Science in Chemistry, 2010

May 2017
University of Arkansas

This dissertation is approved for recommendation to the Graduate Council.

_____
Dr. Julie A. Stenken
Dissertation Director

_____
Dr. Ingrid Fritsch
Committee Member

_____
Dr. David Paul
Committee Member

_____
Dr. Wayne Kuenzel
Committee Member

_____
Dr. Ranil Wickramasinghe
Committee Member

_____
Dr. Dan Davis
Committee Member

Abstract

Affinity agents increase microdialysis protein relative recovery, yet they have not seen widespread use within the microdialysis community due to their additional instrumentation requirements and prohibitive cost. This dissertation describes new affinity agents for microdialysis that require no additional instrumentation to use, have nearly 100% particle recovery, are 7 times more cost efficient than alternatives, and have low specificity enabling their use for a wide variety of proteins. Initially gold nanoparticles were chosen as an affinity ligand support due to their high surface area/volume ratio and colloidal stability. Poly (*N*-isopropylacrylamide) was immobilized to the gold nanoparticles, which served to sterically stabilize the particles and to act as a generic, reversible protein capture agent. A method was developed to reproducibly vary and quantify poly (*N*-isopropylacrylamide) graft density from 0.09 to 0.40 ligands/nm^2 on gold nanoparticles. During characterization of the polymer coated gold nanoparticles, irreversible particle agglomeration was observed at low polymer graft density in ionic solutions, which prevented further development as a protein capture agent. Poly (*N*-isopropylacrylamide) nanogels, which have low nonspecific adsorption, low interparticle attractive forces owing to the low curvature of the particle, and a low Hamaker constant, were synthesized to overcome the agglomeration problem. A generic protein affinity ligand cibacron blue, was immobilized to the nanogels, which enabled rapid determination of particle recovery. The perfusion of the nanogels through a microdialysis probe was optimized yielding ~ 100% particle recovery using a combination of a syringe and peristaltic pump. The microdialysis collection efficiency of CCL2, a physiologically relevant cytokine, was increased 3-fold with addition of the nanogel to the microdialysis perfusion fluid. The reduction in instrumentation

requirements, low cost, and low specificity obtained with the new affinity agents will lead to increased affinity agent use for microdiaylsis protein sampling.

Acknowledgments

I would like to acknowledge and thank my advisor, Dr. Julie Stenken. She has been a continual north star, guiding, directing and supporting me during my graduate career. She has led me to strive for excellence, something I will take with me going forward. I again and always thank her for her help.

I would also like to thank the Cameron Crane, Leanne Mathurin, Tengjiao Wang, Samir Jenkins, and Jingyi Chen for continually educating me in synthesis strategies, characterization methods, and instrument operation.

I would like to thank my wife. She tolerated me working long and complex hours. She knows more about my research than me. She has listened to every presentation, and every brain storm I have had. She has bounced ideas back to me, and offered practical solutions to complex experimental difficulties. I appreciate her stalwart support and understanding.

Finally, I would like to acknowledge the Arkansas Bioscience Institute for funding.

Contents

List of Figures and Tables

Glossary

Abbreviations

AA	Allylamine
AI	Aggregation index
ANOVA	Analysis of variance
APS	Ammonium persulfate
AuNP	Gold Nanoparticle
AuNP-0.09	Gold nanoparticle with a graft density of 0.09
AuNP-0.30	Gold nanoparticle with a graft density of 0.30
AuNP-0.40	Gold nanoparticle with a graft density of 0.40
AuNP-PNIPAM	Gold nanoparticle coated with PNIPAM
AU	Absorbance unit
BCA	Bicinchoninic Acid
BIS	*N*,*N* methylenebisacrylamide
BSA	Bovine serum albumin
CCL2	Chemokine ligand 2
CB	Cibacron blue 3G-A
CV	Coefficient of variation
DLS	Dynamic light scattering
ECS	Extracellular space
ELISA	Enzyme linked immunosorbent assay
E_{tot}	Sum of the steric and van der Waals forces
E_{st}	Sum of the steric
E_{vdW}	Sum of the van der Waals forces
FITC-dextran 10	Fluorescein isothiocyanate dextran with a molecular weight of 10 kDa

HPLC	High performance liquid chromatography
I.D.	Inner diameter
IL	Interleukin
KC/GRO	Keratinocyte chemoattractant/growth regulated oncogene
KPS	Potassium persulfate
LCST	Lower critical solution temperature
LSPR	Localized surface plasmon resonance
LOD	Limit of detection
M_{Au}	Mass attributed to gold
MWCO	Molecular weight cut off
MW_{AuNP}	Molecular weight of a gold nanoparticle
N_A	Avogadro's number
N_{AuNP}	Number of AuNPs
O.D.	Outer diameter
PBS	Phosphate buffered saline
PDI	Polydispersity index
PES	Polyethersulfone
PNIPAM	Poly(*N*-isopropylacrylamide)
RCF	Relative centrifugal force
RR	Relative recovery
SA_{AuNP}	Surface area of a AuNP
SAM	Self assembled monolayer
SDS	Sodium dodecyl sulfate
SDS-PAGE	Sodium dodecyl sulfate polyacrylamide gel electrophoresis
TEM	Transmission electron microscopy

TEMED	Tetramethylethylenediamine
TGA	Thermal gravimetric analysis
TRIS	Tris(hydroxymethyl)aminomethane hydrochloride
Tukey's HSD	Tukey's honest significant difference
VEGF	Vascular endothelial growth factor
V_{AuNP}	Volume of an AuNP

Symbols

C	Center to center distance between particles
d	Particle diameter
D_h	Hydrodynamic diameter
K_D	Dissociation constant
η	Dynamic viscosity of the sample medium
ρ	Density
v	Settling velocity
μ	Ionic strength
λ_D	Debye Length
ε_r	Dielectric constant of the solvent
ε_0	Vacuum permittivity
k_B	Boltzmann's constant
z_i	Charge of an ion
c_i^*	Number concentration of an ion
e	Charge of an electron
C_L	Unbound analyte concentration
C_i	Analyte inlet concentration

C_d	Analyte dialysate concentration
C_o	Analyte sampling medium concentration
R_o	Outer radius of the membrane
Q_d	Flow rate
D_{mem}	Membrane diffusion coefficient
k	Kinetic rate constant
r_α	Radius of the outer cannula
r_β	Radius of the inner membrane
r_o	Radius of the outer membrane
R_d	Resistance to traverse the dialysate
R_e	Resistance to traverse sampling medium
R_m	Resistance to traverse the membrane
D_d	Analyte diffusion coefficient through the dialysate
D_e	Analyte diffusion coefficient through the external sampling medium
ϕ_m	Volume fraction of the membrane accessible to water
ϕ_e	Volume fraction of in the external sampling medium

Chapter 1 Introduction

Cytokines and cytokine quantification

Cytokines are signaling proteins with a molecular weight ranging from 7 to 80 kDa. Cytokines are produced within the cytoplasm of, basophils, eosinophils, lymphocytes, macrophages, and neutrophils.[1-3] Cytokines are responsible for a wide range of cell communication such as regulating inflammation, and directing wound healing processes.[4-8] Once produced, cytokines are excreted into the extracellular space (ECS). They initiate a signaling response by binding their respective cell-surface receptor, where the binding can stimulate the release of other cytokines, or stymie cytokine production in a complex network of interactions with other cytokines which can be additive, synergistic or antagonistic.[9, 10] Cytokines can interact with the cells that secreted them (autocrine), the surrounding cells (paracrine), distant cells (endocrine), or remain bound to the cell (juxtacrine).[11] An imbalance in cytokine concentrations is related to various inflammatory disease states such as arthritis, obesity, anxiety disorders and are commonly used as biomarkers for inflammation.[12-14]

Cytokines are potent molecules that exist at pM concentrations in the ECS.[15, 16] Changes in cytokine concentration are indicative of changes in disease state, or a wound response.[17-20] Sensitive analytical methods with a low limit of detection are required to study cytokine concentration changes as it relates to disease state or wound healing.[21] Optimally one would desire an assay with a low limit of detection (LOD), minimal sample volume requirements, low cost, low variance, high specificity, high reliability, high sensitivity and high throughput. Additionally, the ability to measure multiple cytokines within a single analysis as desired, as it enables the study of the complex network of cytokines and how they interact. These idealistic

traits would allow for an intricate study of the cytokine network, however no one technique to date allows for all. Commonly used methods to detect cytokine protein concentration include; bioassay, enzyme linked immunosorbent assay (ELISA), and the bead array.

Cytokine bioassays allow for the quantification of biologically active protein. This is done by monitoring the proliferation/inhibition of cells due to cytokines,[22] cytokine induced killing of cells,[23] and cytokine stimulated production of other cytokines.[24] As the bioassays are cell-culture based, they suffer from high variance with up to a 100% coefficient of variation (CV%) for inter-assay precision.[25] Additionally, the lengthy time to culture cells impede high-throughput analysis.

A routinely used method for quantifying cytokines is the sandwich ELISA. An ELISA relies on the immobilization of a specific capture antibody to the wells of a well plate. Protein from sample is captured by the immobilized antibody, while unretained material is washed away. An enzyme is attached to the complex through the addition of secondary antibody which recognizes a different epitope than the capture antibody. Detection is performed by adding the enzyme substrate to produce a signal which is proportional to the captured cytokine concentration. ELISAs are specific as they rely on the antigen-antibody specificity, have a wide analytical range (10 pg/mL to ng/mL), have excellent precision with coefficients of variation between 5-10%.[26] However, ELISAs have a 50-100 µL volume requirement, take 6 hr to perform and do not allow for multiplexing.

A bead array relies on similar principles as an ELISA, yet allows for multiplexing. This is accomplished using polymeric particles with immobilized antibodies. Different particles have a different immobilized capture antibody and the particles can be differentiated based on their size and ratio of two internally embedded fluorescent dyes. The signal from beads with different

capture antibodies can be distinguished by determining which particle group signal originates from. The bead arrays have a LOD in the pg/mL range, and require ~25 µL/mL sample volume.[27] The commercially available kits are costly, ~10 times the price of an ELISA. A limitation with bead arrays is their CV,[28, 29] with a reported inter- and intra- assay CV% exceeding 50% and 30% respectively.[30] The CV is defined as the standard deviation over the mean.

Microdialysis sampling

Microdialysis is a diffusion-based sampling technique which allows for the continuous sampling from the ECS. Microdialysis relies on the implantation of a semi-permeable probe which is typically 0.5 mm outer diameter (O.D.) with a 1-10 mm membrane. The probe has a solution that enters the probe (perfusate), diffusion of analyte occurs across a semi-permeable membrane, and analyte containing fluid exits the probe (dialysate), as seen in **Figure 1.1**.

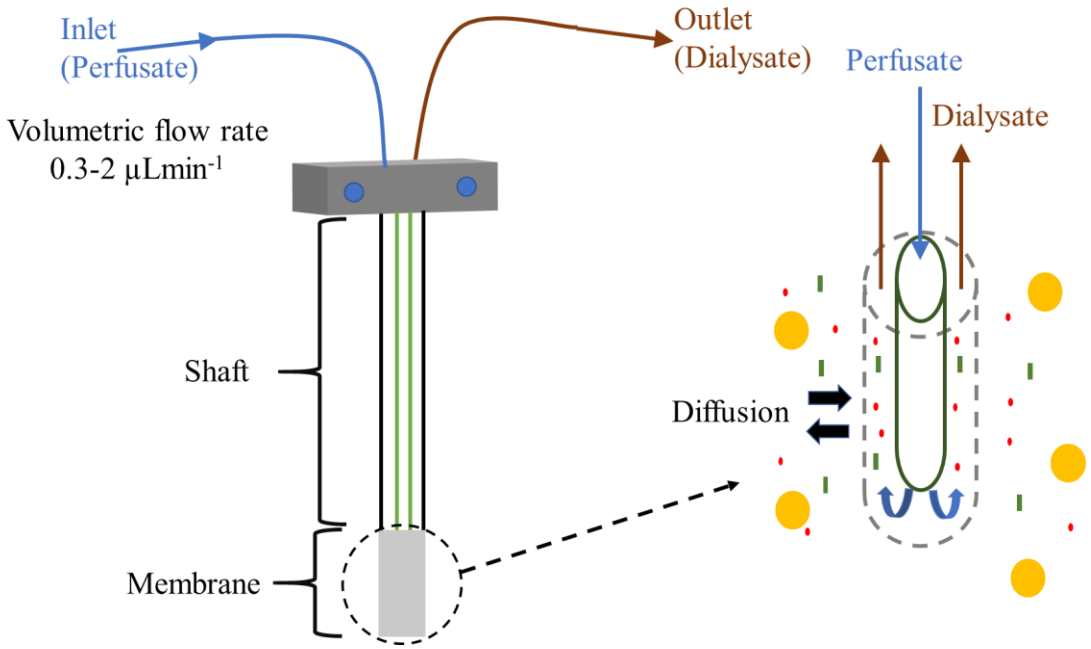

Figure 1.1 Diagram of a microdialysis probe. Diffusion occurs through the water filled pores of the semi-permeable membrane.

Analytes that can diffuse through the water filled pores in the membrane are carried to the outlet of the probe. Once collected, analytes are detected with various on-line or off-line techniques.[31-34] The membrane rejects cells and high concentrations of abundant proteins from entering the dialysate, yielding an analytically clean sample that can be analyzed with minimal sample pretreatment.

Commercially available probe membranes are derived from kidney dialysis membrane. The molecular weight cutoff (MWCO) of these membranes describes the approximate mass at which 90% of analytes are rejected from traversing the membrane.[35] However, the MWCO is determined by an equilibrium experiment where typically the perfusion fluid is continually recycled and perfused. Microdialysis sampling itself is not an equilibrium sampling technique, the perfusion fluid flows along the membrane a single time before collection.

Microdialysis is routinely applied in vivo to a wide range of tissues including, brain,[36] spine,[37] skin,[38] eye,[39] kidney,[40] and is used in a diverse range of species, such as plants.[41] The widespread use of microdialysis is driven from key advantages it has over comparable techniques. Microdialysis allows for continuous sampling from a single animal enabling local concentration changes to be studied for days.[42] Microdialysis can be used to locally deliver drug while sampling.[43, 44] Additionally, two probes, a control and drug delivering probe, may be implanted laterally within a single animal. The use of repeated measurements from a single animal, and implantation of both control and treatment probes within a single animal decreases animal use and minimizes experimental variance.[45] Microdialysis requires minimal instrumentation, typically only requiring a syringe pump, probe, and tubing. Microdialysis has a temporal resolution on the minute to hour time scale, determined by the detection method

requirements.[46-48] The spatial resolution of microdialysis sampling is limited by the size of the probe, which is typically 0.5 mm O.D.

While initially developed as a technique to study small hydrophilic neurotransmitters, microdialysis has a growing interest in being applied to study peptides and proteins[49-61]. The interest in using microdialysis to sample these molecules is due to the inherent advantages microdialysis has, such as drug delivery with simultaneous sampling, and observing local concentration changes over time for a wide variety of analytes. Local drug delivery to the brain enables a broad class of drugs to be studied that normally do not cross the blood brain barrier.[62, 63] Quist *et al.* recently used microdialysis with a multiplexed analysis to study the kinetic profile of 15 cytokines following UV exposure to identify two separate cell recruitment phases involved in the wound healing process.[64] Portnow *et al.* recently used a 100 kDa 10 mm membrane microdialysis probe to study the effect an anti-cancer drug has on 30 different cytokine concentrations peritumoral.[65] Only 17 of the 30 cytokines were above the limit of detection in dialysate.

Challenges for microdialysis sampling of cytokines

The concentration of analyte collected with microdialysis is always lower than then ECS concentration, and the collection efficiency is quantified by the extraction efficiency (EE) as outlined in Eq. 1.1.

$$\boldsymbol{EE} = \frac{\boldsymbol{C_d - C_i}}{\boldsymbol{C_o - C_i}} \qquad \text{Eq. 1.1}$$

Where C_d, C_o, C_i represents the concentration of the analyte in the dialysate, the sampling medium, and the perfusion fluid, respectively. When no analyte is perfused the extraction

efficiency is termed the relative recovery (RR) and is the ratio of analyte concentration in the dialysate and in the sampling medium.

Bungay et al. have developed a model to predict in vitro RR for microdialysis at steady state, as is seen in **Eq 1.2-1.5**.[66] In this model, the RR is inversely proportional to the multiple of the volumetric flow rate of the perfusate (Q_d) and the sum of the mass transport resistances the analyte crosses, namely the dialysate (R_d) , membrane (R_m), and the external sampling medium (R_e). **Figure 1.2** displays the regions and terms used in this model.

$$\boldsymbol{RR = 1 - \exp\left(-\frac{1}{Q_d(R_d+R_m+R_e)}\right)} \qquad \text{Eq. 1.2}$$

$$\boldsymbol{R_d = \frac{13(r_\beta - r_\alpha)}{70\pi L r_\beta D_d}} \qquad \text{Eq. 1.3}$$

$$\boldsymbol{R_m = \frac{\ln\left(\frac{r_o}{r_\beta}\right)}{2\pi L D_{mem}\varphi_m}} \qquad \text{Eq. 1.4}$$

$$\boldsymbol{R_e = \frac{1}{2\pi D_e \varphi_e \sqrt{2 r_o L}}} \qquad \text{Eq. 1.5}$$

Where r_α, r_β, and r_o are radius of the outer cannula, inner membrane, and outer membrane are respectively. L is the effective membrane length, D_d is the analyte diffusion coefficient in the dialysate, D_{mem} is the analyte diffusion coefficient through the membrane, D_e is the analyte diffusion coefficient through the external sampling medium, ϕ_m is the volume fraction of the membrane accessible to water, and φ_e is the volume fraction in the external sampling medium. One can increase the RR by decreasing the flow rate which increase the residence time, or reducing the resistance terms. Experimentally one can reduce the resistance terms by stirring the sampling medium (which minimizes the concentration boundary layer external the probe), increasing the membrane length, or increasing the pore size of the membrane. The dependence on RR with flow rate, and membrane length is displayed in **Figure 1.3** in which a 10 kDa

dextran was sampled from a well stirred solution using a 100 kDa MWCO PES probe with a 4 or 10 mm membrane.

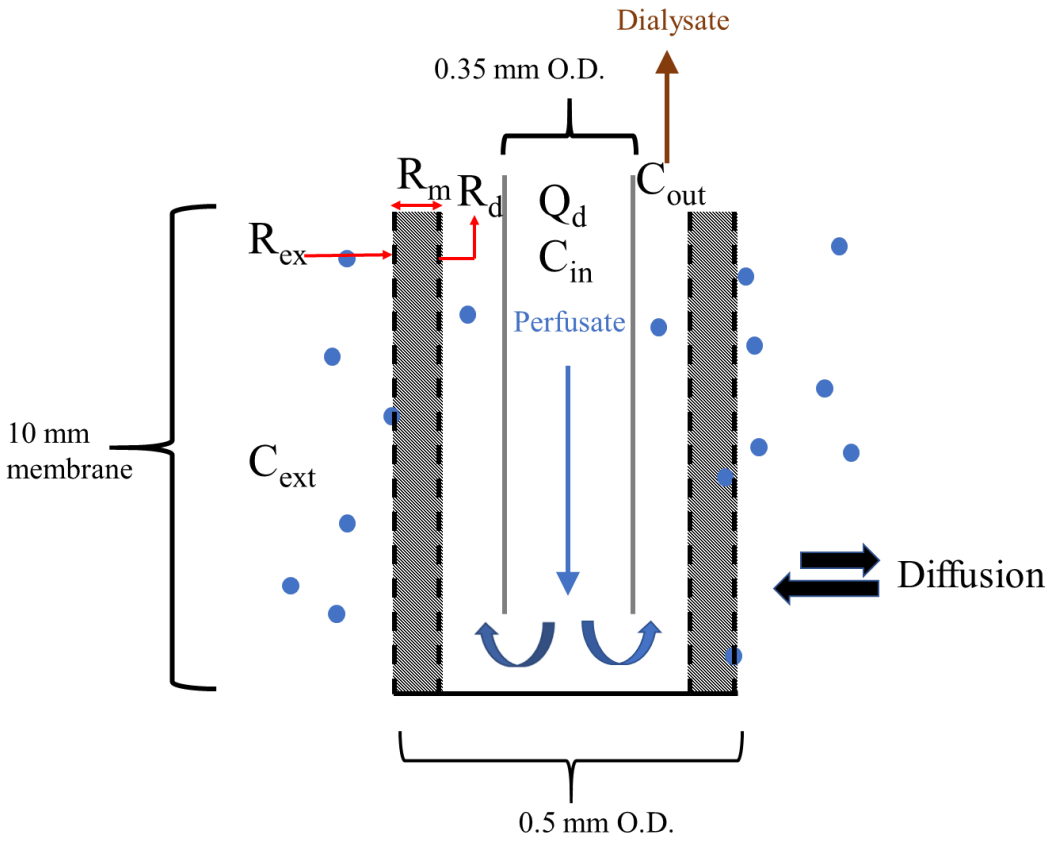

Figure 1.2 Parameters for predicting steady state relative recovery.

Microdialysis was initially pioneered as a method to sample small hydrophilic molecules such as amino acids, monoamines, and neuropeptides which have a RR of 30-40%, 22-30% and 1.5-24% respectively using a 20 kDa MWCO 4 mm membrane at 2 µL/min.[67] However when used for sampling macromolecules, a decrease in RR occurs. The in vitro RR of molecules with a molecular weight greater than 10 kDa at 1 µL/min flow rates using a 100 kDa MWCO 10 mm membrane from a well stirred solution is between 1-10%.[68, 69] The decrease in mass transport with increasing MW is due to lower diffusion coefficients. As seen in **Figure 1.3**, the RR for a

10 kDa dextran at 1 µL/min with a 4 mm 100 kDa MWCO membrane is 6.9 ± 0.4%, while the RR for a 20 kDa dextran under identical conditions is 1.3 ± 0.1%. The aqueous diffusion coefficients for 10 and 20 kDa as determined by dynamic light scattering are 1.47×10^{-6} and 1.06×10^{-6} cm^2/s, emphasizing how a subtle reduction in the diffusion coefficient affects the RR.[68] The aqueous diffusion coefficient of small molecules is typically an order of magnitude greater than proteins. The D_{aq} for dopamine is 5.4×10^{-6} cm^2s^{-1}, while D_{aq} for BSA a 66 kDa protein is 5.38×10^{-7} cm^2s^{-1}.[70, 71]

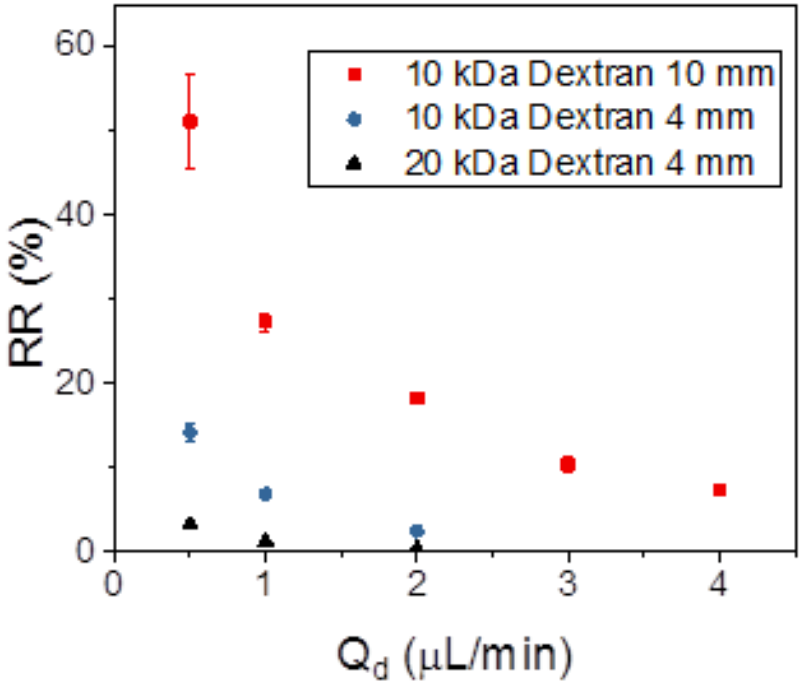

Figure 1.3 RR of 10 and 20 kDa dextran using a 100 kDa MWCO PES membrane with a 4 or 10 mm membrane. Avg ± 1 s.d., n=3.

The drastic reduction in RR with decreasing diffusion coefficient is due to each resistance term in **Equations 1.3-1.5** being inversely proportional to a diffusion coefficient. For macromolecules, the D_m is particularly hindered. With increasing molecular weight the diffusion coefficient through the pores of the membrane decreases exponentially as the size of the molecule approaches the pore size.

Cytokines exist in the ECS at pg/mL-ng/mL concentrations, and their RR is between 1.0-13.1% when sampled at 1 µL/min using a 100 kDa MWCO 10 mm PES probe.[72] The low RR when sampling cytokines and their dilute concentration in the ECS places extraneous strain on the ensuing analytical detection methods. Cytokine detection methods have LODs that are near the concentration of cytokines collected in dialysate, however the dialysate concentration is not always within the LOD. A method to increase cytokine dialysate concentration, i.e. enhance the RR of cytokines, is desired to ease detection method restraints.

Affinity agent enhanced microdialysis sampling

There are five ways to increase the RR of cytokines, 1) use lower flow rates, 2) increase membrane surface area, 3) change material properties, 4) increase membrane pore size, and 5) include the use of affinity agents. A decrease in flow rate reduces the temporal resolution of microdialysis, as both the bead arrays and ELISAs require 25-100 µL of sample. Increasing the membrane surface area is not always possible as there are limited commercially available probe sizes and, increasing the membrane area reduces the spatial resolution of microdialysis. A reduction in spatial resolution makes sampling from tissue spaces impractical, as the tissue may be smaller than membrane used to sample, i.e. specific brain structures. Modifying the material properties is commonly accomplished by including BSA in the perfusion fluid, as it adsorbs to the surfaces of the sampling system reducing nonspecific adsorption.[73] The Dahlin group have

changed the membrane properties by adsorbing a triblock copolymer of poly(ethylene glycol) and poly(propylene) to the membrane in attempt to reduce nonspecific adsorption to the membrane. However, only mild increases in RR were observed for some of the proteins and peptides studied.[74, 75] Increasing the pore size of the membrane causes a reduction in fluid recovery. The use of 100 kDa MWCO ultrafiltration membranes are currently employed for cytokine sampling, and fluid loss is prevented through the addition of high concentrations (0.05-6% w/v) of osmotic agents to the perfusion fluid.[73] However, the use membranes with a MWCO higher than 100 kDa have not been used until recently due to excessive ultrafiltration despite the use of osmotic agents. The recent development of push/pull microdialysis perfusion has led to the use of 1 MDa MWCO probes to sample macromolecules.[76] Push/pull microdialysis consists of the perfusion fluid being pushed using a syringe pump, while the dialysate is pulled with a peristaltic pump reducing fluid loss. The use of 1 MDa MWCO probe with push/pull microdialysis has led to a twofold RR enhancement for IL-6 compared to 100 kDa MWCO.[77] Comparatively the use of affinity agents has seen up to a fourteen fold increase in cytokine RR using 100 kDa MWCO probes.[78]

Affinity agent enhanced microdialysis relies on the perfusion of a high affinity ligand through the microdialysis probe. The addition of a chemical reaction on one side of a membrane is commonly used to facilitate mass transport in separation science, as it couples diffusion with a chemical reaction.[79, 80] The flux of the analyte is increased as the concentration gradient of the unbound form in the dialysate is maximized,[81] as derived by Kramov and Stenken in **Eq 1.6**.[81]

$$\left(\frac{dC_L}{dr}\right) = \frac{2\pi D_{mem}(C_o - C_L)}{Q \ln(r_\alpha / r_\beta)} - \frac{\pi R_i^2 k C_L}{Q} \qquad \text{Eq 1.6.}$$

Where r is any radial point in the membrane, C_L is the unbound analyte concentration in the membrane, C_o is the analyte sampling medium concentration, r_α is the outer radius of the

membrane, r_β is the inner radius of the membrane, D_{mem} is the diffusion coefficient through the membrane, and k is the kinetic rate. Adding a chemical reaction to one side of the membrane reduces the unbound analyte concentration within the membrane. Maximizing the concentration gradient on the inside of the membrane increases flux. A depiction of the recovery with and without affinity agents in the perfusion fluid is displayed in **Figure 1.4**. Affinity agents have been used to enhance the RR of a wide range of analytes collected with microdialysis including proteins, metal ions, lipophilic drugs, prostaglandins, and neuropeptides.[73, 81-84] A compilation of affinity agents, analytes and RR enhancements is shown in **Table 1.1**.

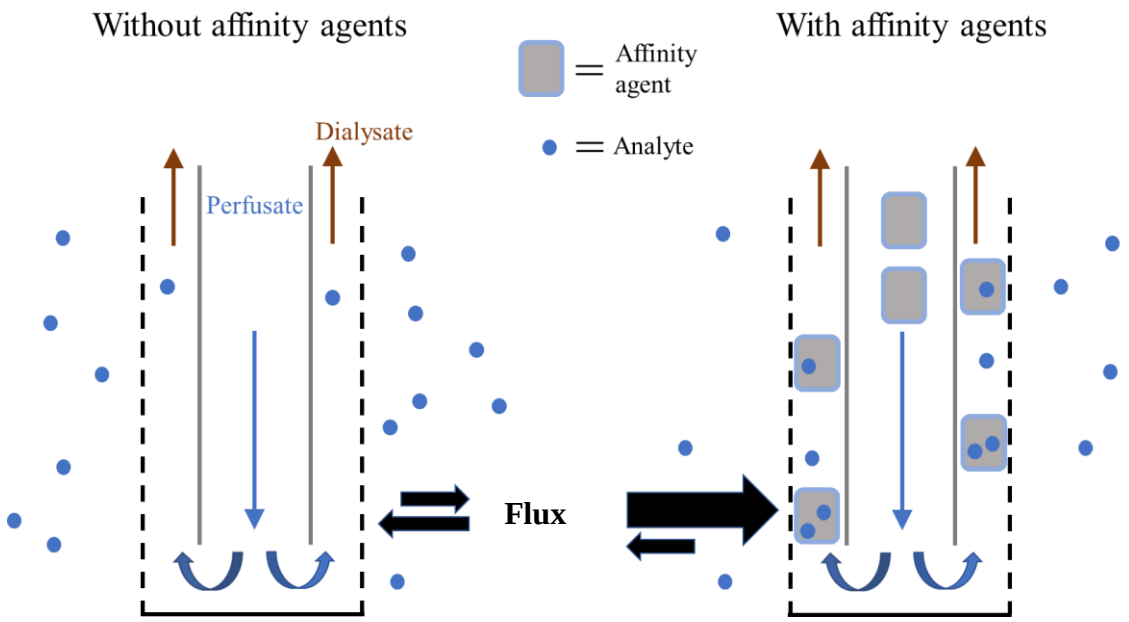

Figure 1.4 Relative recovery enhancement due to affinity agent inclusion in perfusion fluid.

Table 1.1 Analytes with enhanced relative recovery with the perfusion of affinity agents.

Membrane MWCO and length	**Analyte**	**Affinity Agent (AA)**	**Ratio of AA enhanced RR to control RR**	**Notes**
30 kDa 10 mm[82]	Cu (II)	poly-L-aspartic acid	10	Decrease in RR with increasing AA concentration
		poly-L-histidine	7	
CMA20 10 mm[83]	Alkyl parabens	Intralipos® (lipid emulsion)	2-390	RR enhancement factor correlated with lipophilicity of the analyte
30 kDa 10 mm[85]	SB-265123	Hydroxypropyl β-cyclodextrin	36	
20 kDa 4 mm[81]	Ibuprofen	β-cyclodextrin	1.7	Decrease in RR with increasing AA concentration
6 kDa 4 mm[81]			1.3	
29 kDa 4 mm[81]			1.4	
20 kDa 4 mm[86]	Imipramine	β-cyclodextrin	2.7	
	Carbamazepine		1.4	
	Amitriptyline		6.3	
	Desipramine		3	
	Promethazine		10	
20 kDa 10 mm[87]	Carbamazepine	β-cyclodextrin	2.4	
	Hydroquinone		1.2	
	Ibuprofen		4.5	
	4-Nitrophenol		2.3	
29 kDa 4 mm[84]	Prostaglandin B2	β-cyclodextrin	1.6	
	Leukotriene B4		2	

Table 1.1 Analytes with enhanced relative recovery with the perfusion of affinity agents (Cont.).

Membrane MWCO and length	**Analyte**	**Affinity Agent (AA)**	**Ratio of AA enhanced RR to control RR**	**Notes**
20 kDa 4 mm[88]	Met-enkephalin	β-cyclodextrin	1.8	
	Leu-enkephalin		1.9	
	Met-enkephalin	Antibody	2.6	
100 kDa 4 mm[89]	CCL2	Antibody	6.5	
100 kDa 10 mm[90]	IL-4	Heparin	1.7	
	IL-6		2.6	
	IL-7		3	
	CCL2		2	
	TNF-α		2	
100 kDa 10 mm[91]	TNF-α	Antibody immobilized beads	10	Particle settling observed
	IFN-γ		14	
	IL-5		3	
	IL-4		8	
	IL-2		7	
20 kDa 4 mm[92]	FMRFamide	Antibody immobilized beads	1.6	Particle settling observed
	FMRFamide-like peptide I		2.8	
	FMRFamide-like peptide II		2.4	
	Substance P		41.7	
	Somatostatin-14		7.5	
100 kDa 10 mm[93]	aFGF	Heparin immobilized bead	3.5	Particle settling observed
	VEGF		5	
	CCL2		2	
	CCL5		2.7	

When perfusing affinity agents with a molecular weight lower than the MWCO of the membrane, the affinity agent may cross the membrane and enter the sampling medium. This leads to escaped affinity agent interacting with analyte in the sampling medium, altering the diffusion coefficient of the complex, and reducing the unbound analyte concentration in the sampling medium, possibly lowering the RR. A reduction in RR with increasing affinity agent concentrations has been observed.[81, 82] Additionally, the diffusion of affinity agents across the membrane may complicate in vivo studies. In vivo, a biological response may occur due to escaped affinity agent. To prevent affinity agents from cross the membrane, the affinity ligands can be immobilized to a solid support which is unable to cross the membrane pores. The manufacturer for the commonly used Harvard apparatus microdialysis probes reports that the pore size for a 100 kDa MWCO PES membrane is 9 nm, so affinity ligands are immobilized to particles with a diameter larger than 9 nm.[90]Additionally, the perfusion of large affinity ligands, such antibodies, which do not cross a 100 kDa MWCO membrane, can be used. However, perfusing antibodies is costly and the concentration of the antibody is not always known, possibly reducing the maximum RR enhancement due to saturation of antibodies.

The use of solid support to immobilize the affinity ligand has seen use with the application of affinity agents to 100 kDa MWCO probes for macromolecule sampling. Previously used solid supports have consisted of 5-7 µm polystyrene microspheres and 100 nm iron oxide nanoparticles, both of which have been observed to settle in the syringe during perfusion. To hinder particle settling the Stenken and Li groups have used syringe agitators.[92, 93] The use of additional instrumentation slows the development of affinity agents to other groups which desire a method to increase cytokine RR. Additionally, no study has been conducted by either group to determine the length of time syringe agitators can maintain the affinity agent

suspension. For many studies, it is desired to sample continuously for hours to days to observe cytokine profile changes,[64] and affinity agent settling during sampling increases the complexity of the experiment.

Particle settling is due to gravitational forces overcoming Brownian forces, i.e. settling velocity overcomes diffusion velocity.[94] Stoke's law can manipulated to calculate the settling rate of a particle as seen in **Equation 1.7**.[95]

$$\boldsymbol{v} = \frac{\boldsymbol{d^2(\rho_2 - \rho_1)g}}{\boldsymbol{18\eta}} \qquad \text{Eq. 1.7}$$

Where v is the settling rate, d is the particle diameter, ρ_2 is the particle density, ρ_1 is the density of the solution, g is acceleration due to gravity, and η is the solution viscosity. Equation 1.7 displays that the increases in particle diameter, squares the settling velocity, and that the density of the colloid is correlated with settling velocity. The Overbeek criterion estimates particle diffusion velocity as 10 nm/s and is used to predict the settling diameters of particles based on material density and can be used to determine optimal particle sizes which will not settle during microdialysis perfusion.[96] **Figure 1.5a** displays the predicted particle settling diameters based on this benchmark, and was used to guide the forthcoming research in determining optimal particle size of different materials.

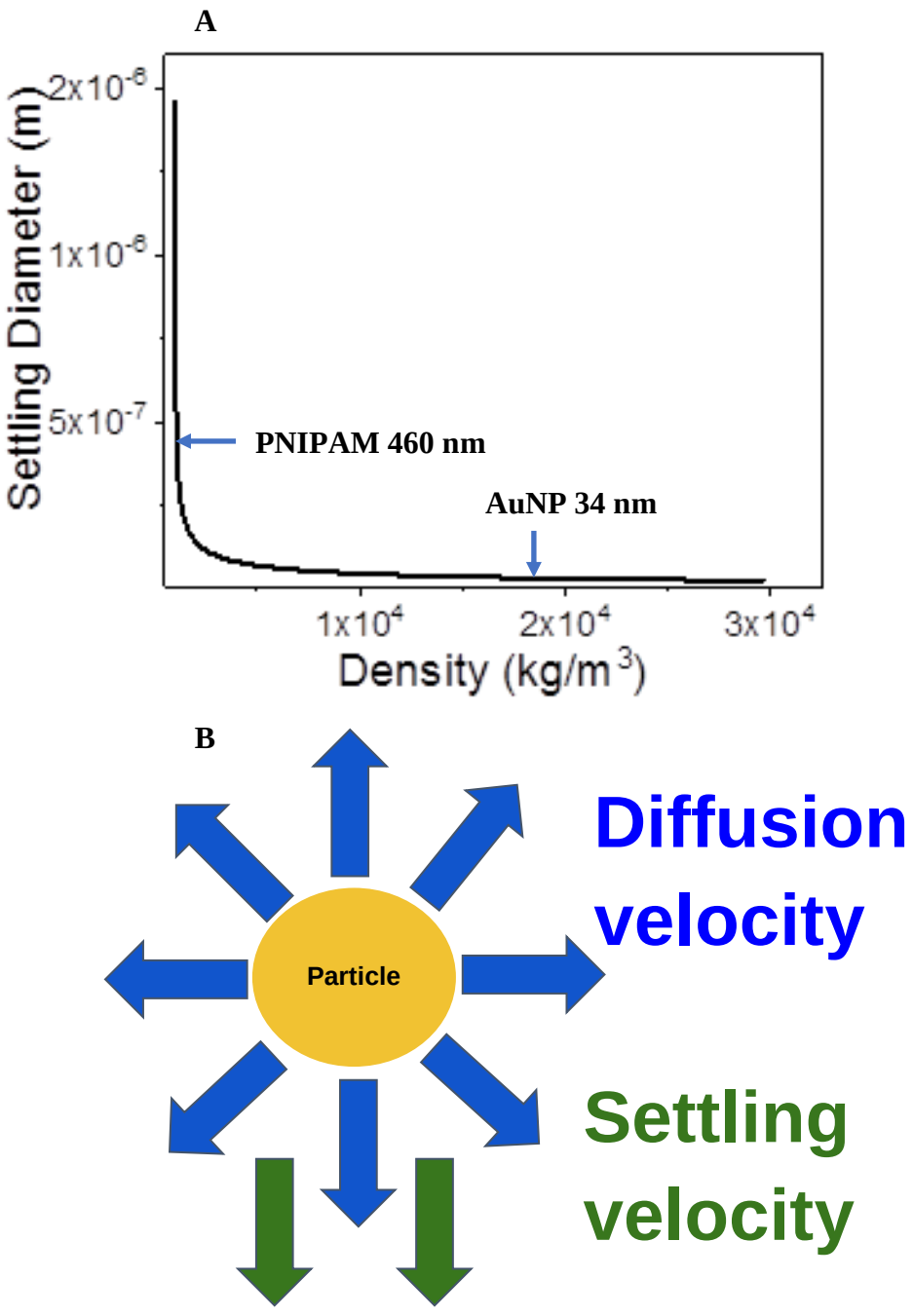

Figure 1.5 (A)Particle settling diameters in water based on material density and a 1 mm/24 hr settling velocity cutoff. Displayed are the settling diameters for PNIPAM and AuNP with densities of 1100 kg/m^3 and 19300 kg/m^3, respectively. (B) Particle settling occurs when settling velocity exceed diffusion velocity.

Gold nanoparticles as an alternative support for affinity agent immobilization

The settling of affinity agents immobilized to a support can be prevented by decreasing the diameter of the particle or decreasing the difference between density and medium. The diameter of the particle is exponentially proportional to the settling diameter, while the particle density is linearly proportional to settling diameter. This highlights the need to decrease particle support size and/or the particle density for the particles' thermal motion to overcome gravitational forces. Gold nanoparticles (AuNPs) have a predicted settling diameter of 34 nm. AuNPs can be readily synthesized with diameters between 10-30 nm using the Turkevich synthesis.[97] AuNPs also have high surface area which enables the exposure of a high density of ligands, display low toxicity, are the most stable aqueous noble metal nanoparticle, and have a wide variety of ligand immobilization chemistries.[98-100] Owing to these properties AuNPs see widespread use for biomedical applications.

The Turkevich synthesis relies on the reduction $Au^{3+}_{(aq)}$ by sodium citrate as displayed in **Figure 1.6**.[97, 101] In this synthesis, the citrate also electrostatically repels adjacent AuNPs, preventing agglomeration which would occur during collisions between nanoparticles.[102] When agglomeration occurs, the size of the particles grow until sedimentation occurs. The citrate ligand can be exchanged with another ligand that has a higher affinity for the gold surface, such as with a thiol, which enables facile grafting of new ligands to the nanoparticle surface.[103] Affinity ligands which have been grafted to AuNPs include aptamers, antibodies, metal complexing agents, small molecules and polymers.[104-111]

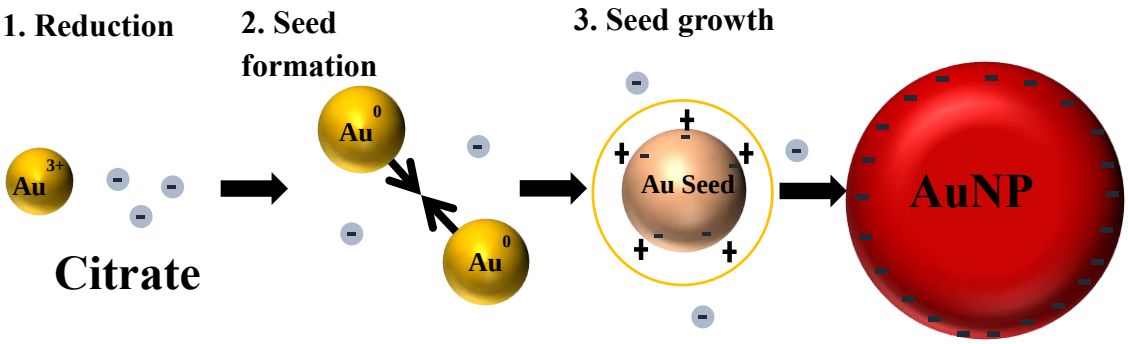

Figure 1.6 Synthesis of AuNPs. Au^{3+} is reduced to neutral gold by citrate ions (blue), neutral Au monomers form seed particles, ionic gold is attracted to seed particles as a counter ion and reduced to form AuNP.

A complication with using citrate stabilized AuNPs in ionic solutions is there tendency to agglomerate when the charge of the citrate ion is screened at high ion concentrations. The Debye length (λ_D) is used to represent the range an electric force extends in solution as defined by **Equation 1.8**. The electric potential decreases by 1/e for each increment of the Debye length away from a surface.

$$\lambda_D = \sqrt{\frac{\varepsilon_r \varepsilon_0 k_B T}{\sum (z_i e)^2 c_i^*}} \qquad \text{Eq. 1.8}$$

Where ε_r is the dielectric constant of the solvent, ε_0 is the vacuum permittivity, k_B is Boltzmann's constant, z_i is the charge of the ion, e is the charge of an electron, c_i^* is the number concentration of the ion. The Debye length is 0.7 nm at 150 mM ionic strength (μ). Charge screening in addition to the high Hamaker constant of gold (1.95 eV),[112] is why citrate stabilized AuNPs agglomerate in salt solutions.[113-115] The Hamaker constant describes the relative van der Waals body-body interaction strength. As particles agglomerate, an increase in particle diameter occurs, leading to and hastening particle precipitation.

Grafting polymer ligands to the nanoparticle surface enables the application of

AuNPs to biological systems with high μ. When polymer ligands are grafted to a nanoparticle surface, a steric hindrance layer is introduced which prevents agglomeration in high ionic solutions. AuNPs need to be sterically stabilized to be used as affinity agent supports in microdialysis perfusion fluid which has a high ionic strength.

Poly(*N*-isopropyl acrylamide)

One polymer that is commonly used to sterically stabilize AuNPS is poly(*N*-isopropyl acrylamide) (PNIPAM).[116-118] PNIPAM is one of the most studied thermoresponsive polymers in part because its lower critical solution temperature (LCST) is ~ 32 °C enabling its use for many potential biological studies[119, 120]. In water below the LCST, the polymer swells forming energetically favorable hydrogen bonds between the acrylamide group and water. Above the LCST, the polymer spontaneously desolvates to form inter- and intra- chain hydrogen bonds which leads to contraction from a coil to a globule and increases its hydrophobicity. Decreasing the separation distance between polymer grafting sites leads to steric hindrance in the polymer chains. The steric hindrance is observed as an increase in chain height, in other words the graft density (chain/nm^2) determines the chain height in solution.[121, 122] **Figure 1.7** illustrates the increase in chain extended and collapsed polymer height with increasing grafting density.

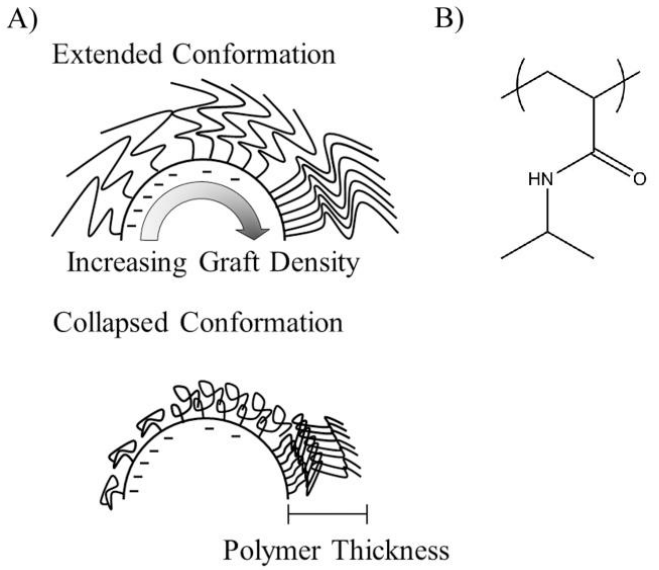

Figure 1.7 A) Extended below the LCST of thep polymer (top) and collapsed above the LCST of the polymer (bottom) with various grafting densities. Increasing graft density increases polymer thickness and decreases the number of citrate ions present on the gold surface. (B) Repeating unit of polymerized NIPAM.

The ability for the polymer to increase/decrease its hydrophobicity has lead to its study as a material for thermally stimulated adsorption/release of cells[123, 124] and proteins.[125-129] PNIPAM displays an ~ ten-fold increase in IgG and fribrinogen adsorption capacity at 40 °C relative to 25 °C.[125, 130] The Leckband group has explored the relationship between protein adsorption to PNIPAM above the LCST of polymer and polymer graft density. With decreasing polymer graft density (0.07/nm^2) an increase in protein adsorption above the LCST is observed. At higher grafting densities (0.15/nm^2) low nonspecific adsorption is observed to the polymer, both above and below the LCST of the polymer.[131, 132] At low graft density a protein can penetrate the polymer network, maximizing polymer-protein interactions. When one extrapolates maximal protein adsorption data at low polymer graft density from flat surfaces to curved 20 nm AuNPs

with a 100 nM particle concentration, between 0.4-0.08 ng of protein may be captured in 1 µL sample volume above the LCST of the polymer.[132, 133]

The citrate ligands on synthesized AuNPs can be exchanged using a thiol terminated PNIPAM chain, as the thiol has a higer affinity for the gold surface than the citrate. The PNIPAM will introduce a steric hindrance layer preventing AuNP agglomeration in ionic solutions, yet the polymer can be stimulated with a thermal response to capture hydrophobic molecules and/or proteins. PNIPAM coated gold nanoparticles (>20 nm diameter) with a low PNIPAM graft density could serve as affinity agents that would not settle during extended microdialysis sampling, not agglomerate in high ionic solutions below the LCST of the polymer, display an increase in protein adsorption above the LCST of the polymer which would occur during in vivo sampling conditions and release adsorbed proteins with a decrease in temperature. However, conflicting observations have been made as to whether AuNPs coated with PNIPAM (AuNP-PNIPAM) agglomerate above the LCST of the polymer.[101, 134-136] The reversibility of AuNP-PNIPAM agglomeration has not been thoroughly studied, and there are no reports of variable graft densities of PNIPAM on AuNPs to date.

Methods to characterize particle agglomeration

The three most prominent means of studying nanoparticle agglomeration are: 1) monitoring the localized surface plasmon resonance (LSPR), 2) dynamic light scattering (DLS), and 3) electron microscopy. Each technique studies a different phenomenon and have inherent measurement biases that can affect the results.[137] The LSPR is a cohesive oscillation of conduction band electrons that are excited by incident light as displayed in **Figure 1.8**. The LSPR is observed as a strong extinction peak (absorbance plus scatter), which occurs at ~520 nm for AuNPs giving them their red color. The SPR wavelength for AuNPs is blueshifted from bulk

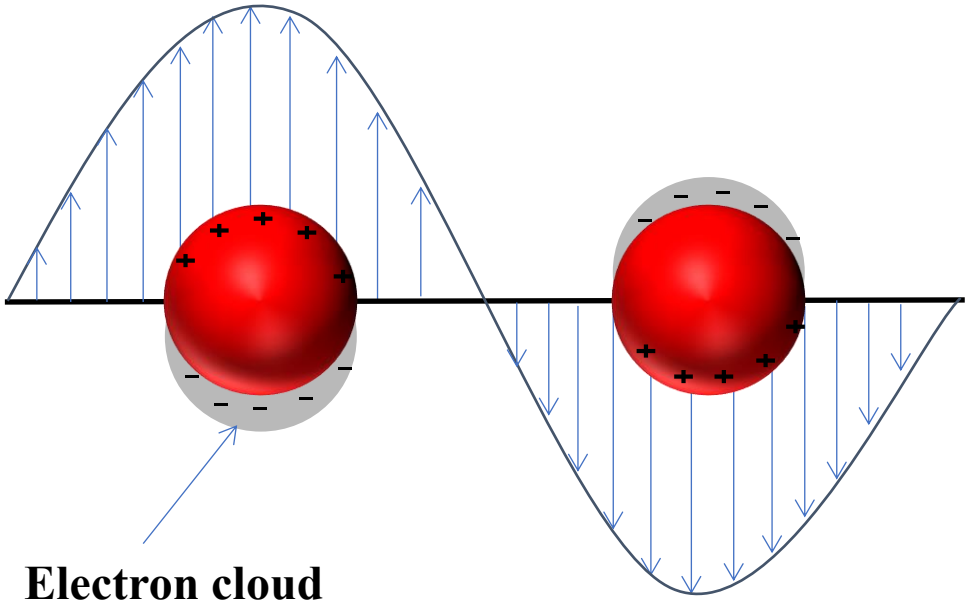

Figure 1.8 Localized surface plasmon resonance for AuNPs (red sphere). Incident light excites the conduction band electrons to oscillate in a cohesive manner.

metal as it requires more energy to polarize the AuNP than bulk material. The LSPR peak position is sensitive to the nanoparticle size, shape, composition, changes in local refractive index, and the separation distance between particles.[138-141] As particle separation distance between adjacent particles decreases to less than five times the radius of the particle, coupling of their plasmon modes causes a redshift in the LSPR peak position.[142] This shift in extinction peak position is commonly used to determine agglomeration of plasmonic nanoparticles.[143, 144]

DLS measures scattered light intensity fluctuations of particles in solution undergoing Brownian motion.[145] A laser passes through the sample and particles in solution scatter light proportional to the size of the particle. The scattered light is detected with a photo-detector and the signal is used to generate an intensity autocorrelation function. Fluctuations of the autocorrelation function at various decay times are related to the diffusion coefficient of the particles scattering light. The hydrodynamic diameters of particles is then calculated using the Stokes-Einstein equation. DLS is biased toward detecting larger particles and/or impurities in

polydisperse samples due to scattering intensity increasing to the sixth power relative to particle diameter ($I \propto d^6$).[146] Increases in the hydrodynamic diameter of particles is indicative of agglomeration.[147]

Transmission electron microscopy (TEM) has been used to study nanoparticle agglomeration/aggregation structures[143, 148] and has been used to study thermal agglomeration of nanoparticles.[149] A benefit of TEM analysis for studying nanoparticle agglomeration is visualization of heterogeneous structures, as both DLS and LSPR are ensemble measurements, with biases towards measuring large agglomerates or decreasing separation distance between particles.

Nanogels as an alternative support for affinity agent immobilization

An additional alternative support material with which affinity ligands may be immobilized to are nanogels, hydrogels with size dimensions in the nm range. Nanogels are a three dimensional network of crosslinked polymers with a diameter below one micrometer.[150] In water the nanogels swell due to the favourable inteeractions between hydrophillic functional groups in the nanogel and water. While nanogels tend to have sizes of 100-1000 nm, their density is lower than a solid particle. The low density of the polymer material is compounded by the fact that water swells the polymer which decreases the density difference between particle and water. Nanogels are a common platoform with which to embed affinity ligands,as they can be synthsized to contain a wide range of monomers with functional groups (such as-NH_2, -OH, -COOH), ease of preperation, tunable size, minimal toxicity, high dispersion stability and ability to entrap macromolecules preventing their degredation due to enzymes.[151-154]

Nanogels have a high suspension stability as they have negligible van der Waals forces of attraction between them; they are hydrated carbonacious materials with low Hamaker

constants.[155, 156] The three dimensional porous structure gives rise to a large area with which ligands can be immobilized. Additionally, responsive nanogels may have a stimuli applied to enhance drug/protein release from the particle.[157, 158] Pan et al. has used PNIPAM nanogels to capture and release lysozyme, observing heightened release kinetics above the LCST of the polymer.[159] Popova et al, has immobilized an affinity ligand within PNIPAM nanogels to separate cytokines from abundant proteins in complex solutions, and observed a 5-fold cytokine release rate at 37°C relative to 22°C.

Nonspecific adsorption is dependent upon the surface area and functional groups of a material exposes to solution. However despite the high surface area of nanogels, PNIPAM nanogels have low nonspecific adsorption amounts. Bisacrylamide crosslinked PNIPAM hydrogels display a 16 mg BSA per gram of material nonspecific adsorption amount, which is comparible to the adsorption of BSA to poly (ethylene glycol) (PEG) nanogels of 4 mg/g.[128] A high level of nonspecific adsorption would inhibit application of the nanogels as affinity agents. Nonspecifically adsorbed protein may undergo conformational changes on the particle surface decreasing the likihood of release (due to increased affinity to the surface occuring after denaturation) and/or possible damage to the epitope causing released protein to not be detected.

Dissertation goals

Cytokines play important roles in initiating and regulating intracellular communications. However the study of cytokines with microdialysis poses a signifigant challenges for the ensuing detection method due to the compounding effects of low extracellular conentrations and low RR. Previously developed affinity agents have been shown in to increase the RR of cytokines, however these affinity agents were insoluble and settled during perfusion unless additional instrumentation was employed. The interest in developing novel affinity agent supports to

enhance cytokine RR while decreasing the complexity of perfusing the affinity agents is the underlying goal of this work.

The first goal of this disseration was to obtain different PNIPAM polymer graft density on AuNPs, which has not been reported prior. The stability of the synthesized AuNP-PNIPAM was studied above and below the LCST of the polymer. Irreversible particle agglomeration affects particle surface area, reactivity, as well as protein adsorption and release amounts. Therefore studying the reversibility of any agglomeration is warranted before AuNP-PNIPAM can be sudied as microdialysis affinity agents.

The second goal of this disseration is to explore the feasibility of affinity ligands immobilized to nanogels synthesized from PNIPAM. A previously developed synthesis for PNIPAM nanogels yield particles with sizes between 700-1200 nm, above the 460 nm predicted settling diameter for PNIPAM. A method to rapidly separate synthesized particles based on settling diameter is used. An affinity dye ligand is immobilized to the nanogels enabling simple quantification of the nanogels (by measuring the absorabance of the immobilizd dye). Perfusion of the nanogels is studied using push and push/pull microdialysis and finally the RR of two cytokines was studied with inclusion of the newly developed nanogels in the perfusion fluid.

Chapter 2 Synthesis of gold nanoparticles with variable graft density and study of their agglomeration reversibility in a salt solution

Introduction

In this chapter, gold nanoparticles (AuNP) with a graft density of 0.09, 0.12, 0.30 and 0.40 chains/nm^2 of poly (*N*-isopropyl acrylamide) (PNIPAM) were reproducibly synthesized by varying the ratio of disulfide terminated poly (*N*-isopropyl acrylamide) to gold nanoparticle in attempt to study protein adsorption as a function of polymer graft density. Low graft densities of PNIPAM have the highest levels of thermally triggered protein adsorption on flat surfaces (0.07 chain/nm^2).[131, 160] Agglomeration of AuNP-PNIPAM in ionic solutions was studied. The reversibility of the particle agglomeration with different graft densities was studied by measurements of their (LSPR), the hydrodynamic radius (D_h), and visualization using electron microscopy. The reversibility of agglomeration correlated with the graft density, with irreversible agglomeration occurring for lower graft densities. The graft density dependence on reversible agglomeration is due to changes in collapsed polymer steric effects.

Experimental

Reagents

Tetrachloroauric (III) acid trihydrate ACS grade was purchased from Acros Organics (New Jersey, NY). Lipoic acid terminated neutral PNIPAM 13 kDa (n ~ 110) as determined by ^{1}HNMR was a gift from Guorong Sun at Texas A&M and used as received. Trisodium citrate, sodium chloride (99.5%) was purchased from Sigma Aldrich (St. Louis, MS). HPLC grade water was used for all experiments and was from Thermo Fisher Scientific (Waltham, MA), as was metal-free nitric acid and hydrochloric acid. Dimethyl sulfoxide (DMSO) was from Electron

Microscopy Sciences (Hatfield, PA) Solutions used for DLS studies were filtered using a 0.2 μm PES from GE Healthcare (Chicago, IL) before nanoparticle dilution.

AuNP Synthesis

All glassware was acid washed with aqua regia consisting of hydrochloric acid and nitric acid at a 3:1 ratio and thoroughly washed with water before use. Gold nanoparticles were synthesized using the Turkevich method as previously described.[97] A total of 300 mL of aqueous tetrachloroauric (III) acid trihydrate (0.5 mg/mL) was brought to a boil with magnetic stirring and 30 mL 1% (w/v) trisodium citrate solution was quickly added. After 8 min, the particles were removed from heat and cooled to room temperature. ^{1}HNMR of the polymer used was performed in deuterated DMSO using a 300 MHz NMR from Bruker (Billerica, MA). A spectrum of the polymer used is shown in **Figure 2.1**.

PNIPAM Modification of AuNP

Gold nanoparticle solutions were purged with nitrogen gas for 30 min, after which a concentrated lipoic acid terminated PNIPAM solution was added drop wise, until a final concentration of the disulfide PNIPAM in the nanoparticle solution was 100, 10, 2 or 1 μM, hereafter referred to as AuNP-0.40, AuNP-0.30, AuNP-0.12 and AuNP-0.09, respectively. The solutions were left sealed for 24 hr. at room temperature with stirring. Residual polymer was removed by centrifuging the solutions at 10 °C, removing the supernatant and suspending the particles in water for a total of three times. PNIPAM modification of the same initial stock of gold particles was repeated at the same polymer concentration on different days to test the reproducibility in obtaining the same graft density.

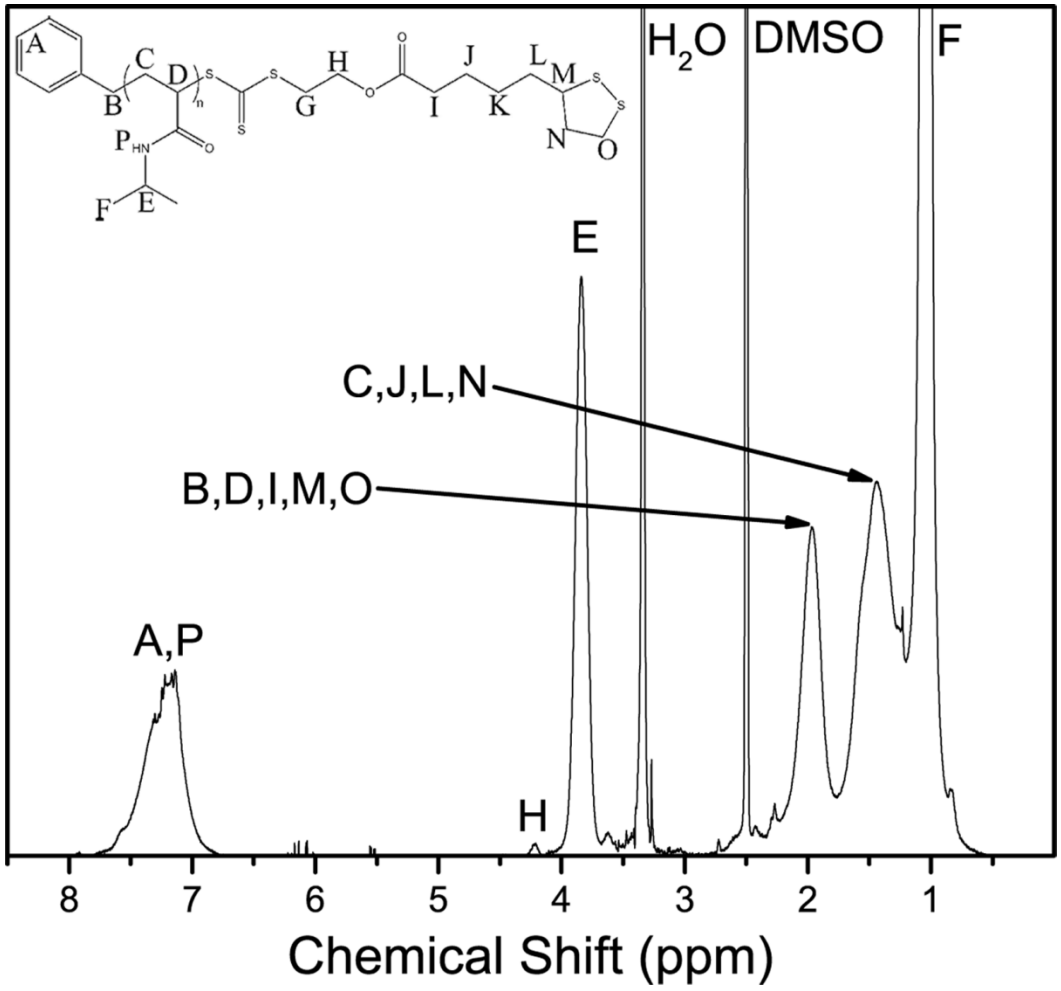

Figure 2.1 [1]HNMR spectrum of PNIPAM 13 kDa in DMSO. Integration of the peaks H from the RAFT agent and E from PNIPAM yielded a value of n=110 corresponding to a calculated molecular weight of 12880 g/mol.

AuNP-PNIPAM characterization

Particle concentration assuming spherical geometry was determined by atomic absorbance using a GBC 932 Plus from GBC Scientific Equipment (Hampshire, IL) Transmission electron microscope (TEM) images of AuNPs were taken using a JEOL-1011 and ImageJ was used to size the NPs. The extinction of AuNPs and AuNP-PNIPAM was measured with 1 nm increments using a Nanodrop 2000c from Thermo Fisher Scientific. The zeta potentials and intensity-weighted hydrodynamic diameter (D_h), or z-average, of the particles was determined using a 90Plus particle sizer from Brookhaven (Holtsville, NY). The source had a λ of 658 nm and the scattering angle was at 90°. The zeta potential was measured in a 1 mM KCl solution. Particles were allowed 10 min to equilibrate at each temperature before a measurement was made. Unless otherwise stated dynamic light scattering (DLS) measurements were made at 23 ± 0.1 °C.

Determination of graft density

Thermogravimetric analysis (TGA) experiments were performed using a Q50 from TA Instruments (New Castle, DE) using a 10 °C/min ramp to 500 °C using lyophilized samples. The graft density was determined using a previously reported method according to **Equations 2.1-3**.[161] The molecular weight of a gold nanoparticle (MW_{AuNP}) was first calculated by dividing the volume of a AuNP (V_{AuNP}) with assumed spherical geometry by the volume of a gold atom (V_{Au}=1.7 ×10^{-29} m^3) and multiplying by the molecular mass of Au. Then the number of AuNPs (N_{AuNP}) was determined by dividing the mass remaining at the end of the TGA (M_{Au}), which is attributed to Au, by the MW_{AuNP} and multiplying by Avogadro's number (N_A). Finally, δ in ligands/nm^2, was determined by dividing the number of polymer ligands lost during heating from 300-425 °C by the surface area of a AuNP (SA_{AuNP}) and the N_{AuNP}. The particle size determined from TEM was used for graft density determination.

$$MW_{AuNP} = \frac{V_{AuNP}}{V_{Au}} \times MW_{Au} \quad \text{Eq. 2.1}$$

$$N_{AuNP} = N_A \frac{M_{Au}}{MW_{AuNP}} \quad \text{Eq. 2.2}$$

$$\delta = \frac{N_{PNIPAM}}{SA_{AuNP} \times N_{AuNP}} \quad \text{Eq. 2.3}$$

AuNP-PNIPAM agglomeration studies

Confirmation of AuNP-0.40 in ionic solutions was observed by diluting AuNP to an absorbance of ~0.3 AU at its LSPR peak in PBS and measuring the D_h of the solutions from 23-37 °C with 2 °C intervals with three measurements made at each temperature, with 10 min intervals between measurements. Samples were equilibrated for 10 min before each measurement.

The temperature at which agglomeration onset was determined by diluting AuNP-0.40 to 1.08 ± 0.07 nM in water or 50 mM NaCl. The 50 mM NaCl concentration was chosen as a previous study reported sedimentation affecting DLS results when AuNP-PNIPAM were heated in higher salt concentrations.[134] The D_h of the diluted AuNP-0.40 was measured from 14 to 37 °C allowing 10 min to equilibrate between each increase in °C.

To test the reversibility of the agglomeration of AuNP-PNIPAM in 50 mM NaCl, particles were diluted to 1.08 ± 0.07 nM in water or 50 mM NaCl and incubated at 37 °C above the LCST of the polymer for up to 6 hr. After heating, all samples were sonicated to disperse flocs, using a bath sonicator for 10 sec. After sonication, the extinction and hydrodynamic diameters of aliquots were measured. Then the solutions were placed at below the LCST of the polymer (~23 °C) to relax the contracted polymer. After 150 min of relaxation at room

temperature, the solutions were agitated by pipetting and the extinction and hydrodynamic diameters of the aliquots were measured in 50 mM NaCl. The change in D_h and in LSPR peak position was recorded with respect to their initial positions in 50 mM NaCl.

Samples in 50 mM NaCl which had undergone a 2 hr heat treatment followed by sonication or remained at room temperature were drop-cast on TEM grids. The average area of AuNPs heated and unheated was determined using ImageJ. Only particles with an area above 67 nm^2 were included in the analysis. This 67 nm^2 threshold was chosen because the smallest measured nanoparticle would have this area assuming circular geometry. Particulate with an area below this threshold is believed to be due to salt.

Jones *et al.* have suggested a methanol wash procedure to remove residual polymer post modification.[162] Residual polymer has been reported to induce thermal agglomeration of AuNP-PNIPAM in water, where residual polymer serves to bridge particles when heated above the LCST of the polymer. To test to see if salt induced thermal agglomeration was caused by a residual polymer, AuNP-PNIPAM was washed for a total of three times in water, followed by washes in methanol. After the third wash in methanol the AuNPs were hydrated in water and lyophilized. The particles were reconstituted in 50 mM NaCl and their D_h measured after 10 min at 37 °C.

Results

AuNP-PNIPAM characterization

Spherical AuNPs with a diameter of 20.5 ± 6.5 nm were synthesized with an initial LSPR of 525 nm. The polydispersity index (PDI) for the synthesized particles was 0.107, which is lower for other reported synthesis.[163] **Figure 2.2** displays a representative TEM image and the

corresponding size histogram. Modification of these particles with PNIPAM was repeated for a total of three times for each graft density studied. The LSPR of the modified AuNPs redshifted to 528 ± 1 nm, 529 ±1, 529 ± 1 and 529 ± 1 nm for AuNP-0.09, AuNP-0.12, AuNP-0.30 and AuNP-40, respectively, as shown in **Table 2.1** and **Figure 2.3**. This red shift is due to an increase in refractive index from essentially water to a carbonaceous polymer, which is in accordance to the report by Zhang *et al.* in which their AuNPs shifted from 525 to 529 nm after PNIPAM modification.[135] The dispersity of the particles increased upon PNIPAM modification, increasing from 0.103 to ~0.22. This increase in dispersity is likely due to dispersity in the polymer, as the dispersity increased similarly for all graft densities The D_h of the AuNPs increased from 31.3 ± 0.3 nm to 55.6 ± 4.6, 56.7 ± 9.1, 56.3 ± 0.9 or 53.7 ± 0.8 nm for AuNP-0.09, AuNP-0.12, AuNP-0.30, and AuNP-0.40, respectively, displayed in **Figure 2.4**. Size analysis by TEM measures the nanoparticle metal core, while DLS measures the core and polymer coating. All graft densities of AuNP-PNIPAM were stable above the LCST in water There was no significant difference in D_h between the grafting conditions studied, and all had essentially the same LSPR peak position and shape. The similarity in D_h is not unexpected as on spherical surfaces the polymer density distribution is less sensitive to increasing graft densities relative to that of flat surfaces.[164] There is an increasing volume the polymer can occupy with increasing distance from the spherical surface.

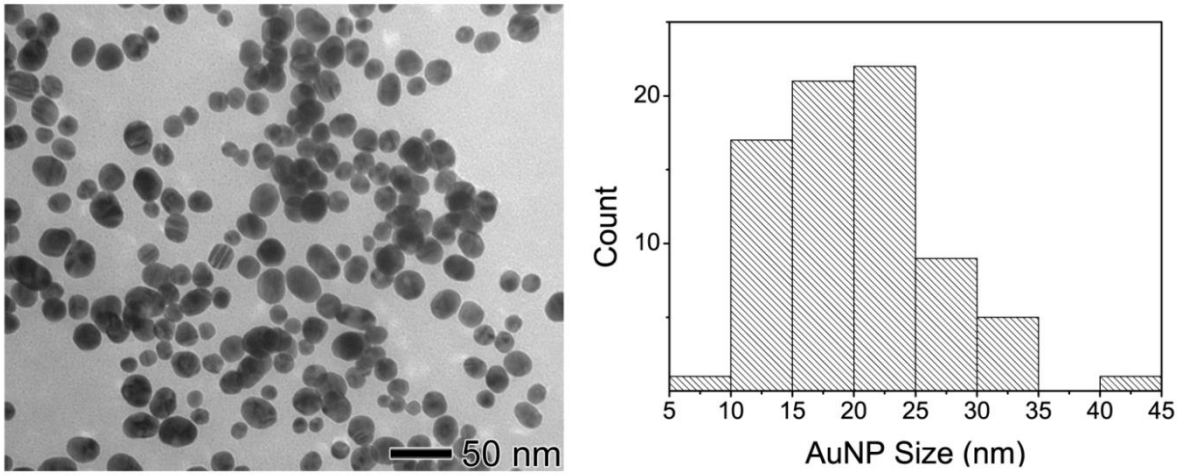

Figure 2.2 (Left) TEM image of the as-synthesized AuNPs, and (right) the corresponding size histogram.

Table 2.1 Characterization of AuNPs

Particle Name	LSPR Position (nm)	Mass % Loss (%)	δ (chains/ nm²)	D_h Water 23°C (nm)	PDI Water 23°C	Zeta Potential (mV)	D_h Water 37°C (nm)	NaCl 23°C (nm)	D_h 50 mM NaCl 37°C (nm)
AuNP	**525**	**NA**	**NA**	**31.3 ± 0.3**	**0.103 ± 0.011**	**NP**	**NP**	**NP**	**NP**
AuNP-0.09	**528 ±1**	**2.6 ± 0.1**	**0.09 ± 0.01**	**55.6 ± 4.6**	**0.226 ± 0.018**	**-17.2 ± 2.1**	**38.6 ± 3.2**	**54.7 ± 6.0**	**179.5 ± 28.6**
AuNP-0.12	**529 ± 1**	**3.6 ±0.3**	**0.12 ± 0.1**	**53.9 ± 3.5**	**0.227 ± 1 0.010**	**NP**	**43.0 ± 0.8**	**55.2 ± 4.2**	**266.1 ± 4.5**
AuNP-0.30	**529 ± 1**	**8.7 ± 0.8**	**0.30 ± 0.03**	**56.0 ± 0.8**	**0.222 ± 0.025**	**-2.1 ± 0.4**	**42.9 ± 1.0**	**56.3 ± 0.9**	**192.6 ± 2.9**
AuNP-0.40	529 ± 1	11.3 ± 0.4	0.40 ± 0.03	53.7 ± 0.8	0.229 ± 0.026	0.3 ± 0.3	41.4 ± 1.3	52.4 ± 1.8	187.4 ± 41.5

n=3 experimental replicates for all except AuNP, in which n=1. Error bars represent ± 1 s.d. NA represents not applicable, and NP represents not performed. For DLS measurements, samples were equilibrated 10 min at the specified temperature before measurements were made.

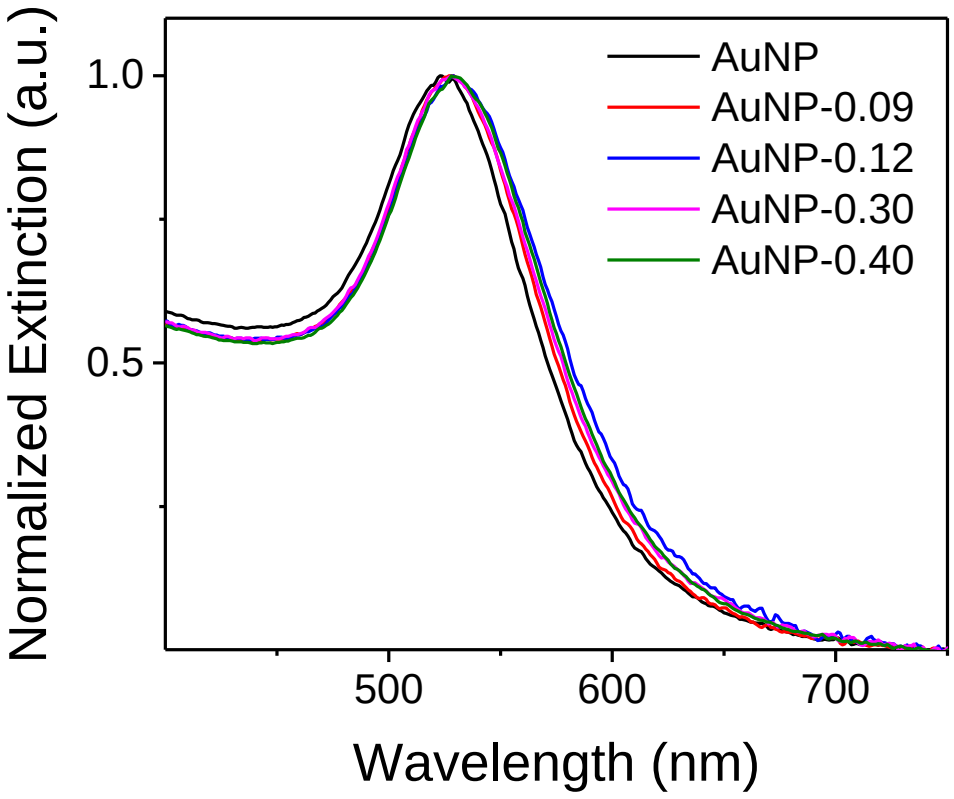

Figure 2.3 Normalized extinction spectra for AuNPs and AuNP-PNIPAM displaying the LSPR peak position in 50 mM NaCl at 23 °C.

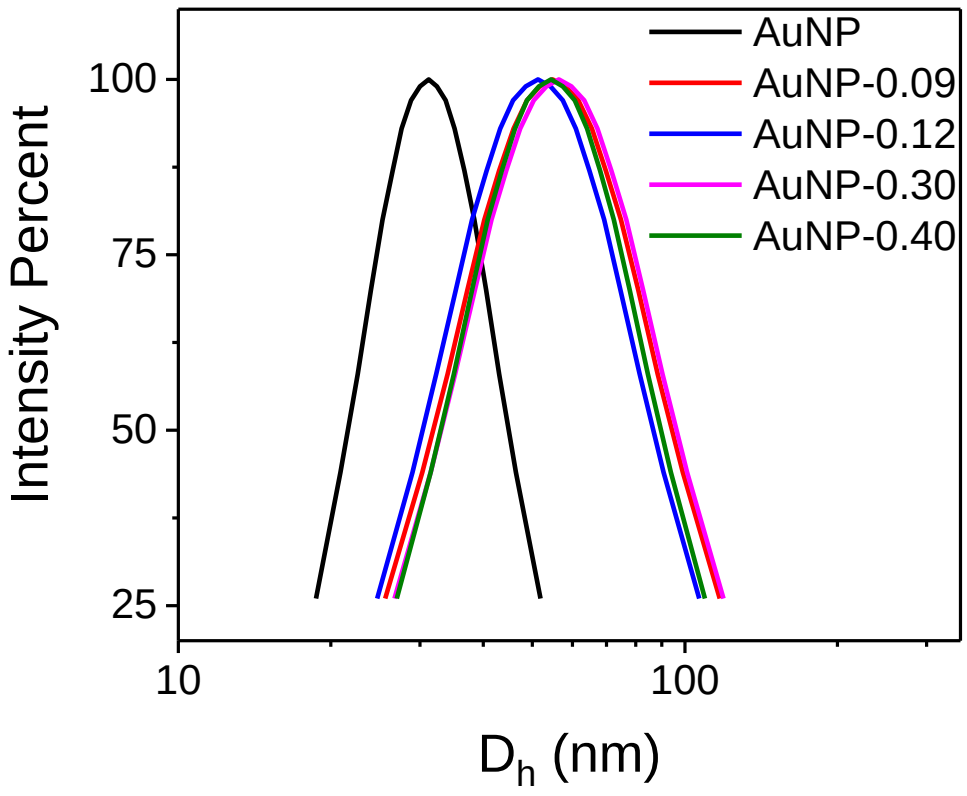

Figure 2.4 Hydrodynamic diameter (z-avg) for AuNPs and AuNP-PNIPAM in water at 23 °C.

Increasing the concentration of PNIPAM ligand while keeping the AuNP concentration the same, led to an increase in mass loss percentage from 300-425 °C as measured by TGA, corresponding to the loss of PNIPAM (**Figure 2.5**). The determined graft densities were 0.40, 0.30, 0.12 and 0.09 chains/nm^2 for AuNP-0.40, AuNP-0.30, AuNP-0.12 and AuNP-0.09, respectively. This is the first time that variable graft densities of PNIPAM have been quantified on AuNPs. Increasing the PNIPAM concentration to 500 μM yielded no observable increase in mass loss compared to 100 μM, indicating saturation of the AuNP surface is reached at 0.40 chains/nm^2. This graft density is lower than previous studies with AuNPs modified with a thiol terminated PNIPAM, which reported 0.9 chains/nm^2.[134] However in this study a lipoic acid terminated polymer (bidentate disulfide anchor) was used, rather than a monodentate thiol anchor, so the reduction in graft density is expected.[165]

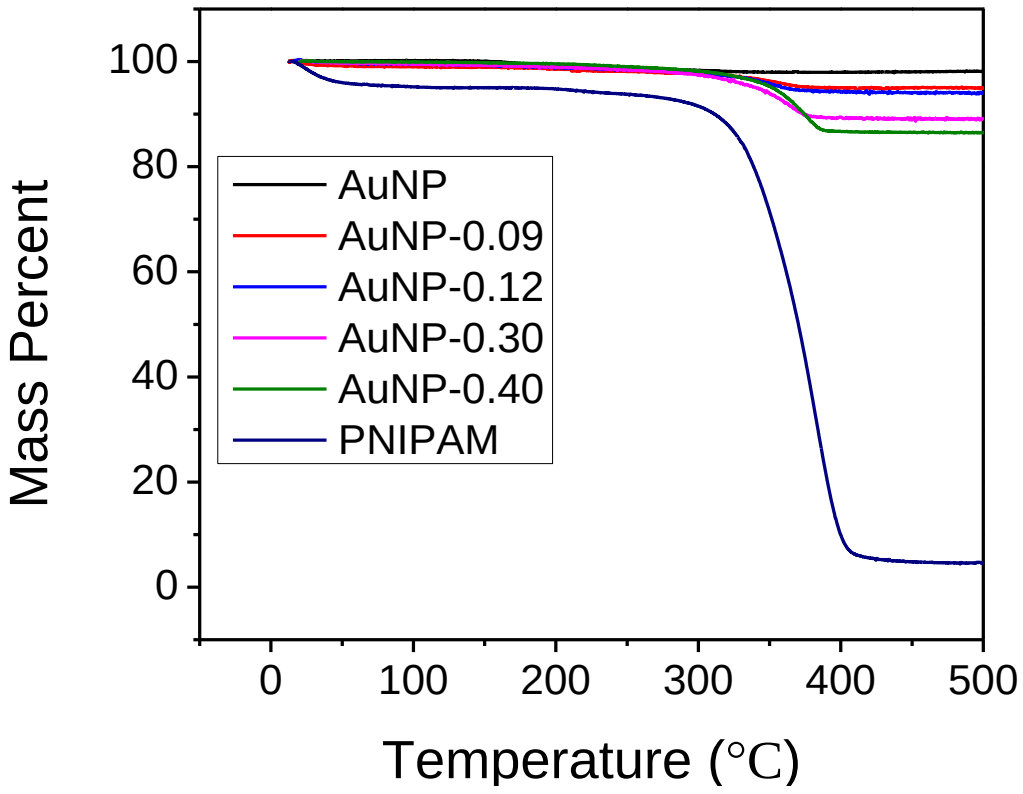

Figure 2.5 TGA of AuNP, AuNP-PNIPAM, and PNIPAM using a 10 °C/min heating ramp.

The zeta potential of the particles increased with increasing graft density, reaching ~ 0 mV at the highest polymer concentration used. The measured zeta potentials were -17.2 ± 2.1, -2.1 ± 0.4 and 0.3 ± 0.3 mV for AuNP-0.09, AuNP-0.30 and AuNP-0.40, respectively. The increase in zeta potential with increasing graft density is expected as the citrate is displaced by the anchor group from the polymer chain. The neutralization in zeta potential displays an increase in polymer coverage and a change in forces that stabilize the particles. At a low polymer graft density and negative zeta potential, particles are stabilized with a combination of steric and electrostatic forces. During polymer collapse in water residual citrate ions on AuNP-0.09 stabilize the particles against agglomeration. As the polymer saturates the particle surface all citrate ions are displaced and the particles are stabilized by steric forces.

The AuNP-0.40 contracted/extended reversibly in water as seen in **Figure 2.6**. Additionally, all AuNP-PNIPAM returned to their initial D_h following a 30-min application of heat at 37 °C (>LCST) and sonication as seen in **Figure 2.7**.

Previous reports have observed salt induced thermal agglomeration of AuNP-PNIPAM. The salt induced thermal agglomeration of AuNP-0.40 was confirmed in PBS as seen in **Figure 2.8**. The sample decreased in D_h from 23 to 25 °C, and agglomeration onset 27 °C with an increase in D_h. The D_h of AuNP-0.40 continued to increase with time heated at 27 °C, indicating continued agglomeration. With further increases in temperature and time, flocculant was observed, complicating DLS due to particles settling outside of the laser path. A similar observation was made by Yusa et al. who observed particle settling at 37 °C in solutions with an ionic strength greater than 100 mM.[134] Due to this complication, further studies of the agglomeration were conducted in 50 mM NaCl.

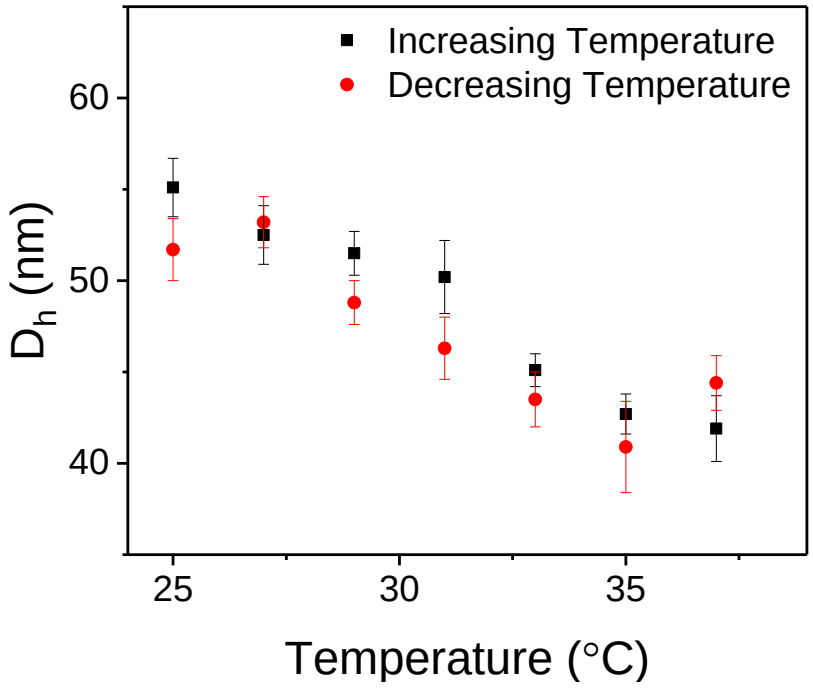

Figure 2.6 Hydrodynamic diameter (z-avg) for AuNP-0.40 in water with increasing temperature (black) and decreasing temperature (red). Samples equilibrated for 10 min at each temperature before measurements were made. Avg ± 1 s.d., n=5

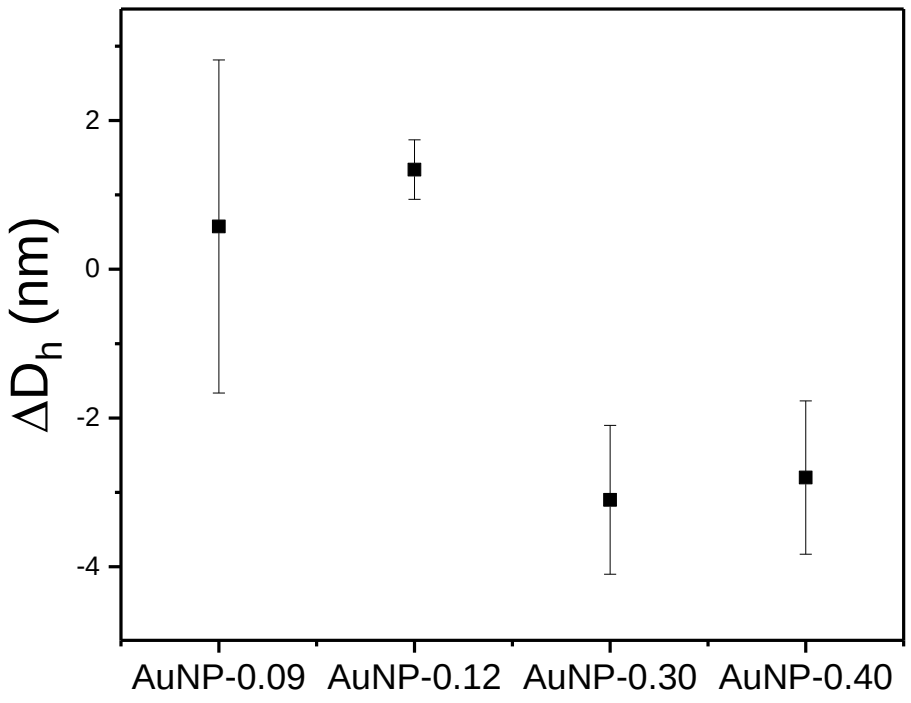

Figure 2.7 Change from initial D_h for AuNP-PNIPAM in water after heating for 30 min at 37 °C followed by sonication at RT. Avg ± 1 s.d., n=5.

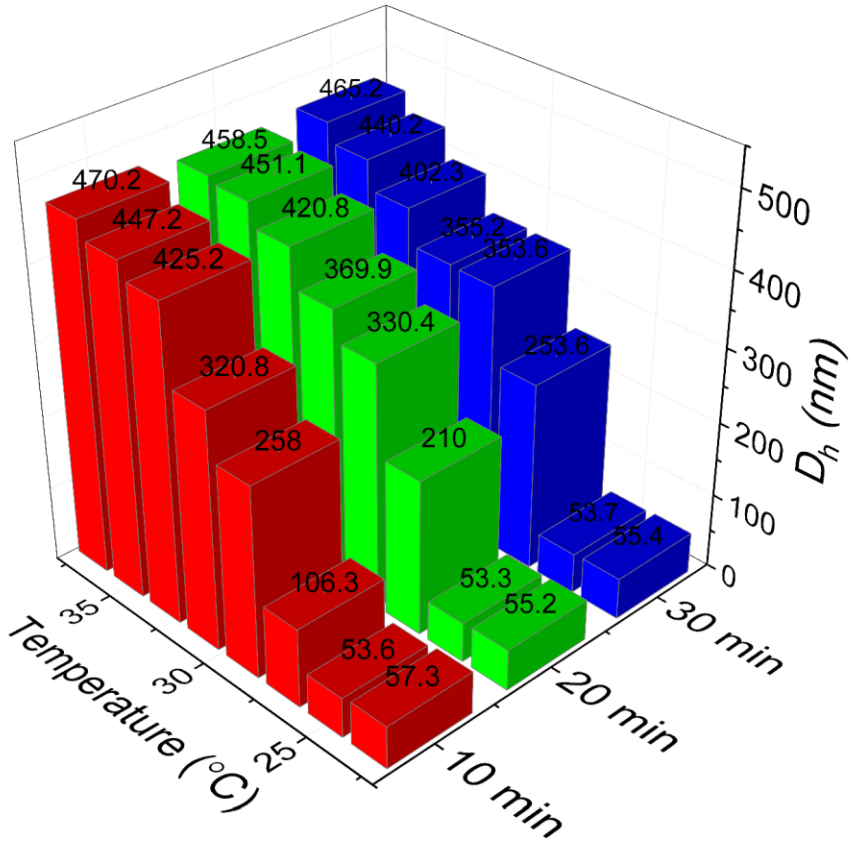

Figure 2.8 D_h of AuNP-0.40 in PBS with varied temperature and times at each temperature. Samples were measured after the first 10 min at each temperature (red), after 20 min (green) and after 30 min (blue). The number above each bar corresponds to D_h at the respective measurement interval.

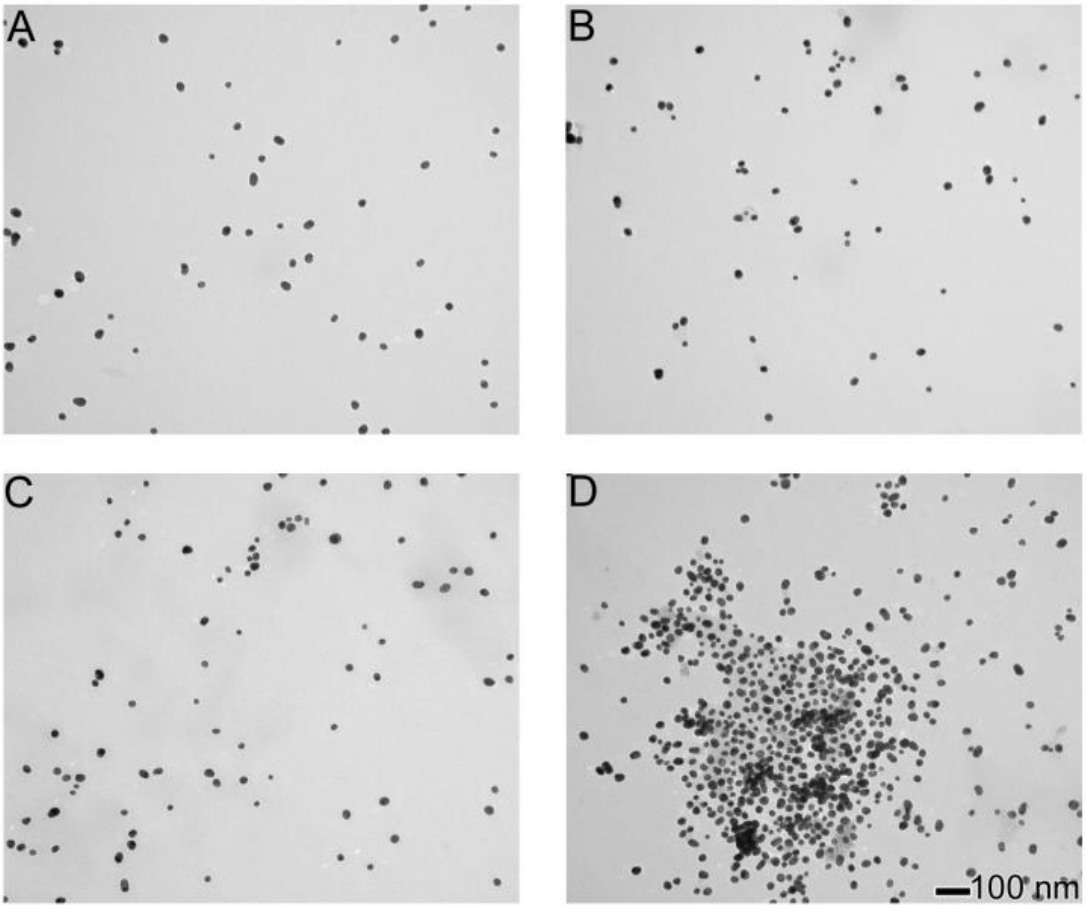

Figure 2.9 TEM image of A) AuNP-0.40 treated with 50 mM NaCl. B) AuNP-0.09 treated with 50 mM NaCl, C) AuNP-0.40 treated with 50 mM NaCl and heated for 120 min, D) AuNP-0.09 treated with 50 mM NaCl and heated for 120 min.

All particles were stable in the salt solution prior to heating as there was no shift in LSPR, the D_h was the same as in water, and TEM images displayed primary particles as seen in **Figure 2.9A**, **2.9B** and **Table 1**. However, when heated in a 50 mM NaCl solution agglomeration onset at ~ 29 °C as seen in **Figure 2.10**. When heated in 50 mM NaCl, the D_h of the particles decreases similarly to those in water, until 28 °C is reached. Any further increases in temperature onset agglomeration. At 15 °C the D_h for AuNP-0.40 was 51.7 ± 0.5 nm and 51.6 ±

0.6 nm in water and 50 mM NaCl, respectively. At 27 °C the D_h contracted to 49.2 ± 0.4 nm and 49.2 ± 0.3 nm in water and salt, respectively. At 30 °C in water the D_h continued to contract to 46.7 ± 0.3nm while in 50 mM NaCl an increase in D_h occurred to 75.9 ± 0.3 nm. It is known that PNIPAM grafted on AuNPs, has two different polymer collapse regions.[117, 166, 167] When grafted to a surface, the polymer adjacent to the surface is less hydrated (due to a high polymer local concentration) and has an LCST that is lower than the outer region. The outer polymer region has more interactions with water. The DLS data display a contraction from 15 to 27 °C in both water and in 50 mM NaCl, which is indicative of polymer collapse at the dehydrated particle core. The particles remained stable at this temperature for 10 min, with no observable agglomeration. However, when further contraction in water was observed at 30 °C, agglomeration onset in 50 mM NaCl. This leads to the conclusion that agglomeration occurs due to a lack in particle stability when the second brush region, which is more hydrated at the water polymer interface, contracts, and/or due to polymer bridges forming as the outer polymer layer form entanglements between polymer chains on adjacent particles.

It has been recently observed that AuNP-PNIPAM agglomeration above the LCST of the polymer occurs in water due to residual polymer from the grafting process bridging nanoparticles.[162] This agglomeration in water has been prevented by removing the residual polymer using a methanol washing procedure. However, the suggested wash procedure did not prevent agglomeration in 50 mM NaCl as seen in **Figure 2.11**.

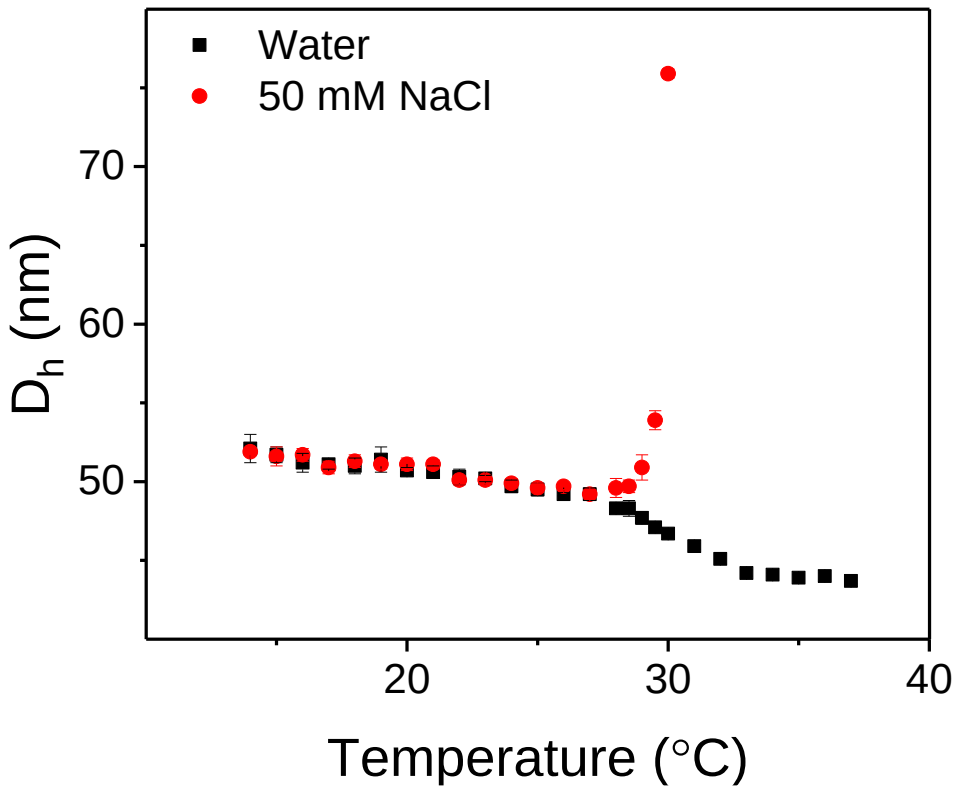

Figure 2.10 D_h of AuNP-0.40 in water (black) and 50 mM NaCl (red). Samples were equilibrated for 10 min before each measurement was taken. Avg ± 1 s.d., n=5.

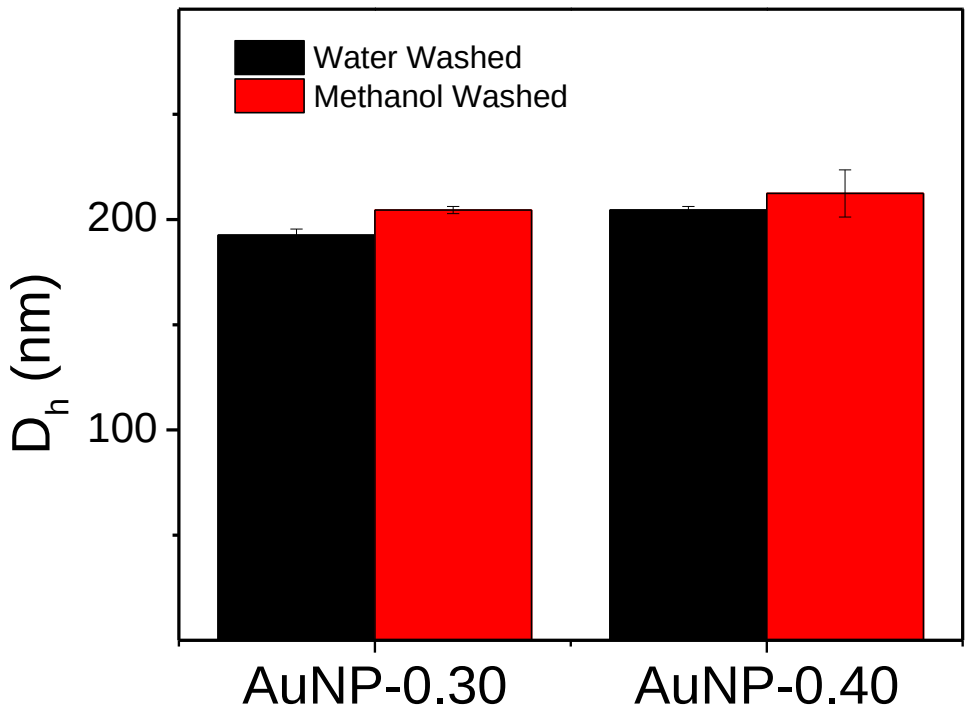

Figure 2.11 Comparison of AuNP-PNIPAM agglomeration in 50 mM NaCl with additional washes in methanol. Samples were washed in water three times and lyophilized. Methanol washed samples underwent an additional three washes in methanol before lyophillization. Gold particles were heated at 37 °C for 10 min before measurements were taken. Avg ± 1 S.D., n=5.

AuNP-PNIPAM agglomeration reversibility studies

Protein adsorption to PNIPAM is highest at low polymer graft densities. All AuNP-PNIPAM were observed to agglomerate above LCST of the polymer hindering protein adsorption studies, as particle surface area would be unknown during agglomeration. Additionally, it is desired to decrease the temperature and release the adsorbed protein. If protein is adsorbed between agglomerated particles its release will be hindered. Therefore, the reversibility of agglomeration as a function of polymer graft density was studied. It should be noted that AuNP-0.12 was excluded from further studies due to sample loss during TGA, a destructive technique.

The reversibility of agglomeration was dependent upon the PNIPAM graft density and the length of time the solution was exposed to 37 °C. The agglomeration of AuNP-0.09 was irreversible despite sonication and the 150-min relaxation period. Both the LSPR peak position and D_h remained significantly different relative to the initial positions for all heating times ($p<0.05$) as shown in **Figure 2.12**. The LSPR peak position redshifted with increasing heating times, up to 107 nm after undergoing a 6 hr heat treatment in 50 mM NaCl as seen in **Figure 2.13**. This occurs due to further contraction of the polymer layer, decreasing the particle separation distance, which couples the plasmon modes. After 150 min at room temperature, the LSPR peak position remained redshifted 78 nm.

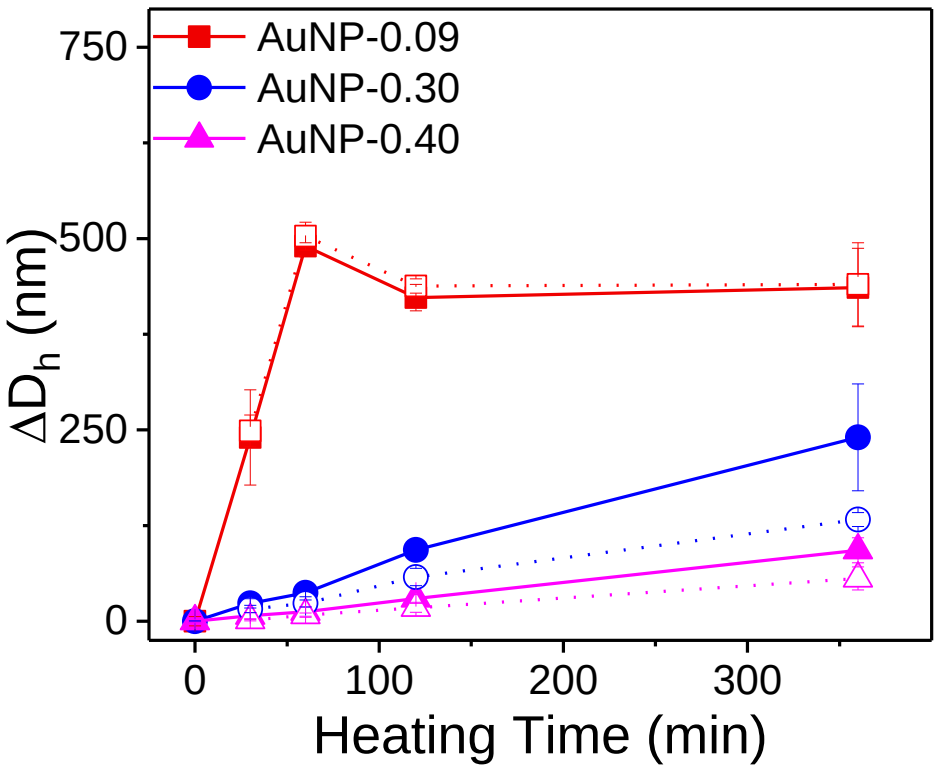

Figure 2.12 Shift from initial hydrodynamic diameter (ΔD_h) for AuNP-0.09 (red), AuNP-0.30 (blue) and AuNP-0.40 (purple) after heating and sonication (filled) and after the relaxation period (unfilled), measurements made in 50 mM NaCl. Avg ± 1 s.d. n=3 experimental replicates.

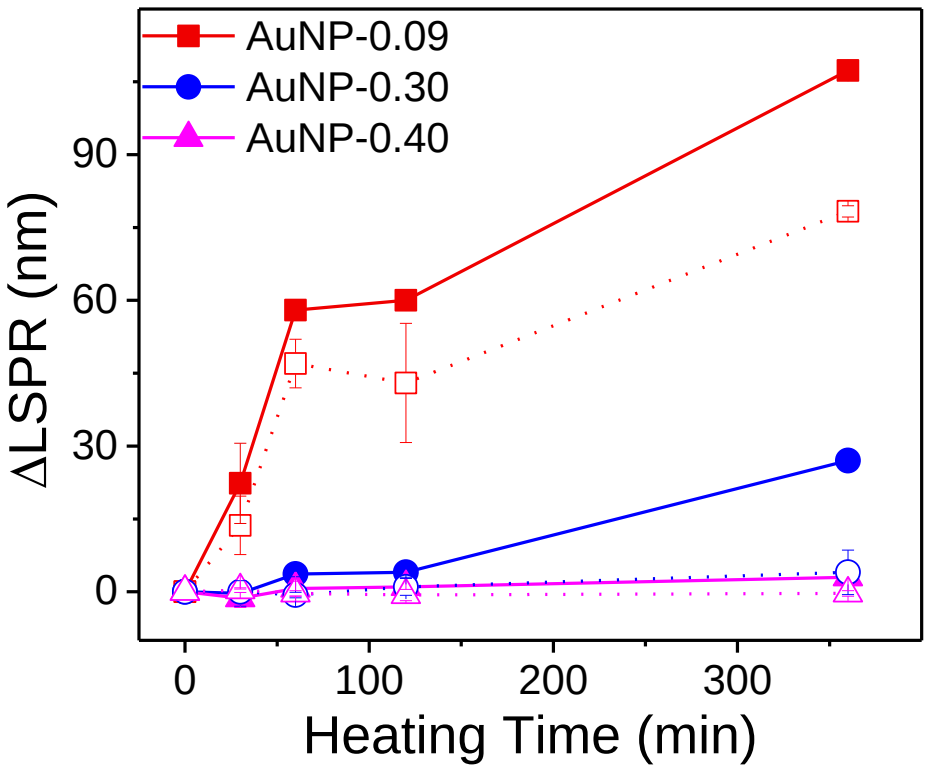

Figure 2.13 Shift from initial localized surface plasmon resonance position (ΔLSPR) for AuNP-0.09 (red), AuNP-0.30 (blue) and AuNP-0.40 (purple) after heating and sonication (filled) and after the relaxation period (unfilled), measurements made in 50 mM NaCl. Avg ± 1 s.d. n=3 experimental replicates.

A slight redshift in LSPR peak position of 2-5 nm during collapse of polymer is predicted due to an increase in polymer density which changes the refractive index.[168] A further redshift is due to decreasing separation distance between particles, with a 57 nm redshift reported for 15 nm AuNP agglomerated using 8 nm DNA spacers.[169] Interestingly the D_h had no appreciable change after the relaxation period. This constant D_h with a blueshift in LSPR is interpreted as agglomerated particles separating during chain rehydration, increasing separation distance between particles. The representative TEM image of heated AuNP-0.09 revealed heterogeneous agglomerated AuNPs surrounded by primary AuNPs with an increase in average particle area and variance as seen in Figure 2.9D and Table 2.2. It is worth noting that several of these agglomerated nanoparticle cores appear adjacent to one another; this is suggestive of attractive particle-particle interactions.

Increasing the polymer graft density lead to less substantial increases in D_h and LSPR peak position after sonication. The increase in D_h and LSPR peak position for AuNP-0.30 was between AuNP-0.09 and AuNP-0.40. The D_h for AuNP-0.40 after 30 min of heat treatment and sonication was significantly different, ($p<0.05$). The increase in D_h for AuNP-0.40 remained significant after the 150-min relaxation period for heating times greater than 30 min. Chain-chain interactions between particles may persist over the relaxation period that was studied. The LSPR peak position for AuNP-0.40 after heating for 6 hr and sonication was redshifted 3 nm. This LSPR peak position returned to its initial value during the 150-min relaxation at room temperature. For AuNP-0.40, the separation distance between AuNP surfaces is sufficient to no longer induce coupling of the plasmon modes (as the LSPR peak position returns to its initial position). LSPR monitoring is insensitive to chain entanglements far from the particle surface that are observable with DLS. The TEM images of AuNP-0.40 heated for 120 min revealed only

primary particles, with no increase in particle area as seen in Figure 2.9C and Table 2.2, suggestive of polymer entanglements that are not seen with TEM, or a reversible agglomeration process during the drying process.

Saturation of the AuNPs was reached at a graft density of 0.40 chains/nm^2, indicating the footprint of the disulfide head is ~ 2.5 nm^2. A 20 nm diameter AuNP with a graft density of 0.09 chains/nm^2 would leave ~ 78% of the AuNP surface area without ligand head groups. This has the repercussion of allowing PNIPAM to collapse against the particle surface, reducing polymer thickness and allowing van der Waals forces to become pertinent.

Table 2.2. Area of AuNPs before and after thermal agglomeration in 50 mM NaCl at 37 °C.

Particle Name	Area (nm^2)
AuNP-0.09	440 ± 530
AuNP-0.09 Agglomerated*	830 ± 3180
AuNP-0.40	430 ± 200
AuNP-0.40 Agglomerated	440 ± 270

The area as determined by ImageJ analysis is reported for at least 250 particles. Error bars represent ± 1 s.d. * indicates significant difference as determined by a t-test assuming unequal variance, $p<0.05$.

To shed light on the cause for graft density dependent reversibility, a soft sphere model is used to calculate the total potential energy (E_{tot}) between particles that are sterically stabilized.[170] This soft sphere model has been used to study the agglomeration of AuNPs stabilized with various molecular weights of poly(oxypropylene)diamine.[171] In this model the E_{tot} is the sum of the steric (E_{st}) and van der Waals forces (E_{vdW}), equation 2.4. A negative E_{tot} indicates attraction between particles.

$$\boldsymbol{E_{tot} = E_{st} + E_{vdW}} \qquad \text{Eq. 2.4}$$

The van der Waals force of attraction (Eq. 2.5) arises due to the high polarizability of the gold cores while the steric repulsion (Eq. 2.6) is due to the polymer coating on the particles. Electrostatic stabilization is neglected as citrate stabilized AuNPs agglomerate in 50 mM NaCl; the Debye length in 50 mM NaCl is 1.36 nm.

$$\boldsymbol{E_{vdW}} = -\frac{\boldsymbol{A}}{\mathbf{12}}\left[\frac{\boldsymbol{d^2}}{\boldsymbol{C^2-d^2}} + \frac{\boldsymbol{d^2}}{\boldsymbol{C^2}} + \mathbf{2\ln}\left(\frac{\boldsymbol{C^2-d^2}}{\boldsymbol{C^2}}\right)\right] \qquad \text{Eq. 2.5}$$

$$\boldsymbol{E_{st}} = \frac{\mathbf{50}\boldsymbol{dl^2}}{\boldsymbol{(C-d)\pi\sigma_a{}^3}}\boldsymbol{k_BTe}^{\left(\frac{-\pi(C-d)}{l}\right)} \qquad \text{Eq. 2.6}$$

Where C is the center to center distance between particles, A is the Hamaker constant (1.95 eV for Au particles),[112] d is the diameter, l is the brush thickness, σ_a is the diameter of the area occupied by the disulfide on the particle (~ 1.6 nm). Graft density determines extended and collapsed polymer thickness. As seen in **Figure 2.14**, an attractive van der Waals force well develops with decreasing polymer thickness. The brush thickness was varied from 12 to 3.5 nm as the hydrodynamic radius of the AuNP increases 12 nm upon polymer modification, which contracts to 3.5 nm with polymer collapse at 37 °C in water. The AuNP-0.09 have a -17 mV zeta potential, stabilizing the particles during thermal collapse in water.

Particles with a high polymer graft density have a thick collapsed polymer layer that prevents van der Waals forces from becoming applicable during polymer collapse in salt solutions. With decreasing graft density, the collapsed polymer thickness decreases, giving rise to attractive van der Waals force between particles. The van der Waals forces inhibit the reversibility of their agglomeration. The TEM images of the AuNP-Low agglomerates show groupings of overlapping particles, which in addition to the dramatic increase in LSPR peak

position suggests AuNP-0.09 surfaces are brought near one another (<10 nm) while AuNP-0.40 are not.

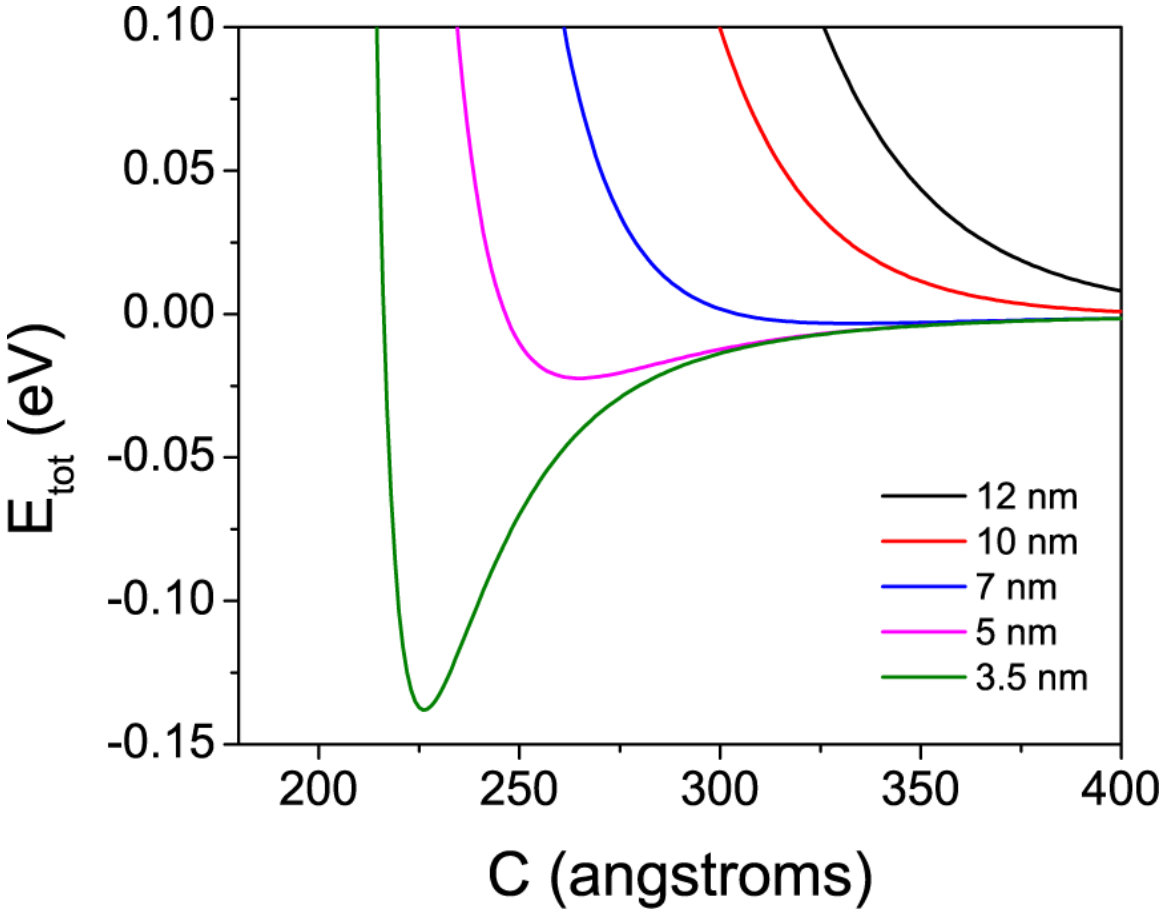

Figure 2.14 Variation in E_{tot} with decreasing C at various polymer thicknesses from 12 nm (black) to 3.5 nm (green).

Summary

Before AuNP-PNIPAM can be applied to an environment, a predictable response in the environment both above and below the LCST must be known. Agglomeration changes nanoparticles surface area, toxicity, and biodistribution. In salt solutions above the LCST of the polymer, AuNP-PNIPAM with a low graft density agglomerate irreversibly. Reversibility is approached by increasing the polymer graft density to 0.40 chains/nm^2, however an increase in D_h is observed for graft densities studied in this work. The irreversible agglomeration of AuNP-PNIPAM at low graft density complicates the development of AuNP-PNIPAM as protein capture/release agents for microdialysis. Thermally stimulated protein adsorption to PNIPAM only occurs at low polymer graft densities where polymer/protein interactions are maximized (as the protein can diffuse into the polymer chain network).[131, 172, 173] Adsorbed protein may not be readily released from the agglomerates.

The graft density dependent agglomeration reversibility results seek to relate the importance of collapsed ligand structure on nanoparticle stability, and guide future design of AuNP-PNIPAM to be used in salt solutions. Additionally, when characterizing the agglomeration of plasmonic nanoparticles, DLS and LSPR monitor different phenomenon which yield complimentary information.

Chapter 3 Synthesis of Protein Binding Nanogels with High Dispersion Stability

Introduction

In this chapter, a modified synthesis for porous nanogels is described. The stability of the nanogel suspensions was studied both above and below the lower critical solution temperature (LCST) of the nanogel, as well as the nanogel's ability to capture/release the proteins, bovine serum albumin (BSA) and lysozyme. Crosslinked poly(*N*-isopropyl acrylamide) (PNIPAM) was chosen for the nanogel support as it displays low nonspecific adsorption (~16 mg/g), and has a previously published synthesis which requires no complex instrumentation.[128, 174] Additionally, the thermal response of PNIPAM gels has been used to release captured dextran and proteins including BSA and VEGF.[175-177]

Cibacron blue 3G-A(CB) is a commonly studied triazine dye that allows for protein purification by affinity chromatography.[178] CB was chosen as the ligand to immobilize to the nanogel due to the simple coupling chemistry, via a substitution reaction, CB is chemically stable, commercially available and binds a wide range of proteins including cytokines through a combination of ionic and hydrophobic interactions.[179-183] The ionic interactions between CB and proteins can be weakened by increasing the ionic strength of the solution and high salt gradients are used to dissociate protein from CB.[184] Additionally, the immobilization of a colorimetric dye to the nanogel enables rapid determination of nanogel concentration.

The synthesized nanogels have the desired characteristics of being water soluble, form stable suspensions, have high surface area, are stable for extended storage periods, have low nonspecific adsorption, and contain amine functional groups allowing for ligand coupling. The hydrodynamic diameters (D_h) of the nanogels was found to decrease from 465 to 261 nm with increasing temperatures above the LCST of the nanogels. The nanogels did not agglomerate in

ionic solutions, or solutions containing protein above the LCST of the nanogel. Nanogels embedded with CB adsorbed and released lysozyme, while BSA bound nonspecifically to the nanogel. These results suggest that nanogels embedded with protein binding ligands may be an alternative support material for microdialysis affinity agents.

Experimental

Reagents

Monosodium phosphate, disodium phosphate, sodium chloride, sodium azide, potassium persulfate (KPS) and NIPAM were purchased from Sigma (St. Louis). Cibacron blue 3G-A was purchased from Abcam (Cambridge, MA). Allylamine (AA) and N, N methylenebisacrylamide (BIS) were purchased from Alfa Aesar (Haverhill, MA). HPLC grade water was used for all experiments and was purchased from Thermo Fisher Scientific (Waltham, MA). Bovine serum albumin (BSA) fraction V was purchased from Rockland (Limerick, PA). Phosphate buffered saline (PBS) solution consisted of 147 mM sodium chloride, 4.7 mM disodium phosphate, 7.3 mM monosodium phosphate, pH adjusted to 7.2 with sodium hydroxide. This solution was used for early studies to test the nanogels in a solution with relatively high ionic strength, 174 mM, which contains kosmotropic salts that are known to affect PNIPAM chain conformations (by dehydrating the polymer), and has been used in microdialysis experiments.[185, 186] The kosmotrope was chosen as due to its ability to buffer the solution, and in attempt to test the nanogel suspension in conditions likely to induce agglomeration. The bicinchoninic acid assay (BCA) kit was purchased from Millipore (Billerica, MA). Lysozyme was purchased from MP Biomedical (Solo, OH).

Synthesis of affinity nanogels

All glassware was acid washed with aqua regia consisting of hydrochloric acid and nitric acid at a 3:1 ratio and thoroughly washed before use. NIPAM was recrystallized in hexane to remove inhibitor prior to use. The synthesis procedure used is a slight modification of previously described synthesis.[174] In brief, 0.89 g of NIPAM and 30 mg of BIS were dissolved in 30 mL of water and syringe filtered using a 0.2 µm filter. The solution was sealed and purged with nitrogen for 15 min. Then 66 µL of AA was added; the solution was purged with nitrogen and heated to 75 °C. Upon reaching 75 °C, precipitation polymerization was initiated with the addition of 1 mL of a 10 mg/mL KPS solution and the solution was stirred for 3 hr.

A separate solution of 0.99 g NIPAM, 30 mg BIS in 30 mL of water was purged with nitrogen for 30 min, and was added dropwise to the initial solution after it had reacted for 3 hr. This combined solution was removed from heat after a further 3 hr and stirred overnight at room temperature.

The synthesis was repeated two times, however one of the nanogel solutions was subjected to an additional centrifugation process to remove aggregate particles. The solution that was subjected to additional was cycles was centrifuged at 5000 relative centrifugal force (RCF) at 8 °C for 5 min and the supernatant recovered, while the precipitate discarded. RCF is reported instead of RPM as RCF relates the force acting on the solution to that of earth's gravitational force and is independent of different rotor sizes. This process was repeated until no further precipitate was observed. This nanogel solution that underwent additional wash steps is denoted as Nanogel 400, and the nanogel solution that did not undergo the additional 5000 RCF centrifugation cycles is denoted as Nanogel 1200. Finally, both nanogel solutions were washed

three times by pelleting the particles at 17,000 RCF at 8 °C for 20 min and suspending the pellet in water. **Figure 3.1** displays the synthesis for the nanogel solutions.

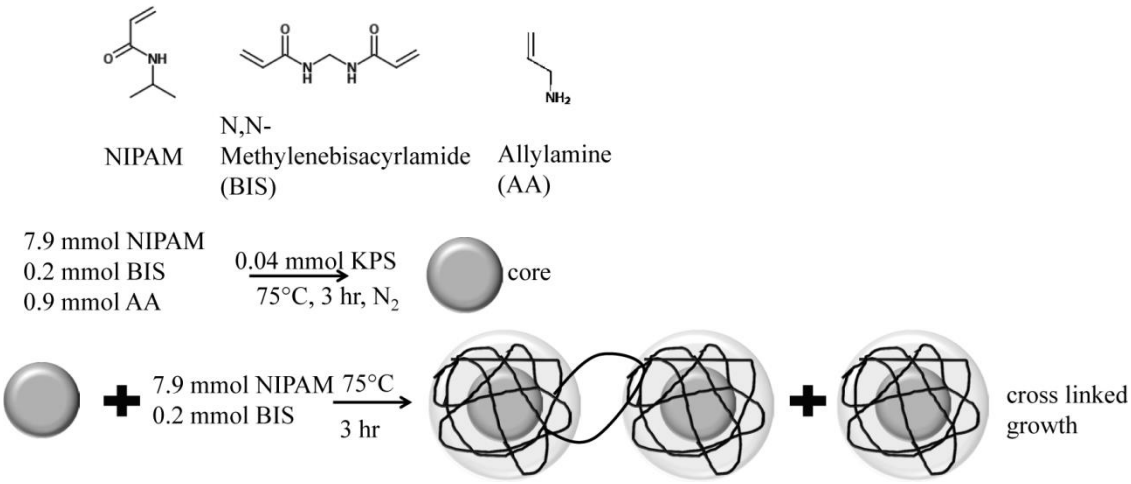

Figure 3.1 Synthesis of Nanogel 1200 and Nanogel 400. Nanogel 400 underwent additional low RCF centrifugation washes before CB modification to remove large agglomerates.

Incorporation of the CB was achieved by adding 0.32 g sodium carbonate to the nanogel solution followed by purging with nitrogen for 30 min. A CB solution was prepared containing 1.5 g CB in 30 mL of 0.1 M sodium carbonate, a 25 µL aliquot was taken to determine the initial CB concentration. The CB solution was added to the nanogel solution and allowed to react at room temperature for two days. The nanogel particles were washed by pelleting the particles at 17,000 RCF at 8 °C for 20 min and suspending the pellet in water, this process was repeated three additional times after the absorbance of the supernatant at 610 nm was zero. Finally, the pellet was suspended in 0.05% (w/v) sodium azide for storage. The supernatant was collected in a volumetric flask, diluted to the mark with water, and the moles of CB in the solution determined by measuring the absorbance at 610 nm, the absorbance peak of CB, using a Nanodrop 200c Thermo Fisher Scientific (Waltham, MA). The moles of CB immobilized into the nanogels was determined by mass balance. **Figure 3.2** displays the wash steps used to differentiate Nanogel 1200 from Nanogel 400 and the CB immobilization.

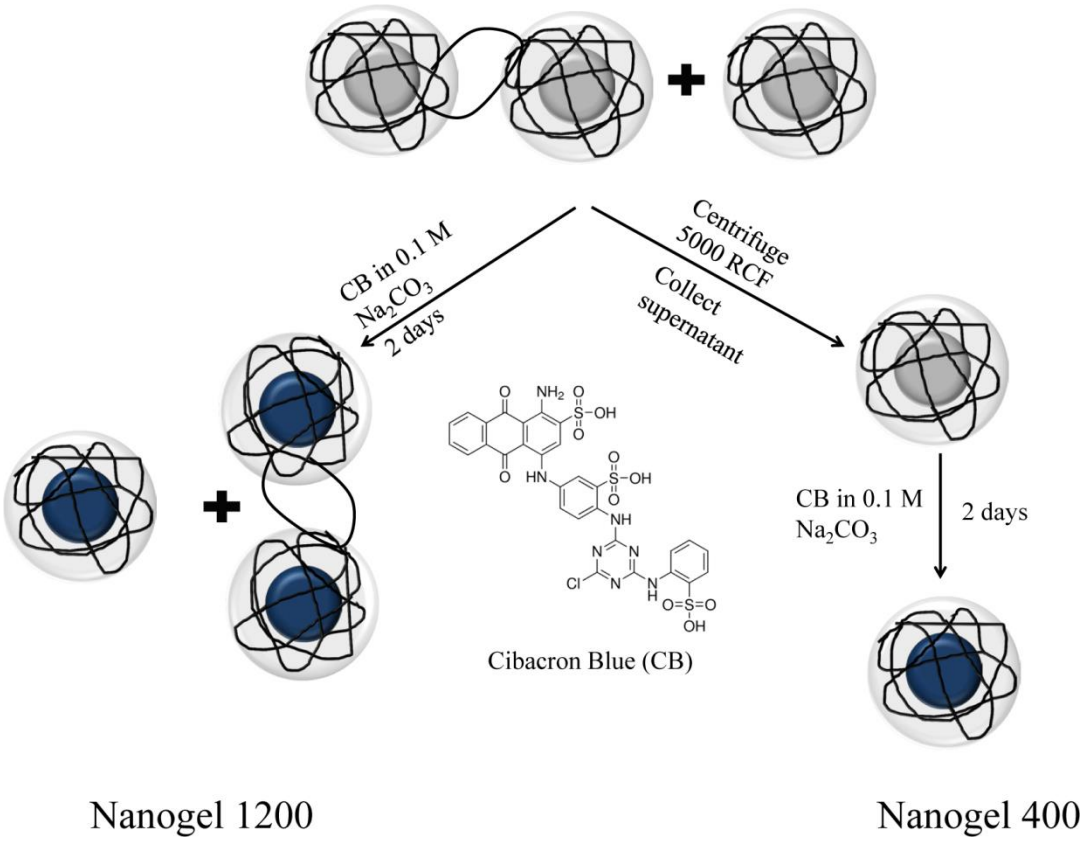

Figure 3.2 CB immobilization process for Nanogel 1200 and Nanogel 400.

Characterization of nanogels

The polymerization procedure used to synthesize Nanogel 400 and 1200 was the same; however Nanogel 400 underwent wash cycles at 5000 RCF to remove large particles. To test what impact additional centrifugation steps had on the stability of nanogel dispersions, both were washed into a PBS with 0.1% (w/v) BSA solution three times to a final concentration of 2 mg/mL nanogel. The solutions were left undisturbed for 8 hr at 21 °C, while monitoring the absorbance at 610 nm every 60 min.

Transmission electron microscope (TEM) images of nanogels were taken using a JEOL-1011 from Jeol (Peabody, MA). TEM images were analyzed using ImageJ. The hydrodynamic diameter of the nanogels at 24 °C was measured with dynamic light scattering (DLS)in water

using a 90Plus particle sizer from Brookhaven (Holtsville, NY), with λ (658 nm) and scattering angle of 90°. To observe thermal collapse of Nanogel 400, DLS measurements were performed on Nanogel 400 in water from 16°C to 40 °C allowing 10 min to equilibrate at each temperature.

To test for nanogel agglomeration above the LCST of PNIPAM, Nanogel 400 was washed into PBS with or without 0.1% (w/v) BSA three times to a final nanogel concentration of 2 µg/mL. This solution was heated to 37 °C for 10 min, after which the z-average (intensity based) hydrodynamic diameter was measured using DLS at 37 °C with 30 s intervals for 10 min. All hydrodynamic diameter (D_h) reported are the z-average. The concentration of nanogels was determined by mass balance after lyophilization. It should be noted that the PBS solution used for these experiments has an ionic strength of 174 mM and contains ionic kosmotropes. This ionic strength is higher than commercially available artificial cerebral spinal perfusion fluid from CMA which has an ionic strength of 155 mM.[187] Agglomeration of PNIPAM nanoparticles is induced with high ionic strength solutions and salt induced collapse of the polymer follows the Hofmeister series.[166, 188-190] As no agglomeration was seen in the PBS solution it is unlikely it will be observed in commercially available perfusion fluids used for microdialysis sampling.

Binding of lysozyme to the nanogels

Nanogel 400 and a nanogel with no cibacron blue incorporated into it (acting as a control) were washed into a PBS solution three times to a final concentration of 8 mg/mL nanogel. The nanogel solution was added to various concentrations of lysozyme in PBS at a 1:1 volume to volume ratio. This solution was incubated for 30 min at 21 °C. After incubation, the solutions were centrifuged at 17,000 RCF at 8 °C for 20 min, the supernatant was collected. This supernatant collected after protein capture is hereafter referred to as the capture supernatant. The

remaining pellet was washed two times with water and suspended to its initial volume in 2 M NaCl. The pellet suspension was incubated for 30 min at 21 °C, after which it was centrifuged and the supernatant collected. This supernatant collected after release is hereafter referred to as the release supernatant. Lysozyme was quantified in the initial solution, the capture supernatant and the release supernatant by a BCA assay. The amount of protein adsorbed (C_a) was determined by mass balance, subtracting the capture supernatant concentration (C_1) from the initial concentration (C_0) as seen in **Eq 3.1**. The percent of lysozyme released ($R_{\%}$) was determined by the ratio of lysozyme in the release solution (C_r) and C_a following **Eq 3.2**.

Eq 3.1 $$\boldsymbol{C_a = C_0 - C_1}$$

Eq 3.2 $$\boldsymbol{R_{\%} = \frac{C_r}{C_a} \times 100}$$

To test lysozyme capture over time, Nanogel 400 was washed into a PBS solution three times to a final concentration of 4 mg/mL nanogel. The nanogel solution was added to a 0.5 mg/mL lysozyme in PBS solution at a 1:1 volume to volume ratio. This solution was incubated for 30, 90, or 180 min at 21 °C. After incubation, the solutions were centrifuged at 17,000 RCF at 8 °C for 20 min, and the supernatant was collected. **Figure 3.3** displays the various steps used for protein binding and release experiments.

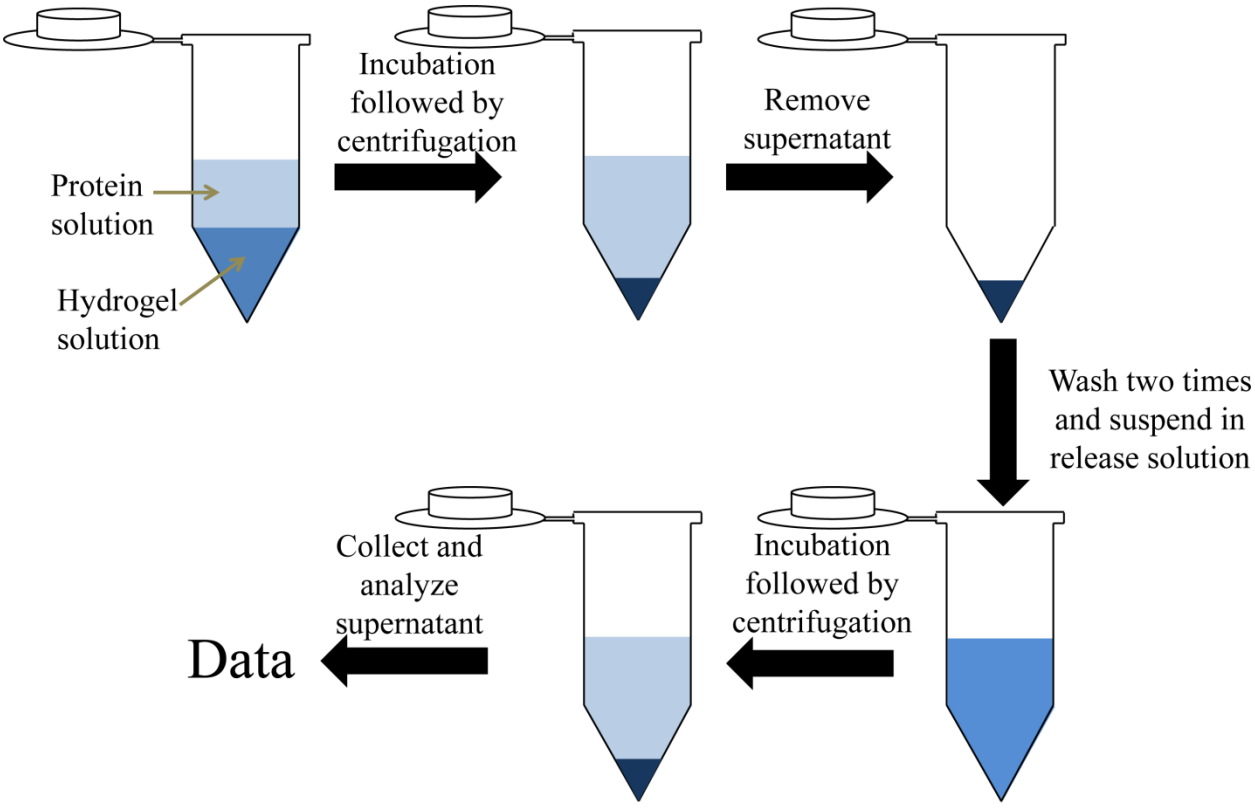

Figure 3.3 Flow diagram for protein capture/dissociation experiments.

BSA exclusion from the nanogels

Nanogel 400 and a control nanogel with no CB were washed into a PBS solution three times to a final concentration of 4 mg/mL. The nanogel solution was added to a 2 mg/mL BSA in PBS solution at a 1:1 (v/v) ratio. This solution was incubated for 30 min at 21 °C. After incubation, the solutions were centrifuged at 17,000 RCF at 8 °C for 20 min, the capture supernatant was collected. The remaining pellet was washed two times with water and suspended to its initial volume in 2 M NaCl. BSA was quantified in the initial solution, the capture supernatant and the release supernatant by the BCA assay. Additionally, a solution containing 2 mg/mL BSA or BSA and lysozyme was added 1:1 with Nanogel 400 or a control nanogel (2 mg/mL) to a final volume of 200 µL. After 30-min the solutions were centrifuged and the

supernatant discarded. The pelleted nanogel was washed two times with water. The concentrated pellet of 40 µL (a fivefold concentration) was then dispersed using a pipette. A SDS-PAGE running gel was made by pipetting 2.25 mL of 40% (w/v) acrylamide, 0.9 mL of a 1% (w/v) BIS, 1.25 mL 1.5 M tris(hydroxymethyl)aminomethane hydrochloride (TRIS) pH 8.5, 25 µL 20% (w/v) sodium dodecyl sulfate (SDS), 0.6 mL of water into a side arm flask. A vacuum was pulled for ~20 min to degas the solution. Polymerization was initiated by adding 25 µL tetramethylethylenediamine (TEMED) and 25 µL of 10% (w/v) ammonium persulfate (APS). The solution was mixed and pipetted into a Bio-Rad casting frame and allowed 45 min to set. The stacking gel was prepared by adding 150 µL of 40% (w/v) acrylamide, 200 µL of 1% BIS (w/v), 375 µL of 0.5 M TRIS pH 6.8, 7.5 µL of 20% (w/v) SDS and 750 µL of water. A vacuum was pulled for ~ 20 min after which, 15 µL of TEMED and 15 µL of 10% (w/v) APS was added. The solution was pipetted into the casting frame and allowed 45 min to set. To the stacking gel, 20 µL of the concentrated nanogel solution was added. The electrophoresis cell was filled with a solution containing 50 mM TRIS pH 8.5, 0.38 M glycine, 8 mM SDS. Electrophoresis was initiated using a mini-Protean from Bio-Rad (Hercules, CA) at 150 V for 90 min. The gel was removed and stained with Coomassie blue for 2 hr, and then destained with 40% (v/v) methanol, 10% (v/v) acetic acid for 1 hr.

Determination of the nanogel viscosity

Diffusion coefficients are inversely proportional to solution viscosity. To confirm that the 2 mg/mL concentration of Nanogel 400 does not significantly increase the viscosity of the perfusion fluid, Nanogel 400 was washed into PBS with 0.1% (w/v) BSA three times. A B89 Canon-Fenske viscometer from Cole-Parmer (Vernon Hills, IL) was calibrated using DI water at

21 °C. Three measurements were made to determine the viscosity of the PBS with 0.1% (w/v) BSA and the 2 mg/mL Nanogel 400 in PBS with 0.1% (w/v) BSA solution at 21 °C.

Results

Characterization of the nanogels

Two nanogel solutions of PNIPAM crosslinked with BIS containing AA in the core were initially synthesized in an identical fashion by free radical precipitation polymerization. Nanogel 1200 had a hydrodynamic diameter of 1240 ± 90 nm. While Nanogel 400 underwent additional centrifugation steps to remove large agglomerates after synthesis and had hydrodynamic diameter of 422 ± 6 nm. The amount of cibacron blue loaded into Nanogel 1200 and 400 was found to be 0.93 ± 0.03 mmol/g and 1.8 ± 0.3 mmol/g respectively, which is similar to that of Patanarut *et al.* which reported a loading of 0.74 to 1.74 mmol/g.[174] The difference in cibacron blue loading between the two groups is not unexpected, as the Nanogel 400 solution had fewer particles with which CB could be immobilized to (due to removal of large agglomerates prior to CB loading). The Nanogel 1200 solution had a total particle mass of 360 mg while Nanogel 400's total particle mass was 185 mg.

It should be noted that the temperature which the nanogels are centrifuged can induce irreversible agglomeration. When Nanogel 1200 was centrifuged at ambient temperature it would agglomerate irreversibly, as seen in **Figure 3.4**. The particles remained agglomerated despite repeated sonication and a two hr relaxation at 4-8 °C. Compaction of polymer chains tethered to a support by centrifugation is not always reversible, as multiple polymer bridges form particles between particles.[191] It is likely the temperature in the centrifuge exceeded the LCST of the polymer, and chains on adjacent particles collapsed together, irreversibly bridging particles.

However, this agglomeration was not studied further as centrifuging the particles at 8 °C did not initiate irreversible agglomeration.

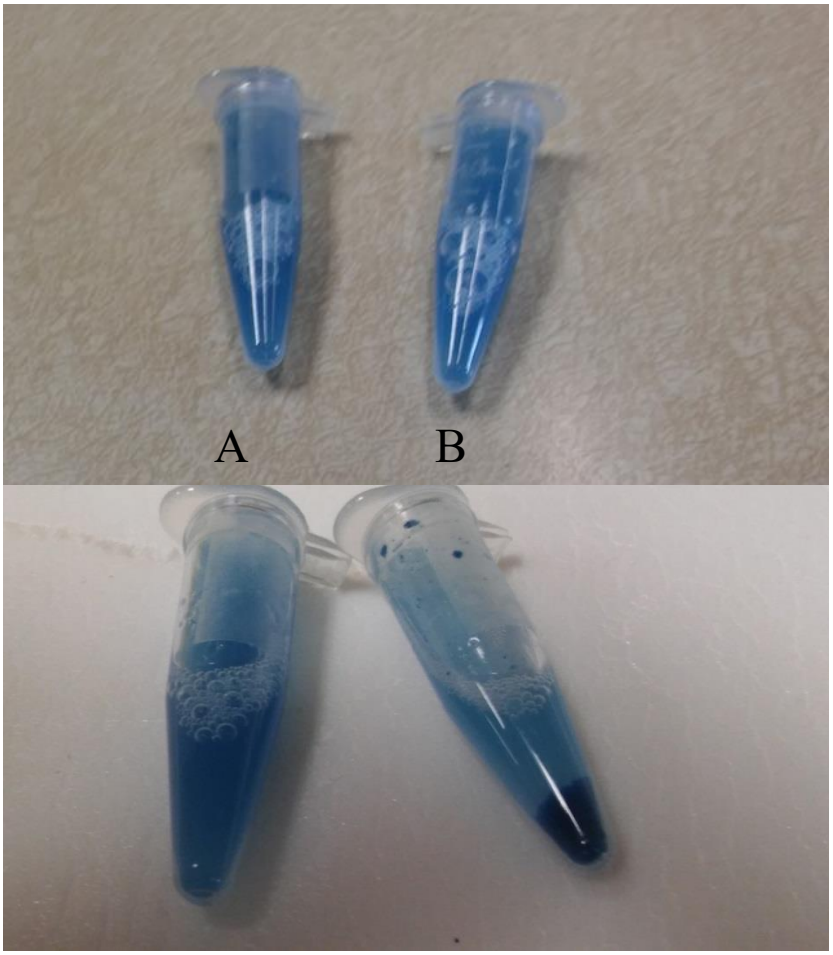

Figure 3.4 Nanogel 1200 centrifugation at 8 °C (A) and ambient temperature (B), before centrifugation (top) and after centrifugation followed by sonication (bottom).

Dispersions of Nanogel 400 were found to be completely stable for up to 8 hr in PBS containing 0.1% (w/v) BSA (no particle precipitation), while Nanogel 1200 precipitated as seen in **Figure 3.5**. After 8 hr at 21 °C, only 42.4 ± 9.8% of Nanogel 1200 remained suspended in solution. Generally, colloids are able to maintain a stable suspension in solution due to

gravitational forces being overcome by Brownian forces.[94] Stoke's law can be used to calculate the settling velocity of a particle.[95]

$$\boldsymbol{v} = \frac{\boldsymbol{d^2(\rho_2 - \rho_1)g}}{\boldsymbol{18\eta}} \qquad \text{Eq. 3.1}$$

Where v is the settling rate, d is the particle diameter, ρ_2 is the particle density, ρ_1 is the density of the solution, g is acceleration due to gravity, and η is the solution viscosity. Equation 3.1 displays that the increases in particle diameter, square the settling velocity. Additionally, the $\Delta\rho$ parameter inhibits usage of dense nanoparticles as 100 nm affinity agent immobilized iron oxide particles precipitate in a microdialysis syringe.[92]

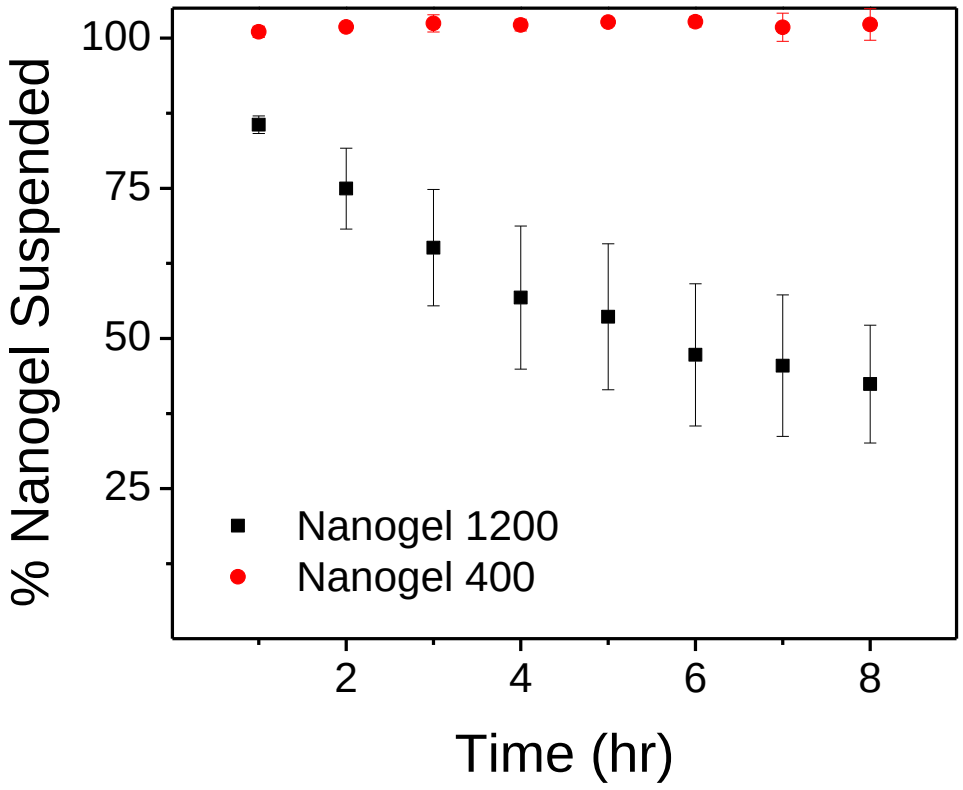

Figure 3.5 Nanogel suspension stability in PBS at 21°C. n= 3. Avg ± 1 S.D.

The Overbeek criterion concludes that particles with a predicted settling velocity less than 1 mm/24 hr will never settle as Brownian motion exceeds gravitational settling.[96] This emphasizes the desire to synthesize small, porous nanoparticles in order to obtain stable dispersions. Using the Overbeek criterion and the viscosity of water, the settling diameter of dense PNIPAM nanogels is 460 nm. However NIPAM-BIS hydrogels form core-shell particles where the shell is less dense than the core,[192] so the settling diameter for PNIPAM nanogels will be larger than this approximation.

Representative TEM images and corresponding size histograms of Nanogel 1200 and 400 are shown in **Figure 3.6** and **Figure 3.7**.

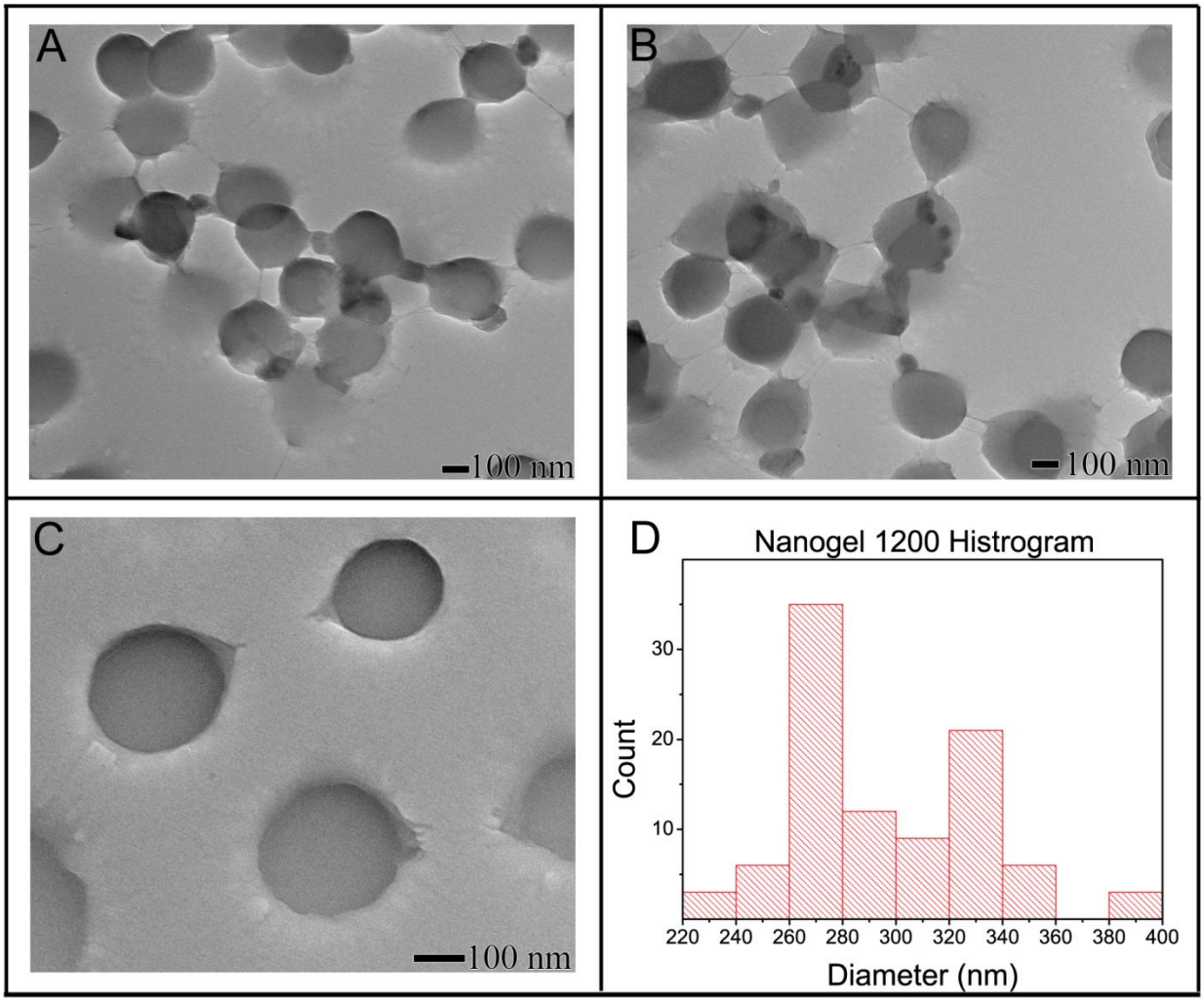

Figure 3.6 TEM images and size histogram for 100 particles of Nanogel 1200.

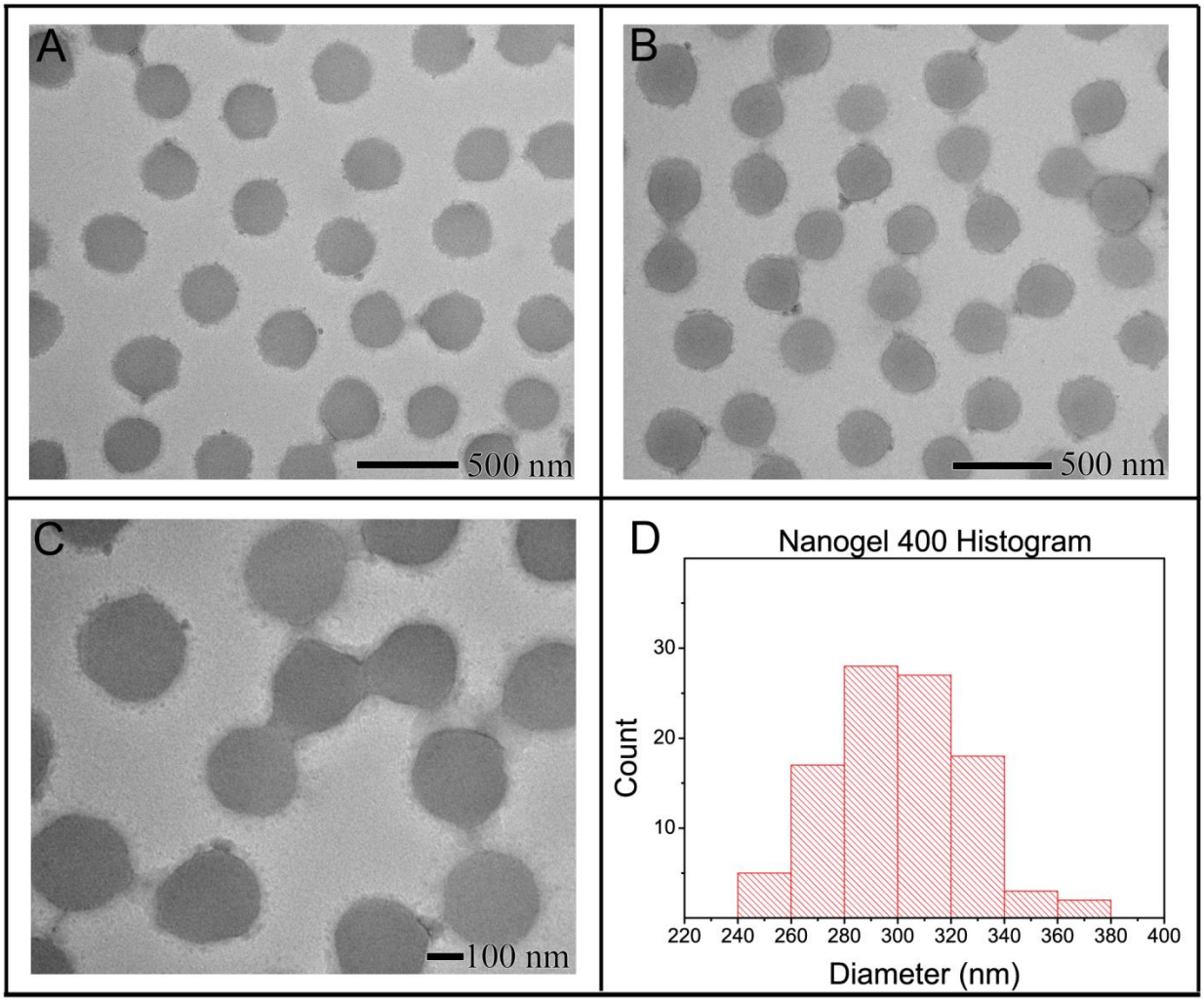

Figure 3.7 TEM images and size histogram for 100 particles of Nanogel 400

The diameters of the dense particle cores as measured by TEM were 297 ± 36 and 298 ± 26 nm for Nanogel 1200 and 400 respectively. Two different TEM's were used to image the particles. The light polymer halo surrounding the core was not included in the TEM size measurements due to poor contrast between the polymer and underlying grid. The TEM images reveal nanogels that are bridged together by polymer, forming aggregates. The degree of bridging appears greater in the Nanogel 1200 sample, owing to its lower dispersion stability. The high degree of particle bridging and extended polymer shell is why the hydrodynamic radius is of Nanogel 1200 is greater than that of Nanogel 400 despite the two particle groups having the same particle core size. Bridged particles accounted for 64% of the total particles in Nanogel 400, as seen in **Figure 3.8**. Nanogel 400 was chosen for further study with the objective to create microdialysis affinity agents that maintain a stable suspension for extended sampling times, as dispersions of it were stable for up to 8 hr.

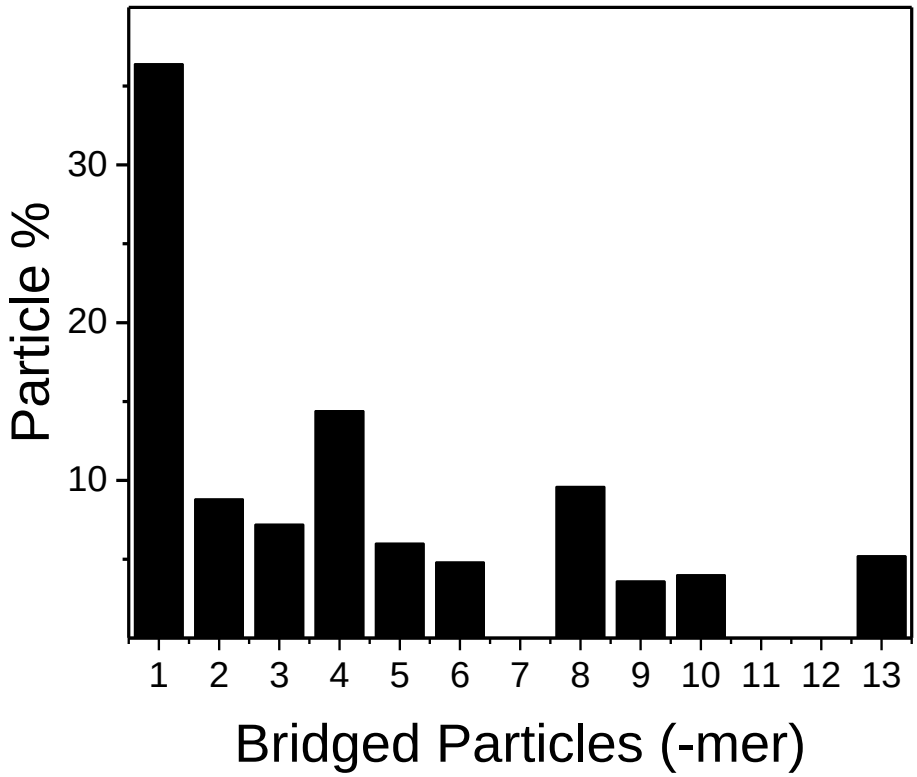

Figure 3.8 Number of particles in a cluster Nanogel 400. n=250 particles. Particles were analyzed using ImageJ with manual counting of bridged particles. Bridged particles are defined as particles with observable polymer contacting an adjacent particle.

Nanogel 400 was found to be stable for up to 3 months when stored at 4 °C. The D_h did not significantly change over three months, 422 ± 6 nm initially and 423 ± 12 nm after 3 months of storage. Additionally, no CB was found in the supernatant after 3 months of storage at 4 °C.

Thermal collapse of Nanogel 400 was found to occur over a broad temperature range from 24 °C to 36 °C as shown in **Figure 3.9**. The hydrodynamic diameter decreased from a maximum of 465± 14 nm at 16 °C to 261 ± 3 nm at 36 °C. The broad temperature collapse for PNIPAM nanogels has been observed and, is due to the dense particle core having fewer

interactions with water molecules. As there are fewer water molecules in the core its LCST is lower than the outer shell.[117, 193]

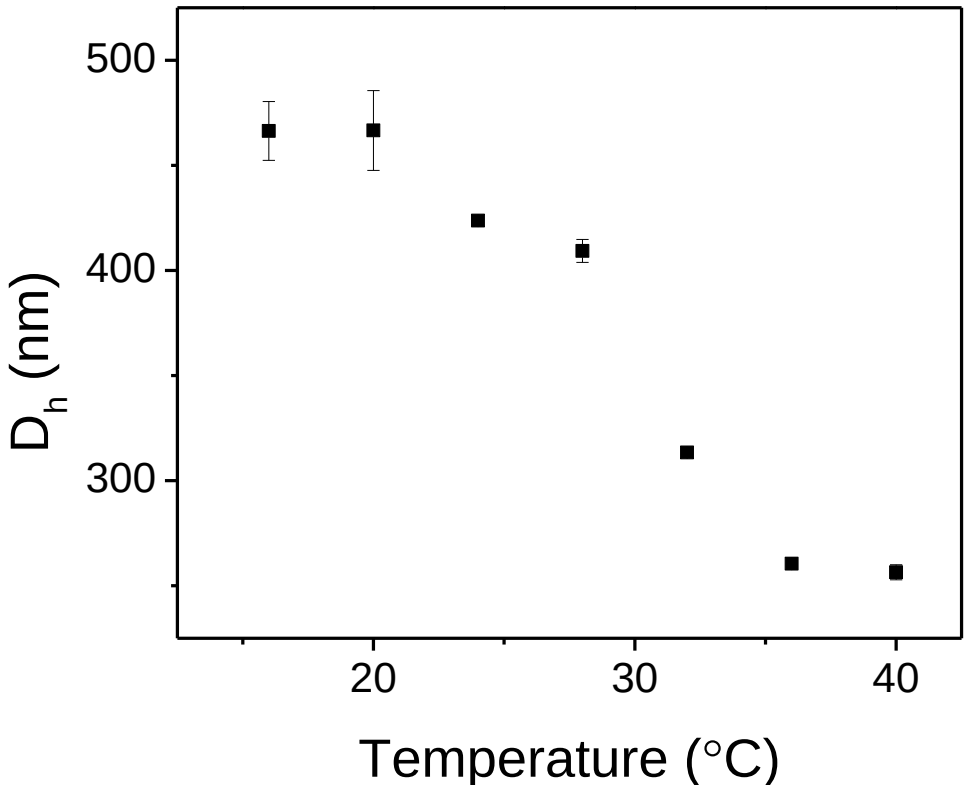

Figure 3.9 Hydrodynamic diameter of Nanogel 400 in water. Avg ± 1 S.D. n=5.

The thermal stability of the nanogels in PBS and PBS with 0.1% (w/v) BSA was studied and no agglomeration was observed at 37 °C, as see in **Figure 3.10**. The CMA 20 10 mm PES microdialysis probe has a 1.2 µL volume, meaning that the particles will not agglomerate in vivo at 37 °C in the probe at 1 µL/min, as the perfusion fluid will only be in contact with elevated temperatures for 72 s. The average hydrodynamic diameter after heating for 20 min at 37 °C was 305 ± 8 nm in PBS and 247 ± 12 in PBS with BSA. The smaller D_h observed in PBS with BSA versus in PBS without BSA is curious. One would expect protein adsorption onto the nanogel

which would yield an observable increase in D_h. DLS is commonly used to study adsorption of proteins onto the surface of nanoparticles by observing an increase in hydrodynamic diameter,[194-197] and has also been used to study temperature triggered protein adsorption onto thermoresponsive nanoparticles.[198] It is possible that BSA adsorbed to the outer polymer layer and prevented bridged particles from interacting. A 10 μM concentration of cetyl-trimethylammonium bromide, which is below its critical micelle concentration, have been show to adsorb to PNIPAM nanogels and prevent thermal agglomeration of PNIPAM nanogels.[199] Adsorption of BSA to gold nanoparticles has been shown to stabilize the nanoparticles by adding a combination of steric and electrostatic barriers in ionic solutions, even in a 200 mM ionic strength solution.[197] It is likely that BSA adsorbs to the PNIPAM nanogels and prevents the bridged particles from interacting in ionic solutions, as the 305 nm D_h in PBS is larger than that observed in water at 37 °C.

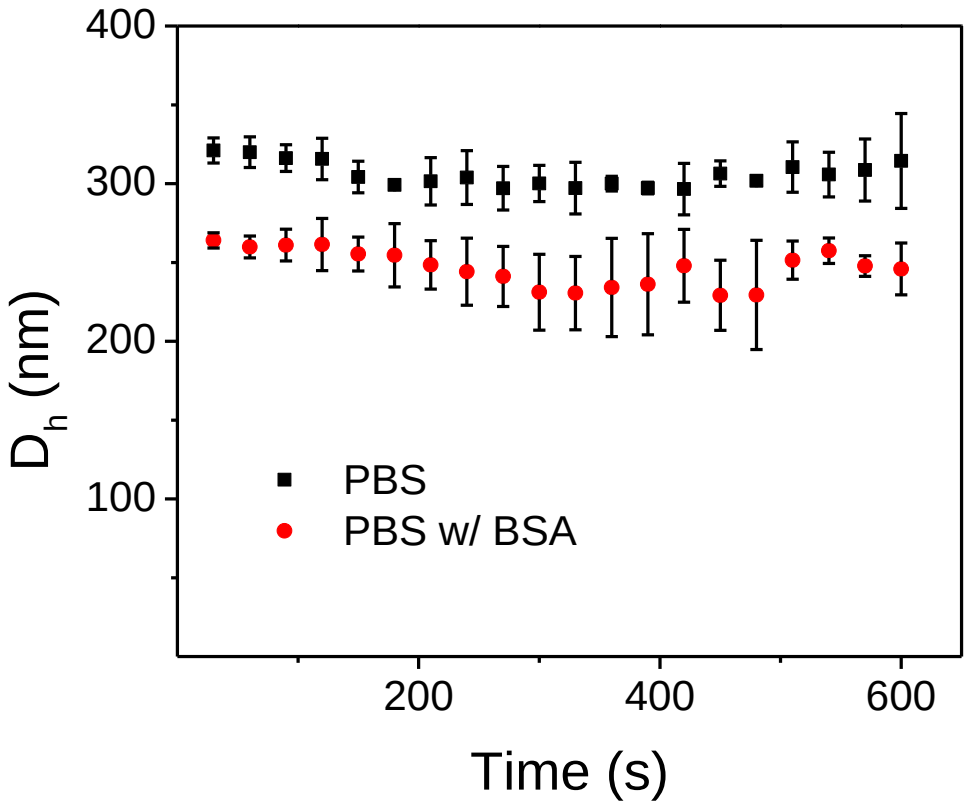

Figure 3.10 Nanogel 400 hydrodynamic diameter at 37 °C in PBS supplemented with or without BSA. n=3. Avg ± 1 S.D. Samples were heated for 10 min at 37 °C before measurements were taken.

Binding of lysozyme to the nanogels

The ability for the nanogels to bind lysozyme was dependent on the inclusion of CB, as nanogels without CB displayed poor lysozyme binding as seen in **Figure 3.11**. The nanogels containing CB adsorbed 79.5 ± 7.1 mg/g lysozyme in 30 min at room temperature in PBS, compared to 9.7 ± 2.6 mg/g for nanogels without CB. This capture amount is similar to crosslinked nanogels containing CB from another study which reported 80 mg/g lysozyme capture with a CB immobilization of 3-5 μg/g.[200]

A low affinity between CB and lysozyme was observed in PBS with 42.0 ± 0.8% of lysozyme captured over 30 min as seen in **Figure 3.12**, possibly due to the high ionic strength reducing the strength of electrostatic interactions. The Debye length in a 150 mM NaCl solution is 0.55 nm. No significant increase in lysozyme binding occurred with increasing incubation time, up to 180 min, $p>0.05$ as determined by a one-way ANOVA. This indicates equilibrium binding for dilute lysozyme concentrations (0.25 mg/mL) is achieved within 30 min.

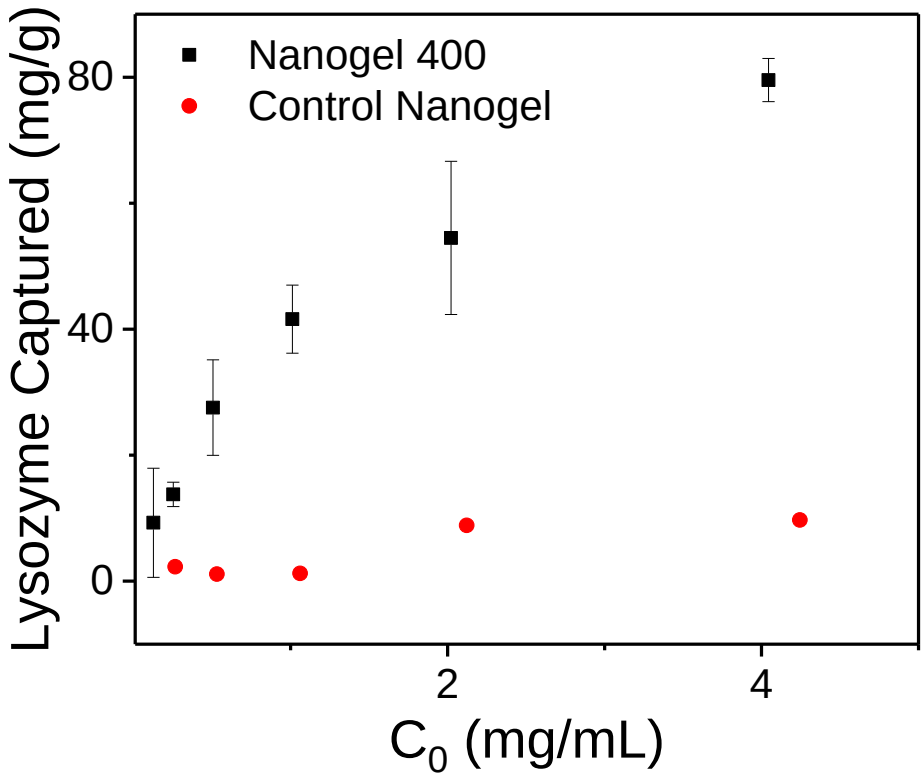

Figure 3.11 Lysozyme captured by Nanogel 400 and a control nanogel in PBS over 30 min. n= 3. Avg ± 1 S.D. C_o is the initial protein concnetation.

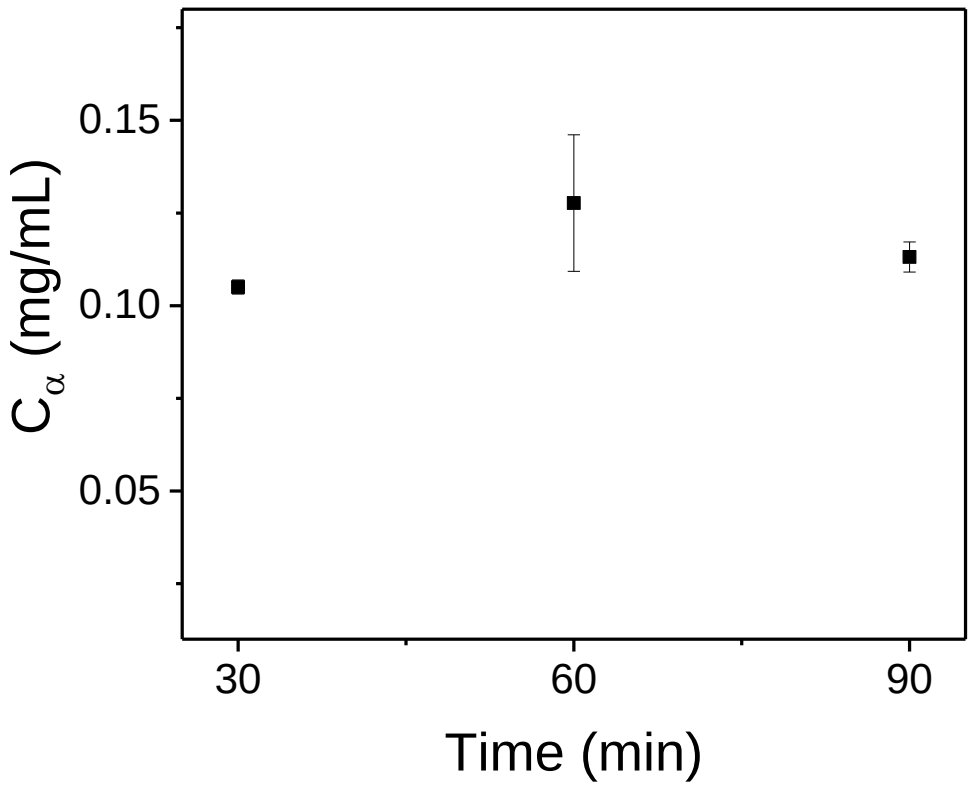

Figure 3.12 Lysozyme captured by Nanogel 400 with an initial protein concentration of 0.25 mg/mL in PBS. n= 3. Avg ± 1 S.D.

When 0.6 mg/mL of lysozyme was captured with Nanogel 400, only 57.4 ± 4.2% was released with a single release cycle using 2 M NaCl as seen in **Figure 3.13**. This hindered dissociation of a relatively high concentration of lysozyme in a high salt solution is not wholly unexpected, as lysozyme expresses reduced solubility with increasing NaCl concentration.[201] At pH 4.5, where lysozyme displays the highest solubility, its solubility is below 1 mg/mL in 2 M NaCl.[202] The 2 M NaCl release solution was chosen as it has previously been shown that lysozyme-CB interaction is weakened with high ionic strength,[203, 204] and that the predominant interaction between proteins and CB is between positively charged amino acids and the sulfonate group on CB. However, there is also hydrophobic interactions between CB and a variety of

proteins with importance placed on location of the aromatic rings relative to the sulfonate groups.[205] The addition of a second 30 min release cycle of 2 M NaCl increased the cumulative release of lysozyme to 81.3 ± 4.8%, while increasing the release time to 90 min increased the release percent to 74.6 ± 3.8%. No CB was detected in the supernatant after incubating Nanogel 400 with 2 M NaCl, confirming no CB dissociation occurs from the nanogels under this condition.

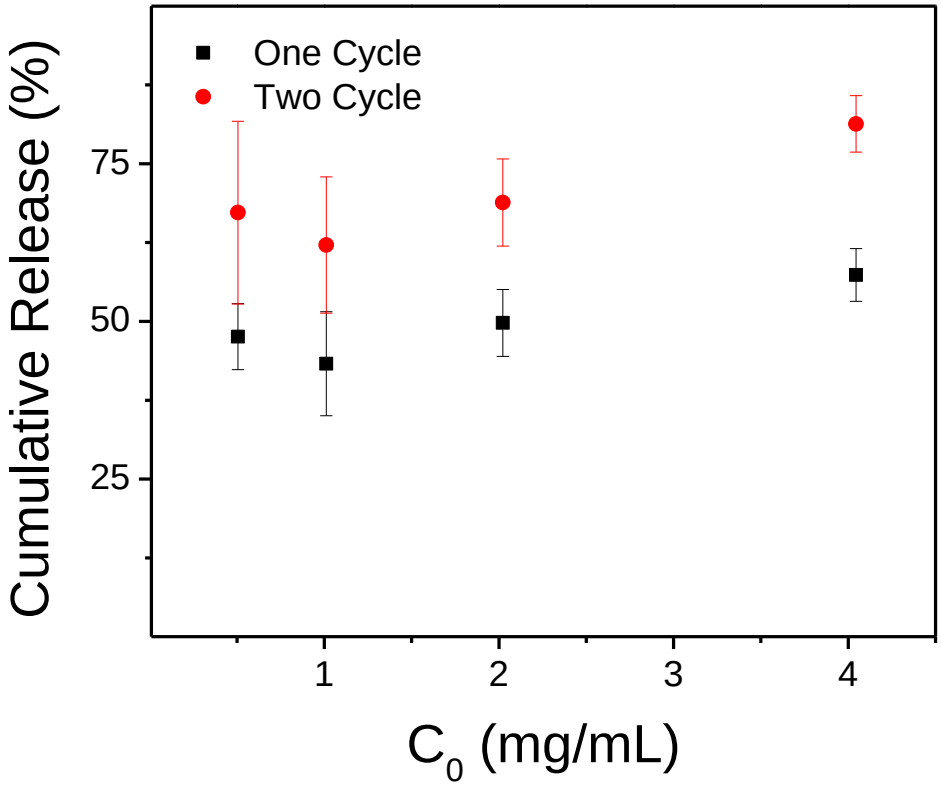

Figure 3.13 Lysozyme released from Nanogel 400 with repeated release cycles of 2 M NaCl for 30 min at room temperature. n= 3. Avg ± 1 S.D.

BSA exclusion from the nanogels

BSA is commonly added to microdialysis perfusion fluid at concentrations of 0.25 to 3.5 mg/mL to enhance the recovery of lipophilic compounds,[206, 207] neuropeptides,[208] and proteins.[73, 209] BSA has been shown to reduce nonspecific adsorption.[73] However BSA is known to bind CB with and K_D of 2.2 μM and CB is routinely used for albumin depletion.[210-213] The BSA-CB interaction must be restricted if Nanogel 400 is to be included in microdialysis perfusion fluid containing BSA to prevent the high concentration of BSA from saturating CB binding sites. Core-shell PNIPAM nanogels have previously shown that the addition of the crosslinked shell can restrict diffusion of large proteins (albumin) into the core of the nanogel, while still allowing diffusion of small proteins such as cytokines.[174, 214, 215] This restricted diffusion of large proteins into the nanogel is similar to restricted access media which prevents proteins from interacting from packing material by size exclusion in solid phase extraction and HPLC. [216, 217]

BSA showed little/no binding to Nanogel 400,the concentration of BSA in the supernatant of Nanogel 400 was found to be 92.5±10.0% of the initial 1 mg/mL concentration, n=2 independent experiments with three separate samples in each experiment measured in duplicate. BSA was not detected in release supernatants. This implies that BSA's interaction with the CB is hindered by the outer polymer layer which does not contain CB.

Figure 3.14 displays a SDS-PAGE result in which BSA adsorbed onto a control nanogel with no CB bound, while both lysozyme and BSA were captured by Nanogel 400. Confirming BSA adsorbs nonspecifically to the outer PNIPAM shell, and lysozyme capture is due to the immobilized CB. It is interesting that the protein band for BSA in lane D (Nanogel 400 and BSA) appears thinner than the BSA band for Lane C and E, control nanogel plus BSA and Nanogel 400 plus lysozyme and BSA. This is likely due to charge repulsion from the sulfonate

groups in CB which have been shown to hinder BSA diffusion at low ionic strength and/or high CB densities.[213, 218] **Figure 3.15** displays lysozyme capture and release to/from CB in the interior of the nanogel, while BSA is excluded from the CB.

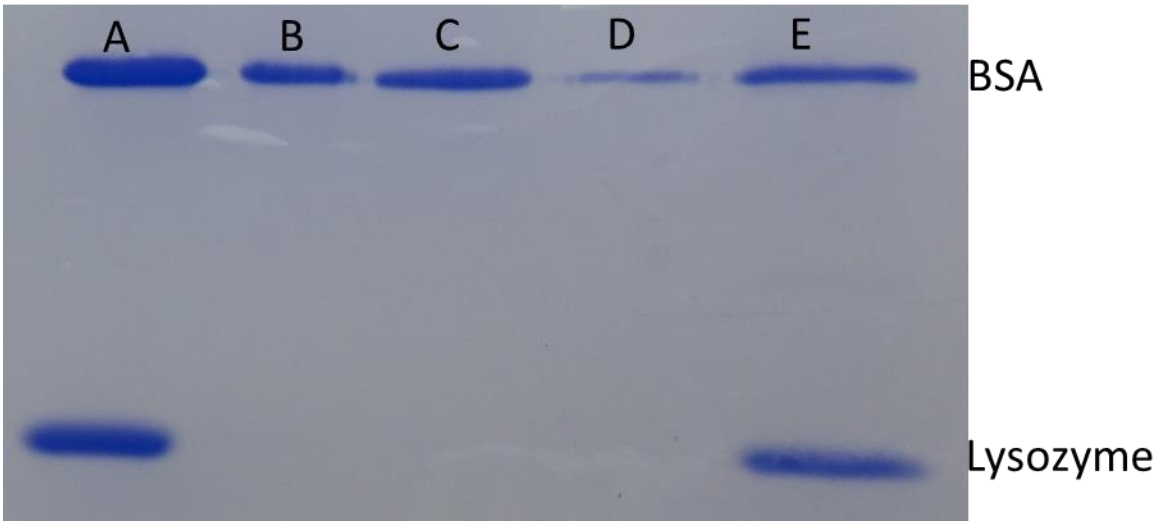

Figure 3.14 SDS-PAGE of BSA and Lysozyme eluted from nanogels. A) 1 mg/mL BSA and Lysozyme in water, B) control nanogel incubated with BSA, C) control nanogel incubated with BSA and Lysozyme, D) Nanogel 400 incubated with BSA, E) Nanogel 400 incubated with BSA and Lysozyme.

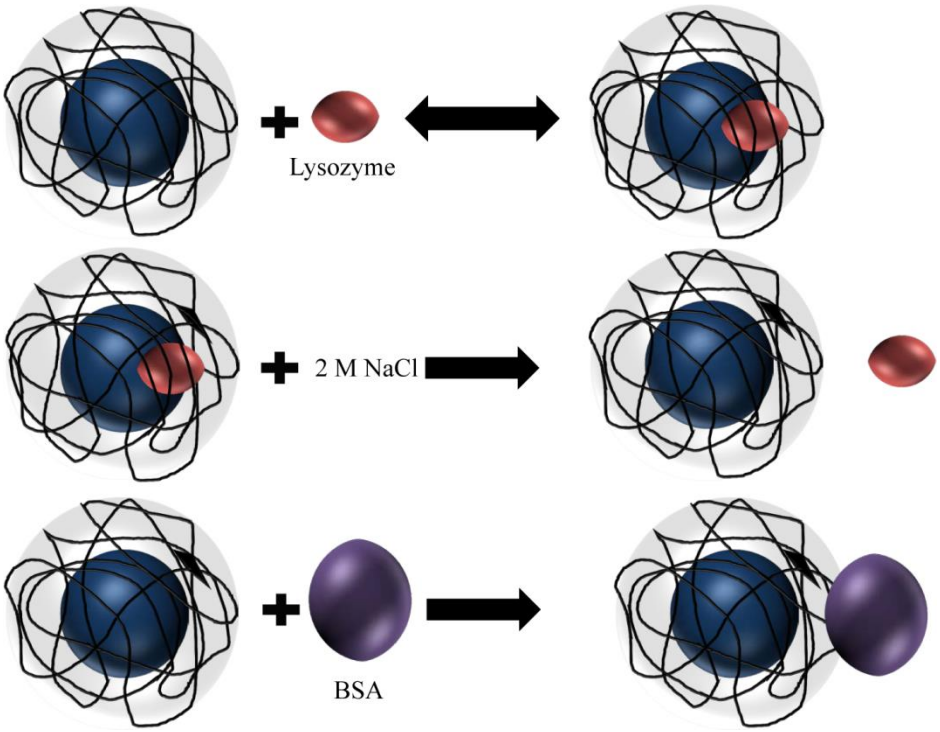

Figure 3.15 Size dependent capture/dissociation to Nanogel 400. CB is immobilized on the interior of the nanogel. The soft porous shell hinders large protein from binding the CB.

CB has affinity for a wide variety of proteins,[184, 219, 220] so a suitable concentration of nanogel must be selected which will be able to capture all protein in the dialysates. For future protein binding experiments a 2 mg/mL nanogel concentration was chosen. This concentration was chosen as it would allow for the capture of 160 µg/mL of protein in dialysates. The total protein content collected from injured human frontal lobe at 0.3 µL/min using a 20 mm membrane length, 100 kDa MWCO probe has been reported to range from 50 to 1520 µg/mL with an average of 234 ± 21 µg/mL.[221] When a 10 mm 100 kDa MWCO probe was perfused at 0.3 µL/min through human subcutaneous tissue, the total protein content ranges from ~2000 to 100 µg/mL with an average of ~500 µg/mL.[222] It should be noted that microdialysis probes used for humans are typically perfused at low flow rates. Both low flow rates and increasing membrane length increase the perfusates residence time with the membrane, thereby increasing

recovery. Additionally the total protein content measured in dialysate from human skin collected at 3 µL/min with a 300 kDa MWCO probe is reported to be ~60-80% albumin.[223] The 2 mg/mL concentration should be sufficient to capture all small protein collected in animal dialysates, as larger albumin is hindered from the CB binding site. However, this will need to be tested in vivo by varying the particle concentration and confirming that saturation of the nanogels is not reached.

Viscosity of the nanogels

The viscosity of the PBS with 0.1% (w/v) BSA was found to be $9.36 \pm 0.008 \times 10^{-4}$ Pa × s while the with the 2 mg/mL Nanogel 400 in the same solution was found to be $9.40 \pm 0.008 \times 10^{-4}$ Pa × s. No significant difference in viscosity was found between the two perfusion fluids, meaning no significant reduction in analyte diffusion coefficient is expected.

Summary

A nanogel solution with CB immobilized to the nanogel was synthesized. The nanogel dispersion was stable for up to 8 hr in an ionic solution with no agitation. The nanogels did not agglomerate in solutions mimicking microdialysis perfusion fluids after 20 min at 37 °C. By selectively loading the CB into the interior of the nanogel, the BSA-CB interaction was prevented. Nonspecific BSA adsorption occurred to the exterior of the nanogel, while lysozyme capture was due to CB immobilization to the nanogel. Adsorbed lysozyme was released from the nanogel, reaching a cumulative release of 81.3 ± 4.8% with two cycles of 2 M NaCl. The nanogels were found to be stable over a three-month storage period. These preliminary data suggest that nanogels may serve as a novel support platform with which to explore as microdialysis affinity agents.

Chapter 4 Water dispersible affinity nanogels enhance microdialysis protein relative recovery

Introduction

In this chapter, the nanogels synthesized in chapter three are studied as affinity agents for microdialysis sampling. The perfusion of the nanogels through a microdialysis system was studied, and compared to previously used affinity agent support material. The recovery of the nanogels was optimized with the use of a syringe push and peristaltic pump. The binding between nanogels and two rat cytokines, CCL2 a 13.1 kDa protein and KC/GRO a 7.8 kDa protein was studied. These two cytokines were initially studied as the mouse and human analog have been shown to have high affinity for CB, and the rat cytokines have been recovered in vivo using microdialysis probes.[47, 182] Various dissociation buffers and temperatures were screened to optimize protein dissociation from the nanogels. Finally, nanogels were included in perfusion fluid, and their effect on RR for CCL2 and KC/GRO studied.

Experimental

Reagents

Monosodium phosphate, disodium phosphate, sodium chloride, sodium azide, potassium persulfate (KPS), NIPAM, and fluorescein isothiocyanate dextran with an average molecular weight of 10 kDa (FITC-dextran 10) were purchased from Sigma (St. Louis). Cibacron blue 3G-A was purchased from Abcam (St. Louis). Allylamine (AA) and N,N methylenebisacrylamide (BIS) were purchased from Alfa Aesar (Haverhill, MA). HPLC grade water was used for all experiments and was purchased from Thermo Fisher Scientific (Waltham, MA). Bovine serum albumin (BSA) fraction V was purchased from Rockland (Limerick, PA). Phosphate buffered

saline (PBS) solution consisted of 147 mM sodium chloride, 4.7 mM disodium phosphate, 7.3 mM monosodium phosphate, pH adjusted to 7.2 with sodium hydroxide. MagPlex 5.6 μm carboxyl functionalized microspheres were purchased from Luminex (Austin, TX). Rat CCL2 ELISA kit was purchased from BD Biosciences (San Jose, CA). Rat KC/GRO ELISA kit was purchased from R&D Systems (Minneapolis, MN).

Recovery of Nanogel 400 and microspheres through a microdialysis probe

Nanogel 400 or microspheres were washed into a PBS with 0.1% (w/v) BSA three times to a final concentration of 2 mg/mL or 1×10^6 beads/mL. The syringe containing microspheres was placed in a BASi syringe pump which was attached to an in house custom rotator to agitate the microsphere suspension (10 rotations/min). The syringe containing the nanogels was placed in a syringe pump on top of the SFC Fluidics push/pull pump. A CMA 20 from Harvard Apparatus (Holliston, MA) with a 10 mm PES 100 kDa MWCO membrane was placed in water and connected to the syringe containing the particles. To account for dead volume in the system, two flushes were discarded before collections were made at each position. A 10-min flush at 3 μL/min was performed and followed by another flush at 1 μL/min for 30 min. Following flushes, collections were made at 1 μL/min with three collections made at each position (15 μL/collection). Collections were made at positions depicted in **Figure 4.1**. A newly dispersed solution was prepared and placed in the syringe when changing sampling positions. This was done to prevent possible particle settling from biasing results during extended sampling. When sampling from position 4 with microspheres, the outlet was connected to dialysate collection unit one, a push/pull peristaltic pump from SFC Fluidics (Fayetteville, AR) or a MAB 20 peristaltic pump from SciPro (San Francisco, CA). Particle recovery was determined relative to the concentrations in the syringes. Microspheres were quantified using a hemocytometer, while

nanogels were quantified by measuring the absorbance of the solutions at 610 nm using a Nanodrop 200c from Thermo Fisher Scientific (Waltham, MA).

Particle recovery during extended sampling times was studied using a CMA 20 10 mm PES 100 kDa MWCO probe and a flush procedure as previously described. Following the flush collections were made at 1 µL/min every 60 min, for 5 hrs using the syringe rotator for the microspheres or the SFC Fluidic push/pull pump for Nanogel 400, as these were found to give the highest particle recovery for the microspheres and Nanogel 400.

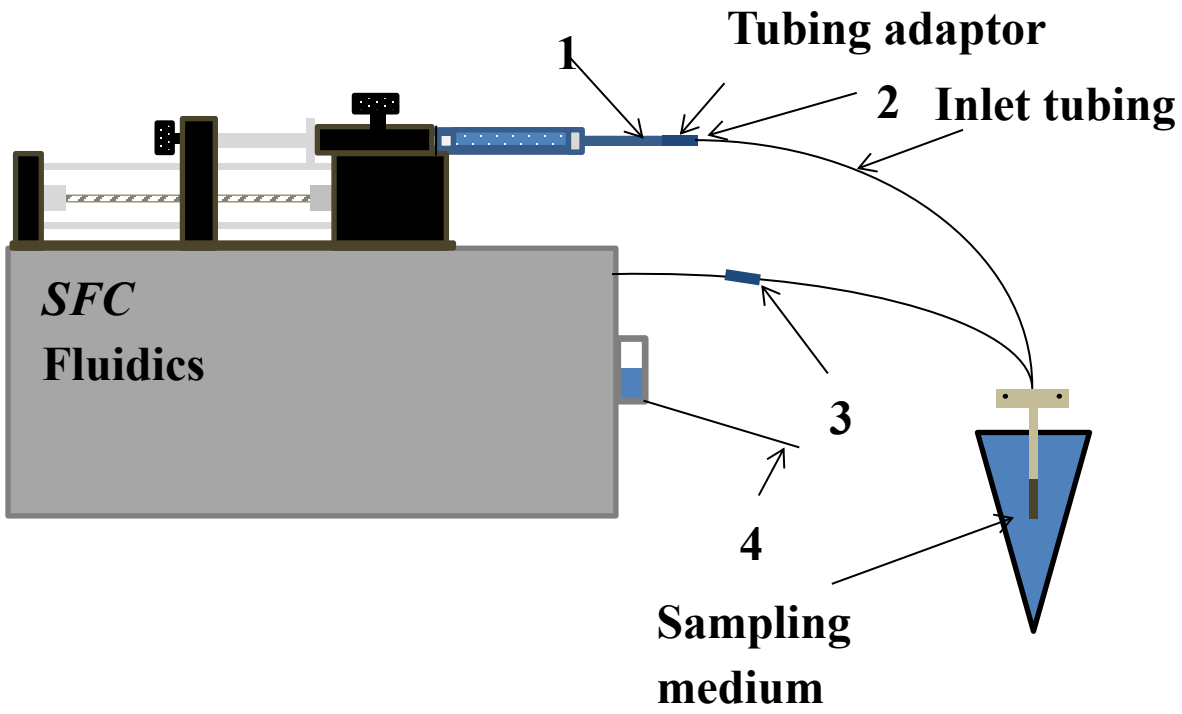

Figure 4.1 Particle recovery was determined at the syringe outlet (1), at the tubing adaptor (2), at the probe outlet (3), and at the peristaltic pump outlet (4).

Protein binding to Nanogel 400

Initial experiments were conducted to confirm CCL2 binding to Nanogel 400, and confirm the binding is not inhibited by BSA, which is added to microdialysis perfusion fluid to act as a blocking agent. A 4 ng/mL CCL2 (standards from the ELISA kit) in PBS with 0.1% (w/v) BSA and without BSA was added 1:1 (v/v) with 4 mg/mL of Nanogel 400 in a protein LoBind centrifuge tube from Eppendorf. The solutions were incubated for 30 min at room temperature, after which the solutions were centrifuged and the supernatant collected. The amount of CCL2 captured was determined by mass balance.

Confirmation that protein binding was due to the immobilization of CB to the nanogel was performed by adding 4 ng/mL CCL2 in PBS with 0.1% (w/v) BSA was added 1:1 to PBS with 0.1% (w/v) BSA, a control nanogel with no CB immobilized, or Nanogel 400. The solutions were incubated for 30 min at room temperature, after which the solutions were centrifuged and the supernatant collected. The amount of CCL2 captured was determined by mass balance. Confirmation of KC/GRO binding to Nanogel 400 was performed in the same fashion, using a 2 ng/mL KC/GRO concentration.

To test for CCL2 saturation of the nanogels, solutions of CCL2 ranging from 10 ng/mL to 250 pg/mL in PBS with 0.1% (w/v) BSA were mixed 1:1 (v/v) with a 4 mg/mL solution of Nanogel 400 in PBS with 0.1% (w/v) BSA. The solutions were incubated for 30 min at room temperatures, after which they were centrifuged at 17,000 RCF at 8 °C for 20 min, the capture supernatant was collected and the amount of CCL2 captured was determined by mass balance. To obtain a K_D value for the CB -protein interaction a 4 ng/mL CCL2 or 2 ng/mL KC/GRO in PBS with 0.1% (w/v) BSA was added 1:1 (v/v) with concentrations of Nanogel 400 from 8 mg/mL to 400 ng/mL in PBS with 0.1% (w/v) BSA and incubated at room temperature for 30

min. After incubation, the solutions were centrifuged and the supernatant collected. The amount of CCL2 captured was determined by mass balance. The K_D was determined at 50% free ligand using a Klotz plot.[224]

Protein dissociation from Nanogel 400

Nanogel 400 was washed into PBS with 0.1% (w/v) BSA three times to a final concentration of 4 mg/mL. A 4 ng/mL CCL2 or 2 ng/mL KC/GRO solution in PBS with 0.1% (w/v) BSA was added 1:1 to Nanogel 400. The mixed solutions were incubated at room temperature for 30 min, after which the solutions were centrifuged at 17,000 RCF at 8 °C for 20 min, the capture supernatant and an aliquot of the initial protein solution were collected and stored at -20 °C for no more than three days. The nanogel-protein pellet was washed two times with water, and suspended in a release solution for up to twelve hr. The released protein was detected via an ELISA, and the percent dissociated determined by mass balance.

In vitro microdialysis sampling

The push/pull syringe/peristaltic pump used for Nanogel 400 perfusion was a prototype provided by SFC Fluidics. Verification that steady state conditions were reached using the SFC Fluidics push/pull pump, a 30 μM FITC-dextran 10 solution in PBS was sampled. A CMA 20 with a 10 mm PES 100 kDa MWCO membrane was connected to the SFC Fluidics push/pull pump. A 20-min flush at 3 μL/min was performed, after which collections were made at 1 μL/min, 60 min/collection for 5 hr. An aliquot of the FITC-dextran sampling medium was taken to create standards. The RR of the dialysates was determined by measuring the absorbance of the solutions and standards at 495 nm using a Nanodrop 200c from Thermo Fisher Scientific. The

dead volume of the microdialysis probe and SFC Fluidics push/pull pump was estimated by measuring the time it took for FITC-dextran 10 to be detected in the dialysate.

In vitro microdialysis sampling was performed at room temperature, from a 10 ng/mL CCL2 solution in PBS with 0.1% BSA. A CMA 20, 10 mm PES 100 kDa MWCO probe was perfused using PBS with 0.1% (w/v) BSA supplemented with or without Nanogel 400 at 2 mg/mL. Flow was initiated at 3 µL/min for 20 min, followed by 60 min at 1 µL/min. Both samples were not analyzed, as previous FITC-dextran 10 sampling experiments displayed steady recovery occurred after these collections. Then four collections were made at 1 µL/min with 60 min/collection. An aliquot of the sampling medium was taken before sampling, in the middle of sampling and after sampling. The average CCL2 concentration of these aliquots was used to determine protein RR. After collection, dialysates without nanogels were stored at -20 °C until analysis, which was performed within two days. Collections made with nanogels were washed twice with water and suspended in 2 M NaCl, 10 mM NaH_2PO_4 pH 7 and left to dissociate at 37 °C for 12 hr. Released samples were centrifuged, the supernatant collected and stored at -20 °C until analysis, which was performed within 24 hr. Samples were measured using a reduced volume ELISA (50 µL) for both sample and standards.

Results

Recovery of Nanogel 400 and microspheres through a microdialysis probe

Immobilizing affinity ligands to support materials can lead to affinity agent settling. This is due to the size of the support material and its density. Affinity agent precipitation complicates continuous sampling. As the affinity agent precipitates, its concentration in the syringe will decrease, allowing for unpredicted saturation of protein binding sites to the affinity agents as

their suspended concertation decrease over time. Saturation of the protein binding sites on the particle will reduce the RR enhancements observed. It is not uncommon for microdialysis to be applied for lengthy sampling periods up to 12 or 24 hr.[60, 74, 225] In order to reduce affinity agent precipitation during continuous perfusion, the Stenken and Li group have used syringe rotators which agitate the solution during sampling.[92, 93] However, particle recovery over time was not studied in these previous works. In this work, the recovery of 5.5 μm polystyrene microspheres over 5 hr was compared to that of Nanogel 400. The microspheres used were identical to those used for previous affinity agent immobilization.[93] No microspheres were found in dialysate when they were perfused at 1×10^6 beads/mL using a push syringe pump, while Nanogel 400 had a particle recovery of 87.6 ± 3.5 %, as seen in **Figure 4.2**. The high recovery of Nanogel 400 without the use of instrumentation that agitates the particles is an advantage over microsphere supports.

The particle recovery was studied at various positions in the microdialysis system, as denoted in **Figure 4.1**. The loss of Nanogel 400 occurred at the syringe tip when using a syringe pump as seen in **Table 4.1**. Particle loss at the syringe tip agrees with a previous particle perfusion study.[93] When a push/peristaltic pull system was employed, 100% of the nanogels could be collected at a1 μL/min flow rate. Microspheres were unable to be collected using a push/pull system. Microsphere adsorption to small inner diameter tubing has been reported, and their loss during the contraction of tubing using a peristaltic pump is expected.[226] Particle concentration is modeled to be highest at the walls of the compressed peristaltic tubing.[227-229] The particle concentration is highest in the middle of the tubing where the flow rate is faster than at the walls. Compression of the tubing shifts the tubing wall boundaries while the particle concentration positions unperturbed for short compression time scales. Microsphere recovery

was reestablished by disconnecting the peristaltic pump, indicating it as the source for particle loss either due to adsorption or restriction of passage in the compressed tubing. A different peristaltic pump (MAB 20 from SciPro) was also tested for microsphere recovery, and no particles were recovered using either peristaltic pump.

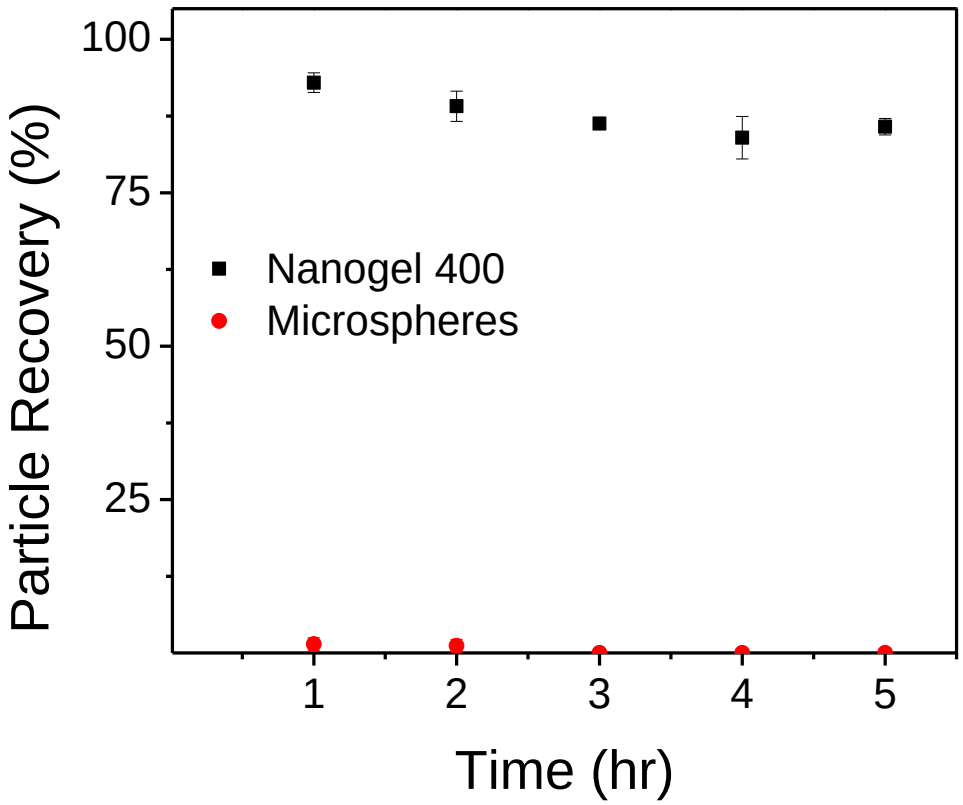

Figure 4.2 Particle recovery at 1 µL/min flow rate using PBS sampled from position 3. Avg ± 1 S.D., n=3.

Table 4.1 Particle recovery at various sampling positions at 1 µL/min flow rate.

Position Number	Nanogel Recovery (%)	Microsphere Recovery (%)	Fluid Drive Mechanism
1	85.5 ± 3.9	69.4 ± 8.9	Push
2	79.1 ± 5.5	80.7 ± 5.3	Push
3	84.7 ± 5.3	66.0 ± 2.2	Push
4	99.8 ± 2.9*	ND	Push/Pull

* Indicates significant difference from the other positions in column, $p<0.05$ as determined by a one-way ANOVA with Tukey HSD post hoc test, ND indicates no recovery observed, avg ± 1 S.D., n=3

The addition of a syringe rotator hinders particle settling; however, in this work microsphere settling was observed during extended sampling using a syringe rotator, as seen in **Figure 4.3**. The microsphere recovery decreased from 65% to 35% over 3 hr despite using a syringe rotator. Interestingly the particle recovery for hours 3-5 remained constant. This may be due to particle precipitation occurring at the walls of the syringe, while the particles in the center of the syringe maintained suspension over the time studied. The maximum diameter for a stable polystyrene microsphere suspension is 720 nm; further increases in particle diameter hasten particle settling. Nanogel 400 was found to have a consistent particle recovery that did not decrease over time with the use of a syringe push and peristaltic pull pump. The average particle recovery for Nanogel 400 using push/pull perfusion at 1 µL/min for 8 hr was 100.1 ± 1.7 %.

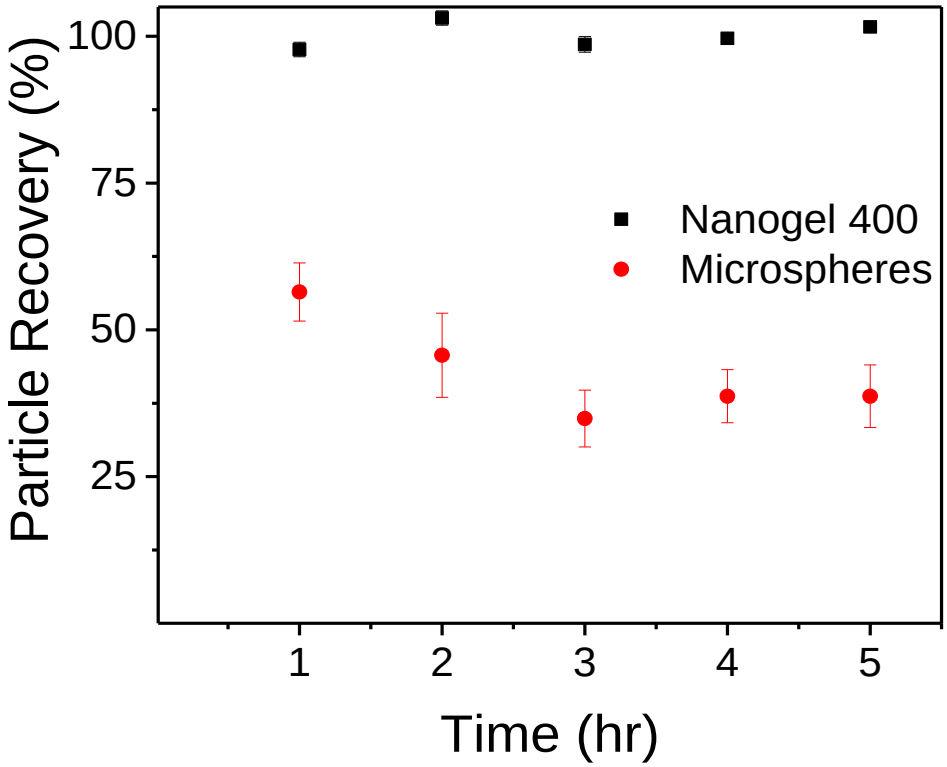

Figure 4.3 Particle recovery at 1 µL/min flow rate in PBS using optimized sampling conditions. Samples taken from position 3 for microspheres or 4 for Nanogel 400. Microspheres were perfused using a syringe rotator, while Nanogels were perfused using a push/peristaltic pull pump. Avg ± 1 S.D., n=3.

Protein binding to Nanogel 400

BSA is commonly included in microdialysis perfusion fluid to act as a blocking agent. BSA has an affinity for a wide range of proteins and acts as a carrier protein for small molecules, and was found to nonspecifically bind to Nanogel 400 in chapter 3.[230, 231] However, inclusion of BSA in PBS did not inhibit the binding between CCL2 and Nanogel 400, as 95.1 ± 0.3% of a 2 ng/mL CCL2 solution was captured in the absence of BSA and 95.1 ± 1.0 % of CCL2 was captured in the presence of BSA.

The ability for CCL2 to bind the nanogel was due to the immobilization of CB. After a 30-min incubation with 5 ng/mL CCL 4810 ± 360 pg/mL CCL2 remained in a control centrifuge tube with no nanogel, 4445 ± 205 pg/mL remained in the supernatant with a control nanogel (with no CB immobilized), while 1015 ± 370 pg/mL CCL2 remained uncaptured when Nanogel 400 was used as seen in **Figure 4.4**. The K_D for CB and CCL2 was estimated to be 110 μM as seen in **Figure 4.5**.

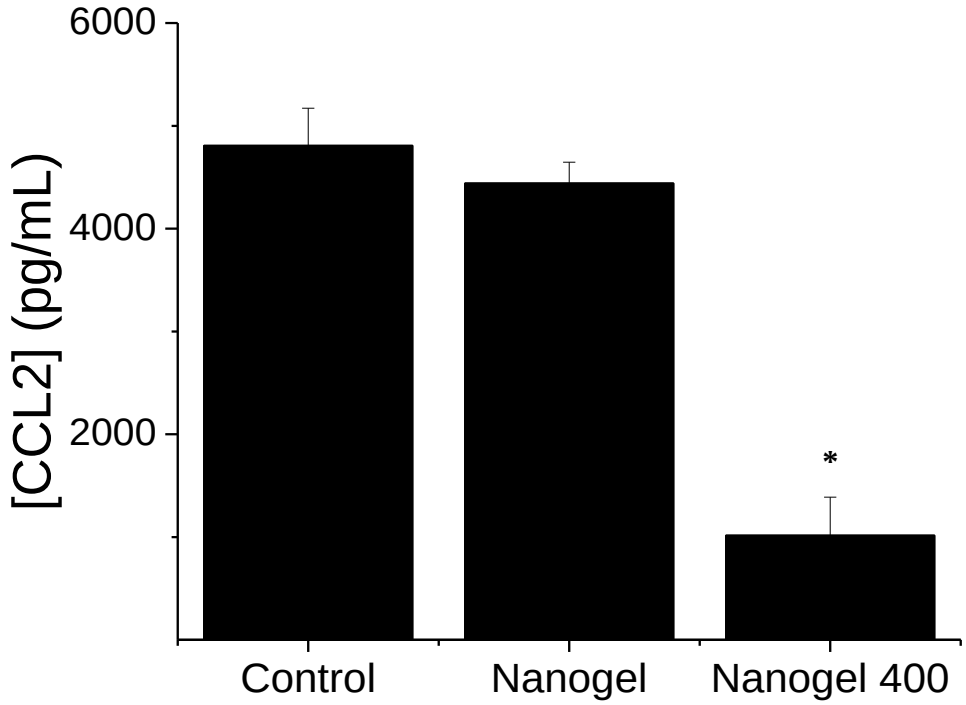

Figure 4.4 CCL2 supernatant concentration following a 30-min incubation in PBS with additional PBS added as control, a 2 mg/mL nanogel solution without CB, or 2 mg/mL Nanogel 400 solution. Avg ± 1 S.D., n=3. * indicates signifigant difference from control and nanogel, $p<0.01$ as determined by a one-way ANOVA with a Tukesy HSD post-hoc test.

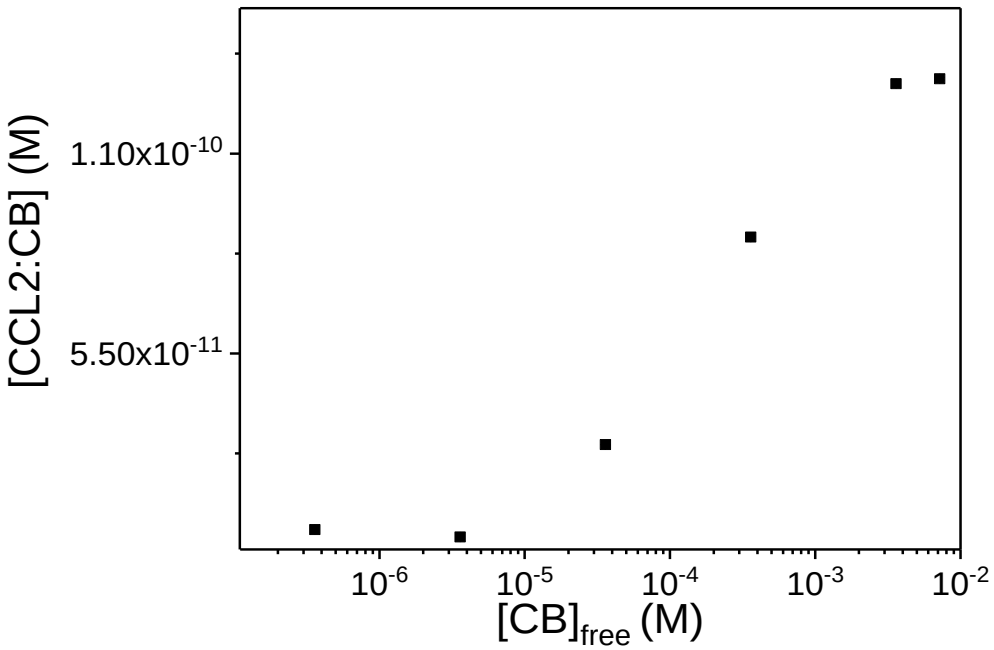

Figure 4.5 Binding isotherm for CCL2 and CB immobilized to Nanogel 400 in PBS. Avg ± 1 S.D., n=3.

KC/GRO was found to have a low affinity for Nanogel 400 with a K_D of 720 μM as seen in **Figure 4.6**. A previous report displayed CB has a K_D of 0.4 μM for human IL-8, the human analog for rat KC/GRO.[182] However rat KC/GRO has a 46% identity match with human IL-8. Additionally, the positive amino acid residues are believed to play an important role in protein binding to CB; human IL-8 has 16 positive amino acids while rat KC/GRO has 11. Protein information was obtained using uniprot software.[232] The concentration of KC/GRO in a control centrifuge tube was found to decrease by 29% over a 30 min incubation, possibly due to nonspecific adsorption. This occurred despite the inclusion of BSA as a blocking agent. When Nanogel 400 (2mg/mL) was added to the KC/GRO solution, 51.1 ± 1.1% of KC/GRO was not

detected as seen in **Figure 4.7**. This implies that the K_D between KC/GRO and CB is higher than 720 μM as ~60 pg of the KC/GRO was lost not to Nanogel 400. It is unlikely that the loss of KC/GRO is due to solely degradation as many studied cytokines remain stable for 6 hr at room temperature, and KC/GRO standards left at room temperature for 1 hr yield the same signal as those freshly made.[233] Nonspecific adsorption of dilute analytes and/or its degradation are persistent complications when determining K_D by measuring free analyte concentrations.[234, 235] The low K_D between CB and KC/GRO emphasizes the complexity in predicting protein affinity to affinity dyes *a priori*.

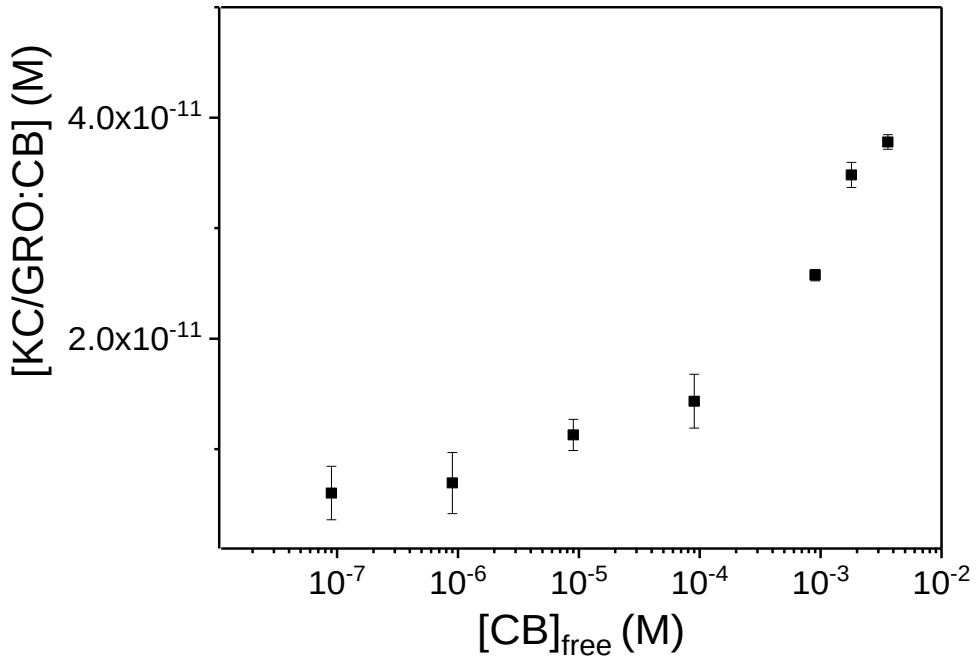

Figure 4.6 Binding isotherm for KC/GRO and CB immobilized to Nanogel 400 in PBS. Avg ± 1 S.D., n=3.

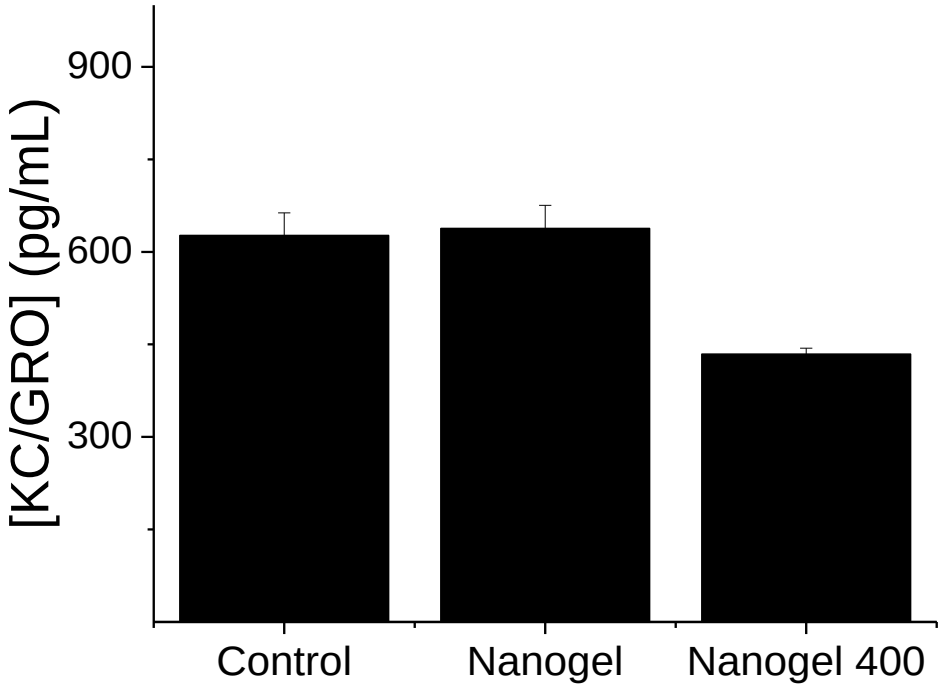

Figure 4.7 KC/GRO supernatant concentration following a 30-min incubation in PBS with additional PBS added as control, a 2 mg/mL nanogel solution without CB, or 2 mg/mL Nanogel 400 solution. Avg ± 1 S.D., n=3.

Protein dissociation from Nanogel 400

It is desired to develop affinity agents that can capture and release protein, so the protein may be diluted to a concentration within working the range of an analysis. To this end batch dissociation experiments were performed screening various dissociation buffers. **Table 4.2** lists the various dissociation buffers/conditions and the percent CCL2 released. Initial experiments using a 2 hr dissociation step were performed comparing organic dissociation solutions to ionic solutions. In previous work, a 30% acetonitrile solution was found to dissociate 92% of CCL2 from heparin, a sulfonated glycosaminoglycan using a batch process.[93] However for this work only 21.5% of bound CCL2 was found to dissociate from Nanogel 400 using the 30%

acetonitrile solution. This low dissociation is likely due to the poor solubility of the nanogel in acetonitrile, and a more ionic interaction between CCL2 and CB. The insoluble nanogel would have collapsed pore structure hindering diffusion. The performance of the CCL2 immunoassay was compromised when standards were made in 2 M NaCl pH 4, the signal of standards made under these conditions was significantly different from controls as determined by a Student T-test, $p<0.01$. Cibacron blue did not dissociate from the nanogel under any of the dissociation conditions.

Table 4.2 Protein dissociation from Nanogel 400.

Dissociation Solution 2 hr	Percent CCL2 Dissociated	Percent KC/GRO Dissociated
30/70 Acetonitrile/PBS 4 °C	**21.5 ± 2.3**	
2 M NaSCN 4 °C	**23.3 ± 0.4**	
2 M NaCl 4 °C	**49.8 ± 3.0**	
2 M NaCl 37 °C	**60.7 ± 4.2**	
2 M NaCl 10 mM Phosphate 37 °C		
pH 10, 2 hr	**47.2 ± 4.0**	
pH 7, 2 hr	**75.7 ± 2.9**	
pH 4, 2 hr*	**73.3 ± 10.1**	
pH 7, 12 hr	**90.2 ± 6.2**	**79.3 ± 1.8**

*Indicates performance of the immunoassay was compromised. Avg ± 1 S.D., n=3.

During the initial screening of dissociation buffers, the highest percent CCL2 dissociation was observed using 2 M NaCl pH 7 solution at 37 °C (above the LCST of PNIPAM). Further experiments revealed a time dependent dissociation with an increase dissociation occurring when the dissociation was performed above the LCST of PNIPAM, as seen in **Figure 4.8**. A maximum release was observed with a 12 hr dissociation time reaching 90.2 ± 6.2% of CCL2 dissociated of using 2 M NaCl pH 7. KC/GRO reached 79.3 ± 1.8% dissociation during a 12 hr release at 37 °C

in 2 M NaCl pH 7. The lower percent dissociation for KC/GRO may be attributed to protein irreversibly bound to the centrifuge tube/nanogel, or the interaction between KC/GRO and CB has additional nonionic interactions.

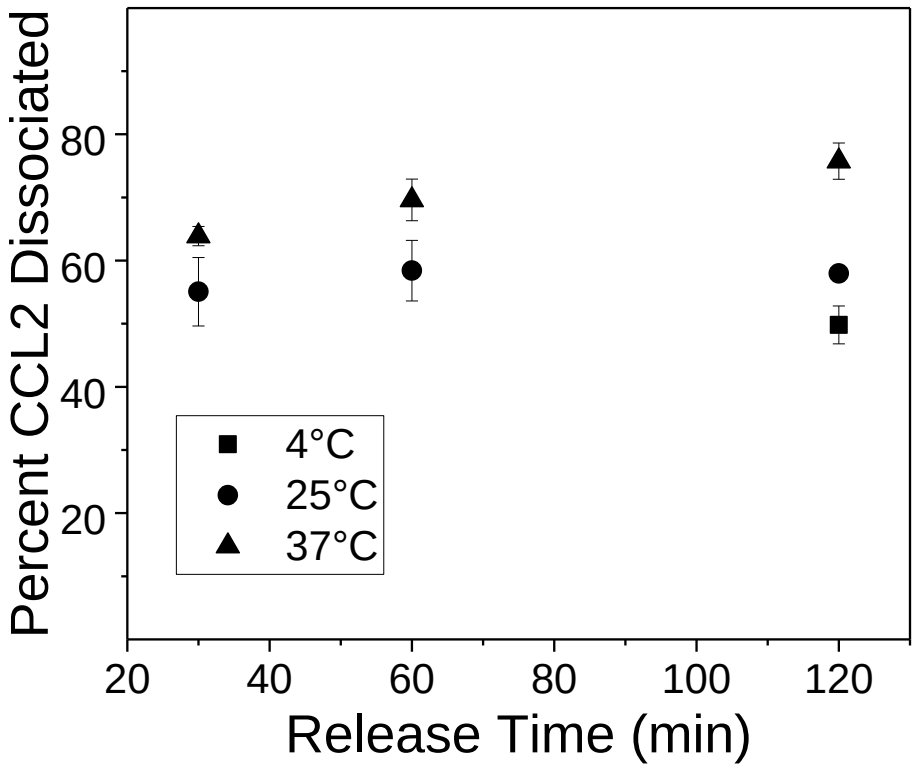

Figure 4.8 Percent CCL2 dissociated from Nanogel 400 in 2 M NaCl pH 7. Avg ± 1 S.D. n=3, except 25 °C at 120 min in which n=2.

In vitro microdialysis sampling

The dead volume of the microdialysis probe attached to the SFC Fluidics push/pull pump must be accounted for when changing perfusion fluid. Sampling begun before this volume has been accounted for, is performed using a previous perfusion fluid. The determined dead volume of this space with 30 cm of fluorinated ethylene propylene tubing (0.12 mm I.D. 1.2 µL/10 cm) attaching the probe to the pump is ~30 µL. To account for this volume a 3 µL/min flow rate for 20 min was performed before sampling. After the initial flush, the flow rate was decreased to 1 µL/min and steady state sampling of FITC-dextran 10 was reached 60 min later, as displayed in **Figure 4.9**. The first collected sample was significantly different from the four succeeding collections, $p<0.01$ as determined by a one-way ANOVA and Tukey HSD post hoc test. The relative recovery is lower in the first sample collected as a portion of this perfusate had a lower residence time as a portion was perfused at a 3 µL/min. Flow rate is inversely proportional to relative recovery.[236] As the first sample collected using the SFC pump was not indicative of steady state sampling, it was discarded in protein sampling experiments.

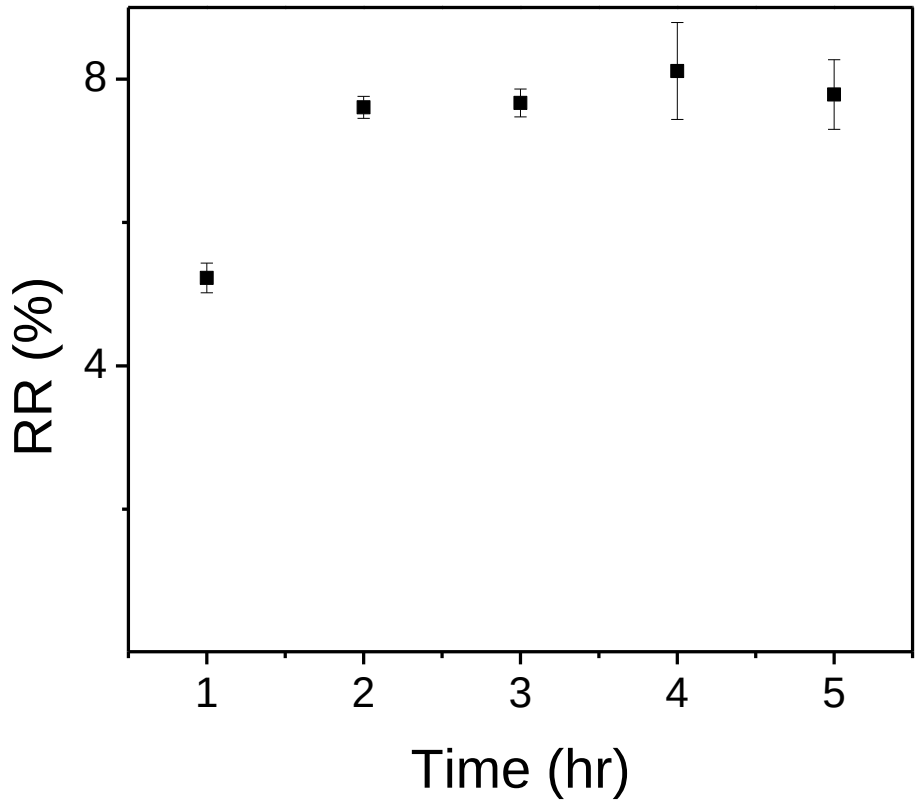

Figure 4.9 FITC-dextran 10 RR at 1 µL/min using SFC push/pull pump. Collections were made at 1 µL/min. Avg ± 1 S.D., n=3

With the inclusion of Nanogel 400 in the perfusion fluid, the RR for CCL2 was enhanced, while it was not for KC/GRO. The control and Nanogel 400 enhanced RR are displayed in **Table 4.3**. The RR for CCL2 at 1 µL/min increased from 1.2 ± 0.3% to 4.0 ± 0.6% with inclusion of Nanogel 400, n=3 where n is the number of probes from the same lot. The RR for CCL2 is statistically different between control and Nanogel 400 ($p<0.05$). The control RR for CCL2 using a CMA 20 microdialysis probe at 1 µL/min is in close agreement with previously reported CCL2 RR of 1.0 ± 0.3% using the same probe model.[237] The RR for KC/GRO at 1 µL/min decreased from 31.2 ± 2.5% to 9.2 ± 1.7%. The decrease in RR is likely due to a

combination of the low affinity between KC/GRO and CB, and nonspecific adsorption to the nanogels at time periods that were not studied. Previous experiments that tested for nonspecific adsorption to the nanogels were performed using a 30-min incubation time, while the during microdialysis experiment protein remained in solution with the nanogels for up to 2 hrs after encountering the nanogels. The nonspecific adsorption over a longer incubation period may enable the protein to irreversibly adsorb to the nanogels.

Table 4.3 Protein RR at 1 µL/min.

	CCL2 RR (%)	**KC/GRO RR (%)**
Control	1.2 ± 0.3	31.2 ± 2.5
Nanogel 400	4.0 ± 0.6*	9.2 ± 1.7

Average ± S.D., n=3 experimental replicates for CCL2, while n=4 technical replicates for KC/GRO. * indicates significant difference as determined by a Student's T-test, $p<0.01$.

Lot to lot variation in commercially available microdialysis probes can cause probes to have variable relative recoveries for the same molecule. An example of this lot to lot variation was observed when a microdialysis probe was perfused under identical control conditions as those used earlier, yet the RR for CCL2 was 7.1 ± 1.2%. The RR for CCL2 collected with this probe was enhanced to 12.7 ± 1.8% with the inclusion of Nanogel 400, which returned to 7.5 ± 0.7% when Nanogel 400 was removed from the perfusion fluid, as seen in **Figure 4.10**. There was no significant change in the control CCL2 RR before and after Nanogel 400 was perfused indicating that the increase in RR is due to the nanogel in the perfusion fluid, and that the nanogel does not irreversibly adsorb to the membrane or block pores, which would hinder transport into the dialysate during extended sampling.

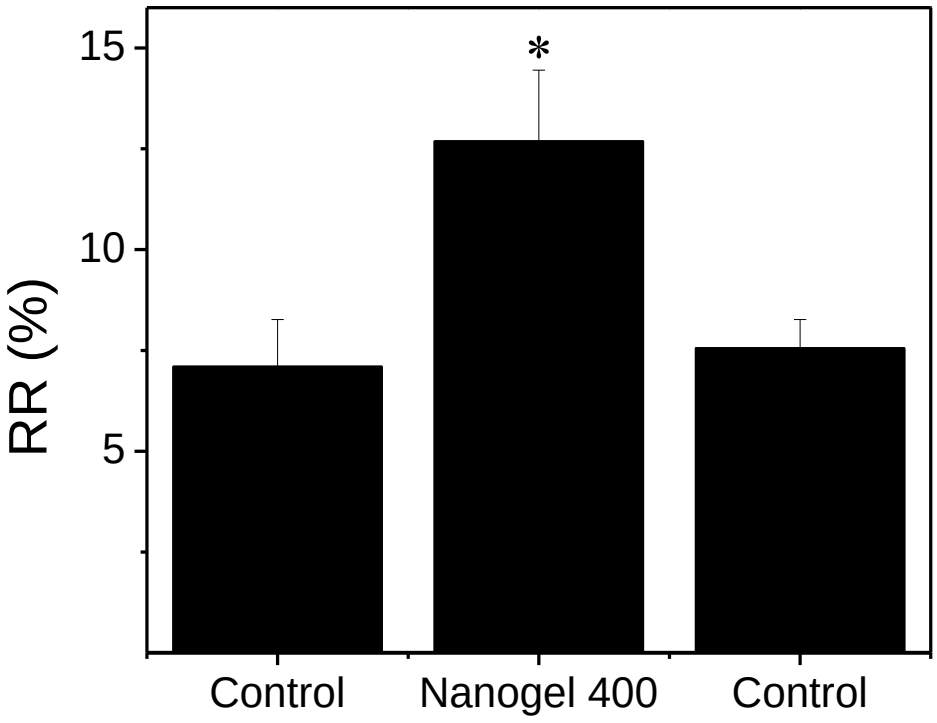

Figure 4.10 CCL2 RR without Nanogel 400 (control) and with Nanogel 400 in the perfusion fluid. Avg ± 1 S.D., n=4 one hr collections using 1 probe. Perfusion fluid was changed between bars to include or remove the affinity agent. *indicates significant difference between Nanogel 400 and both Control sampling periods as determined by one-way ANOVA and Tukey HSD post hoc test, $p<0.01$.

Previously developed affinity agents have ranged in cost, from $136/mL of perfusion fluid for free antibodies to $0.01/mL of perfusion fluid for free heparin as seen in **Table 4.4**. However, the addition of a support material, which prevents free affinity ligands exodus from the probe, increases the cost of affinity agents. The nanogels used in this chapter cost $2.40/mL of perfusion fluid, with 97% of the cost associated with the affinity ligand used, CB. The as synthesized nanogels have amine functional groups which are amenable to a range of common coupling chemistries such as substitution reaction (used in chapter 3), reductive amination and

carbodiimide crosslinking (EDC/NHS). The use of heparin in lieu of CB would reduce the cost of the nanogels, and there is a wide range of known physiologically relevant heparin binding proteins with nM K_D's.[238-243] The use of heparin could serve to increase the affinity between the protein and nanogel, and reduce the trial and error aspect of determining which proteins bind to CB.

Table 4.4 Comparison of affinity agent RR enhancement factors and cost.

Affinity Agent	Particle Diameter	Analytes	Working Concentration	Cost/1 mL of Working Solution* ($)	Ratio of AA enhanced RR to control RR
SPE packing material[244]	90 μm	Kemptide, Leu-enkephalin, Met-enkephalin, oxytocin, [Arg8]vasopressin, LHRH	6.2 mg/mL	0.45	1-10
Flow Cytometry Antibody Beads[78]	7 μm	TNF-α, IFN-γ, IL-2, IL-4, IL-5	1:1 or 1:4 dilution of stock	100-40	2.4-13.6
Heparin-immobilized beads[93]	5.5 μm	aFGF, VEGF, CCL2, CCL5	2.25×10^7 beads/mL	18.10	1.6-4
Cibacron Blue Nanogels (this work)	400 nm	CCL2	2 mg/mL	2.40	3.3
Antibody[88]	molecule	Met-enkephalin	0.15 μM	136.5	2.5
Heparin[90]	molecule	IL-4, IL-6, IL-7, CCL2, TNF-α	0.1 μM	0.01	2-3.9

*Cost of working solution accounts for commercial cost from reported venders of materials required for synthesis or direct use for a single analyte.

Summary

In vitro affinity microdialysis is described by including nanogels immobilized with CB in the perfusion fluid. The RR of CCL2 was enhanced with the inclusion of the nanogels, and not enhanced for KC/GRO. A 100% nanogel recovery over 8 hr was obtained by adding a peristaltic pump to the microdialysis system. CCL2 displayed specific capture to CB embedded nanogels. CCL2 and KC/GRO were capable of being dissociated from the nanogels which could then be detected by commercially available ELISAs. The cost associated with the nanogels is 7.5 times lower than that for previously developed heparin-immobilized microspheres, while yielding similar RR enhancement factors for CCL2. This work displays that nanogels can serve as a novel support material for affinity ligands to be immobilized to, for affinity enhanced microdialysis sampling.

Chapter 5 Conclusion and Future Work

Microdialysis sampling of proteins and peptides is of growing interest. In recent years, microdialysis has continued to be used by a wide number of labs to collect cytokines, tau proteins, and amyloid beta oligomers.[58, 60, 61] Appropriate methods to increase the relative recovery of large/dilute molecules collected with microdialysis are desired, as this would reduce the complexity placed on the ensuing detection method. The low recovery can be offset by increasing the residence time of the perfusion fluid in the probe or increase the surface area of the probe. However, in vivo these alterations will decrease the temporal resolution, as common analysis methods have 25-100 µL volume requirements, or increase the trauma due to surgical implantation of a large probe. Recent improvements to the design of microdialysis probes have allowed for the use of 1-3 MDa molecular weight cutoff probes to be developed, which has seen rapid commercialization by microdialysis probe manufacturers.[77] The new high molecular weight cut off probes typically display a two-fold increase in RR, while affinity agent enhanced sampling has seen up to a 14-fold increase in relative recovery.[91] The high RR enhancements observed with affinity agents warrants their further development. Previously developed affinity agents have relied on perfusable affinity ligands, however if the ligands are small enough to pass through the semipermeable membrane they may alter in vivo results. To prevent this, ligands have been immobilized on support materials that do not cross the membrane. Formerly developed support materials have consisted of costly microspheres or dense iron oxide nanoparticles, both which readily precipitate. The precipitation of these agents increases the complexity of their use. This dissertation developed a cost-effective affinity agent support that does not precipitate. This would allow for the simple perfusion of affinity agents immobilized to the new nanogel support and broaden their use in microdialysis studies.

In chapter two gold nanoparticles were initially chosen to study as a support material due to the simple synthesis of <20 nm diameter particles, high surface area, long term stability, and simple immobilization strategies. Poly (*N*-isopropyl acrylamide) (PNIPAM) was initially chosen as generic to immobilize to the gold nanoparticles as it would act as both a stabilizing ligand and capture ligand. PNIPAM can switch hydrophobicity with subtle changes in temperature, thereby allowing for the capture and release hydrophobic molecules with a temperature change.[245] Gold nanoparticles immobilized with various PNIPAM graft densities were synthesized. The graft densities studied were similar to those studied for protein capture and release on flat surface.[160] Rapid agglomeration of the particles was observed during the thermal response in salt solutions. To elucidate the reversibility of the agglomeration three complimentary techniques were used, dynamic light scattering, monitoring the localized surface plasmon resonance and electron microscopy. The agglomeration was determined to be irreversible for low polymer graft density; thermally triggered protein adsorption to PNIPAM occurs only at low graft densities. The cause for agglomeration in salt solutions was studied and evidence suggests the agglomeration onsets due to a second brush layer that collapses. However further studies using differential scanning calorimetry and nanoparticle tracking analysis need be performed to confirm this observation. Differential scanning calorimetry can be used to identify two separate brush regions that collapse, while nanoparticle tracking analysis can determine agglomerate size distribution without a particle size bias. The cause for the irreversible agglomeration at low graft densities was determined to be due to polymer collapsing to the particle surface, causing a low collapsed polymer thickness and/or screening of residual surface charge at high ionic strength. These compounding issues develop a secondary van der Waal's energy well which inhibits the reversibility of agglomeration. The rapid and irreversible agglomeration of low polymer graft

density particles where protein adsorption is highest inhibited protein adsorption studies by causing changes in surface area, and particle precipitation. Due to these complexities, a new support platform was sought.

Cibacron blue is a ligand commonly used in affinity separations owing to its affinity with a large number of proteins, and nanogels immobilized with cibacron blue are being developed as cytokine delivery agents due to its μM to nM dissociation constant with cytokines.[183] In chapter three nanogels with embedded Cibacron blue were synthesized. Cross linked PNIPAM was chosen for as the support material due to its low density, simple polymerization, low nonspecific adsorption, low cost and it has a thermal response which hastens protein dissociation. Centrifugation was used to rapidly remove large particles yielding a monodisperse stable suspension. The stability of the thermoresponsive nanogels was studied in perfusion fluids with high ionic strength and high protein concentrations at temperatures above the lower critical solution temperature of the polymer. No agglomeration was observed under the conditions tested, and the particles were found to be stable for up to three months. The nanogels were used to capture, release and concentrate lysozyme, acting as a model protein. BSA was excluded from interacting with cibacron blue, however BSA nonspecifically adsorbed to the nanogel.

The recovery of perfused nanogels through a 10 mm PES 100 kDa MWCO microdialysis was 88% at 1 $\mu L min^{-1}$ over a 5 hr period without the use any additional instrumentation. A consistent 100% particle recovery was obtained using a combination of push/pull pumps. Optimized conditions for microspheres, through constant rotation of the syringe, did not prevent particle precipitation, hindering their use as affinity agent supports. The dissociation constant between the nanogels and two rat cytokines, CCL2 and KC/GRO were determined and found to be higher than previously reported for the human and mouse analogs.[182] Previous studies on the

interaction of cibacron blue and cytokines were performed using human/mouse proteins, however in this work the interaction was studied using rat proteins. Rat proteins were chosen with the goal to develop affinity agents to be used for sampling from rat. Captured proteins were efficiently dissociated (>80%) from the nanogels using 2 M NaCl pH 7. Dissociated protein was detected using commercially available ELISA's. The dissociation conditions did not affect the performance of the ELISAs. The RR of CCL2 was enhanced three-fold with the inclusion of the nanogels, while the RR of KC/GRO decreased, possibly due to nonspecific adsorption to the nanogels. The mass recovery KC/GRO decreased with the use of the nanogel, and further experiments to verify the cause are warranted. Further in vitro studies of the nanogels needs be performed to validate use at enhancing protein RR with a multiprotein sample. In vivo use of the nanogels needs to be studied to confirm that the nanogels are not saturated with proteins, as many collected proteins are likely to interact with cibacron blue.

Further work to immobilize heparin, a glycosaminoglycan, to the nanogels in lieu of cibacron blue should be performed. A wide range of rat cytokines have a known nM K_D with heparin. The lower K_D between heparin and cytokines relative to cibacron blue will lead to lower required concentrations of nanogels to efficiently capture cytokines. Heparin has previously been used as a free and immobilized ligand to enhance cytokine RR.[93] The as synthesized nanogels have primary amines due the allyl amine which enables carbodiimide crosslinking between a primary amine and a carboxyl functional group on heparin. Additionally, reductive amination can be used to attach heparin via the aldehyde to the both primary and secondary amines (secondary amines from PNIPAM). A comparison between heparin immobilization strategies and protein dissociation constants, adsorption amounts, and RR enhancements is a desired study. Additionally, a study determining maximum cytokine RR by combining high MWCO probes

with affinity agents is warranted using nanogels which can be collected using a peristaltic pump. The compounding enhancements between affinity agents, and high MWCO probes may lead to dialysate samples that can be diluted before detection, which would increase the temporal resolution of cytokine sampling.

In conclusion, this dissertation describes a method to vary PNIPAM graft density on gold nanoparticles, and synthesize monodisperse nanogels that form a stable suspension. The thermoresponsive gold nanoparticles were found to be unsuitable to the ionic environments encountered with microdialysis. The nanogels were found to be cost efficient support material which form a stable suspension and enhanced the RR of CCL2.

References

1. Fitzgerald, K. A.; O'Neill, L. A. J.; Gearing, A. J. H.; Callard, R. E., In *The Cytokine FactsBook and Webfacts (Second Edition)*, Academic Press: London, 2001.

2. Mizgerd, J. P.; Spieker, M. R.; Doerschuk, C. M., Early response cytokines and innate immunity: essential roles for TNF receptor 1 and type I IL-1 receptor during Escherichia coli pneumonia in mice. *J Immunol* 2001, *166* (6), 4042-8.

3. Gouwy, M.; Struyf, S.; Proost, P.; Van Damme, J., Synergy in cytokine and chemokine networks amplifies the inflammatory response. *Cytokine Growth Factor Rev* 2005, *16* (6), 561-80.

4. Anderson, J. M.; Rodriguez, A.; Chang, D. T., FOREIGN BODY REACTION TO BIOMATERIALS. *Semin. Immunol.* 2008, *20* (2), 86-100.

5. Lefkowitz, D. L.; Lefkowitz, S. S., Macrophage-neutrophil interaction: a paradigm for chronic inflammation revisited. *Immunol Cell Biol* 2001, *79* (5), 502-6.

6. Dinarello, C. A., Proinflammatory cytokines. *Chest* 2000, *118* (2), 503-8.

7. Tripepi, G.; Mallamaci, F.; Zoccali, C., Inflammation markers, adhesion molecules, and all-cause and cardiovascular mortality in patients with ESRD: searching for the best risk marker by multivariate modeling. *J Am Soc Nephrol* 2005, *16 Suppl 1*, S83-8.

8. Ljubimov, A. V.; Saghizadeh, M., Progress in corneal wound healing. *Prog Retin Eye Res* 2015, *49*, 17-45.

9. Brodbeck, W. G.; Nakayama, Y.; Matsuda, T.; Colton, E.; Ziats, N. P.; Anderson, J. M., Biomaterial surface chemistry dictates adherent monocyte/macrophage cytokine expression in vitro. *Cytokine* 2002, *18* (6), 311-9.

10. Gaudet, S.; Janes, K. A.; Albeck, J. G.; Pace, E. A.; Lauffenburger, D. A.; Sorger, P. K., A compendium of signals and responses triggered by prodeath and prosurvival cytokines. *Mol Cell Proteomics* 2005, *4* (10), 1569-90.

11. Keustermans, G. C.; Hoeks, S. B.; Meerding, J. M.; Prakken, B. J.; de Jager, W., Cytokine assays: an assessment of the preparation and treatment of blood and tissue samples. *Methods* 2013, *61* (1), 10-7.

12. Feldmann, M.; Maini, R. N.; Bondeson, J.; Taylor, P.; Foxwell, B. M.; Brennan, F. M., Cytokine blockade in rheumatoid arthritis. *Adv Exp Med Biol* 2001, *490*, 119-27.

13. Netea, M. G.; Joosten, L. A.; Lewis, E.; Jensen, D. R.; Voshol, P. J.; Kullberg, B. J.; Tack, C. J.; van Krieken, H.; Kim, S. H.; Stalenhoef, A. F.; van de Loo, F. A.; Verschueren, I.; Pulawa, L.; Akira, S.; Eckel, R. H.; Dinarello, C. A.; van den Berg, W.; van der Meer, J. W., Deficiency of interleukin-18 in mice leads to hyperphagia, obesity and insulin resistance. *Nat Med* 2006, *12* (6), 650-6.

14. Hou, R.; Garner, M.; Holmes, C.; Osmond, C.; Teeling, J.; Lau, L.; Baldwin, D. S., Peripheral inflammatory cytokines and immune balance in Generalised Anxiety Disorder: case-controlled study. *Brain, Behav., Immun.*

15. Waern, I.; Karlsson, I.; Pejler, G.; Wernersson, S., IL-6 and IL-17A degradation by mast cells is mediated by a serglycin:serine protease axis. *Immun., Inflammation Dis.* 2016, *4* (1), 70-79.

16. Budzyńska-Włodarczyk, J.; Michalska-Jakubus, M. M.; Kowal, M.; Krasowska, D., Evaluation of serum concentrations of the selected cytokines in patients with localized scleroderma. *Advances in Dermatology and Allergology/Postępy Dermatologii i Alergologii* 2016, *33* (1), 47-51.

17. Fu, A. K. Y.; Hung, K.-W.; Yuen, M. Y. F.; Zhou, X.; Mak, D. S. Y.; Chan, I. C. W.; Cheung, T. H.; Zhang, B.; Fu, W.-Y.; Liew, F. Y.; Ip, N. Y., Proc. Natl. Acad. Sci. U. S. A. *Proc. Natl. Acad. Sci. U. S. A.* 2016, *113* (19), E2705-E2713.

18. Feng, B.; Tang, Y.; Chen, B.; Xu, C.; Wang, Y.; Dai, Y.; Wu, D.; Zhu, J.; Wang, S.; Zhou, Y.; Shi, L.; Hu, W.; Zhang, X.; Chen, Z. Transient increase of interleukin-1β after prolonged febrile seizures promotes adult epileptogenesis through long-lasting upregulating endocannabinoid signaling *Sci. Rep.* [Online], 2016, p. 21931. PubMed.

19. Ersoy, O. F.; Ozkan, N.; Ozsoy, Z.; Kayaoglu, H. A.; Yenidogan, E.; Celik, A.; Ozugurlu, A. F.; Arabaci Cakir, E.; Lortlar, N., Effects of melatonin on cytokine release and healing of colonic anastomoses in an experimental sepsis model. *Ulus Travma Acil Cerrahi Derg* 2016, *22* (4), 315-21.

20. Resan, M.; Vukosavljevic, M.; Vojvodic, D.; Pajic-Eggspuehler, B.; Pajic, B., The acute phase of inflammatory response involved in the wound-healing process after excimer laser treatment. *Clin. Ophthalmol.* 2016, *10*, 993-1000.

21. Stenken, J. A.; Poschenrieder, A. J., Bioanalytical chemistry of cytokines--a review. *Anal Chim Acta* 2015, *853*, 95-115.

22. Au-Yeung, B. B.; Smith, G. A.; Mueller, J. L.; Heyn, C. S.; Jaszczak, R. G.; Weiss, A.; Zikherman, J., IL-2 Modulates the TCR Signaling Threshold for CD8 but Not CD4 T Cell Proliferation on a Single-Cell Level. *J. Immunol.* 2017.

23. Hehner, S. P.; Hofmann, T. G.; Ratter, F.; Dumont, A.; Droge, W.; Schmitz, M. L., Tumor necrosis factor-alpha-induced cell killing and activation of transcription factor NF-kappaB are uncoupled in L929 cells. *J Biol Chem* 1998, *273* (29), 18117-21.

24. Guo, L.; Junttila, I. S.; Paul, W. E., Cytokine-induced cytokine production by conventional and innate lymphoid cells. *Trends Immunol* 2012, *33* (12), 598-606.

25. Meager, A., Measurement of cytokines by bioassays: theory and application. *Methods* 2006, *38* (4), 237-52.

26. de Jager, W.; Rijkers, G. T., Solid-phase and bead-based cytokine immunoassay: a comparison. *Methods* 2006, *38* (4), 294-303.

27. Morgan, E.; Varro, R.; Sepulveda, H.; Ember, J. A.; Apgar, J.; Wilson, J.; Lowe, L.; Chen, R.; Shivraj, L.; Agadir, A.; Campos, R.; Ernst, D.; Gaur, A., Cytometric bead array: a multiplexed assay platform with applications in various areas of biology. *Clin Immunol* 2004, *110* (3), 252-66.

28. Fichorova, R. N.; Richardson-Harman, N.; Alfano, M.; Belec, L.; Carbonneil, C.; Chen, S.; Cosentino, L.; Curtis, K.; Dezzutti, C. S.; Donoval, B.; Doncel, G. F.; Donaghay, M.; Grivel, J. C.; Guzman, E.; Hayes, M.; Herold, B.; Hillier, S.; Lackman-Smith, C.; Landay, A.; Margolis, L.; Mayer, K. H.; Pasicznyk, J. M.; Pallansch-Cokonis, M.; Poli, G.; Reichelderfer, P.; Roberts, P.; Rodriguez, I.; Saidi, H.; Sassi, R. R.; Shattock, R.; Cummins, J. E., Jr., Biological and technical variables affecting immunoassay recovery of cytokines from human serum and simulated vaginal fluid: a multicenter study. *Anal Chem* 2008, *80* (12), 4741-51.

29. Garrigan, C.; Han, J.; Tolomeo, P.; Johnson, K. J.; Master, S. R.; Lautenbach, E.; Nachamkin, I., Evaluation of a research use only luminex based assay for measurement of procalcitonin in serum samples. *Am. J. Transl. Res.* 2016, *8* (10), 4362-4369.

30. Malekzadeh, A.; Twaalfhoven, H.; Wijnstok, N. J.; Killestein, J.; Blankenstein, M. A.; Teunissen, C. E., Comparison of multiplex platforms for cytokine assessments and their potential use for biomarker profiling in multiple sclerosis. *Cytokine* 2017, *91*, 145-152.

31. Davies, M. I.; Cooper, J. D.; Desmond, S. S.; Lunte, C. E.; Lunte, S. M., Analytical considerations for microdialysis sampling. *Adv. Drug Delivery Rev.* 2000, *45* (2–3), 169-188.

32. Nandi, P.; Lunte, S. M., Recent trends in microdialysis sampling integrated with conventional and microanalytical systems for monitoring biological events: a review. *Anal Chim Acta* 2009, *651* (1), 1-14.

33. Saylor, R. A.; Lunte, S. M., A review of microdialysis coupled to microchip electrophoresis for monitoring biological events. *J Chromatogr A* 2015, *1382*, 48-64.

34. Perry, M.; Li, Q.; Kennedy, R. T., Review of recent advances in analytical techniques for the determination of neurotransmitters. *Anal Chim Acta* 2009, *653* (1), 1-22.

35. Van der Bruggen, B.; Vandecasteele, C., Modelling of the retention of uncharged molecules with nanofiltration. *Water Res* 2002, *36* (5), 1360-8.

36. Ngo, K. T.; Varner, E. L.; Michael, A. C.; Weber, S. G., Monitoring Dopamine Responses to Potassium Ion and Nomifensine by in Vivo Microdialysis with Online Liquid Chromatography at One-Minute Resolution. *ACS Chem. Neurosci.* 2017.

37. Phang, I.; Zoumprouli, A.; Papadopoulos, M. C.; Saadoun, S., Microdialysis to Optimize Cord Perfusion and Drug Delivery in Spinal Cord Injury. *Ann Neurol* 2016, *80* (4), 522-31.

38. Joshi, A.; Patel, H.; Stagni, G., Pharmacokinetic applications of cutaneous microdialysis: Continuous+intermittent vs continuous-only sampling. *J Pharmacol Toxicol Methods* 2017, *83*, 16-20.

39. Klaus, R.; Jin, C.; Maier-Salamon, A.; Jager, W.; Knopf, C.; Zeitlinger, M.; Richter-Muksch, S.; Schmidl, D.; Schmetterer, L.; Garhofer, G., An Exploratory Microdialysis Study to Assess the Ocular Pharmacokinetics of Ciprofloxacin Eye Drops in Rabbits. *J Ocul Pharmacol Ther* 2016, *32* (6), 390-5.

40. Post, E. H.; Su, F.; Hosokawa, K.; Taccone, F. S.; Herpain, A.; Creteur, J.; Vincent, J.-L.; De Backer, D., Changes in kidney perfusion and renal cortex metabolism in septic shock: an experimental study. *J. Surg. Res.* 2017, *207*, 145-154.

41. Pretti, L.; Bazzu, G.; Serra, P. A.; Nieddu, G., A novel method for the determination of ascorbic acid and antioxidant capacity in Opuntia ficus indica using in vivo microdialysis. *Food Chem* 2014, *147*, 131-7.

42. Hifumi, T.; Kawakita, K.; Yoda, T.; Okazaki, T.; Kuroda, Y., Association of brain metabolites with blood lactate and glucose levels with respect to neurological outcomes after out-of-hospital cardiac arrest: A preliminary microdialysis study. *Resuscitation 110*, 26-31.

43. Smith, T. S.; Bennett, J. P., Jr., Mitochondrial toxins in models of neurodegenerative diseases. I: In vivo brain hydroxyl radical production during systemic MPTP treatment or following microdialysis infusion of methylpyridinium or azide ions. *Brain Res* 1997, *765* (2), 183-8.

44. Bourne, J. A., Intracerebral microdialysis: 30 years as a tool for the neuroscientist. *Clin Exp Pharmacol Physiol* 2003, *30* (1-2), 16-24.

45. Keeler, G. D.; Durdik, J. M.; Stenken, J. A., Effects of delayed delivery of dexamethasone-21-phosphate via subcutaneous microdialysis implants on macrophage activation in rats. *Acta Biomater* 2015, *23*, 27-37.

46. Zhang, J.; Jaquins-Gerstl, A.; Nesbitt, K. M.; Rutan, S. C.; Michael, A. C.; Weber, S. G., In vivo monitoring of serotonin in the striatum of freely moving rats with one minute temporal resolution by online microdialysis-capillary high-performance liquid chromatography at elevated temperature and pressure. *Anal Chem* 2013, *85* (20), 9889-97.

47. Vasicek, T. W.; Jackson, M. R.; Poseno, T. M.; Stenken, J. A., In Vivo Microdialysis Sampling of Cytokines from Rat Hippocampus: Comparison of Cannula Implantation Procedures. *ACS Chem Neurosci* 2013.

48. Dankoski, E. C.; Wightman, R. M., Monitoring serotonin signaling on a subsecond time scale. *Front Integr Neurosci* 2013, *7*, 44.

49. Stanley, M.; Macauley, S. L.; Caesar, E. E.; Koscal, L. J.; Moritz, W.; Robinson, G. O.; Roh, J.; Keyser, J.; Jiang, H.; Holtzman, D. M., The Effects of Peripheral and Central High Insulin on Brain Insulin Signaling and Amyloid-beta in Young and Old APP/PS1 Mice. *J Neurosci* 2016, *36* (46), 11704-11715.

50. Fisher, J. R.; Wallace, C. E.; Tripoli, D. L.; Sheline, Y. I.; Cirrito, J. R., Redundant G(s)-coupled serotonin receptors regulate amyloid-β metabolism in vivo. *Mol. Neurodegener.* 2016, *11*, 45.

51. Macauley, S. L.; Stanley, M.; Caesar, E. E.; Yamada, S. A.; Raichle, M. E.; Perez, R.; Mahan, T. E.; Sutphen, C. L.; Holtzman, D. M., Hyperglycemia modulates extracellular amyloid-β concentrations and neuronal activity in vivo. *J. Clin. Invest.* 2015, *125* (6), 2463-2467.

52. Takeda, S.; Hashimoto, T.; Roe, A. D.; Hori, Y.; Spires-Jones, T. L.; Hyman, B. T., Brain interstitial oligomeric amyloid beta increases with age and is resistant to clearance from brain in a mouse model of Alzheimer's disease. *Faseb j* 2013, *27* (8), 3239-48.

53. Abrahamsson, A.; Rzepecka, A.; Romu, T.; Borga, M.; Leinhard, O. D.; Lundberg, P.; Kihlberg, J.; Dabrosin, C., Dense breast tissue in postmenopausal women is associated with a pro-inflammatory microenvironment in vivo. *Oncoimmunology* 2016, *5* (10), e1229723.

54. Khan, F.; Pharo, A.; Lindstad, J. K.; Mollnes, T. E.; Tonnessen, T. I.; Pischke, S. E., Effect of Perfusion Fluids on Recovery of Inflammatory Mediators in Microdialysis. *Scand J Immunol* 2015, *82* (5), 467-75.

55. Tabatabaei, P.; Visse, E.; Bergstrom, P.; Brannstrom, T.; Siesjo, P.; Bergenheim, A. T., Radiotherapy induces an immediate inflammatory reaction in malignant glioma: a clinical microdialysis study. *J Neurooncol* 2017, *131* (1), 83-92.

56. Taguchi, H.; Aono, Y.; Kawato, T.; Asano, M.; Shimizu, N.; Saigusa, T., Intragingival injection of Porphyromonas gingivalis-derived lipopolysaccharide induces a transient increase in gingival tumour necrosis factor-alpha, but not interleukin-6, in anaesthetised rats. *Int J Oral Sci* 2015, *7* (3), 155-60.

57. Xu, H.; Gelyana, E.; Rajsombath, M.; Yang, T.; Li, S.; Selkoe, D., Environmental Enrichment Potently Prevents Microglia-Mediated Neuroinflammation by Human Amyloid beta-Protein Oligomers. *J Neurosci* 2016, *36* (35), 9041-56.

58. Schiefecker, A. J.; Dietmann, A.; Beer, R.; Pfausler, B.; Lackner, P.; Kofler, M.; Fischer, M.; Broessner, G.; Sohm, F.; Mulino, M.; Thomé, C.; Humpel, C.; Schmutzhard, E.; Helbok, R., Neuroinflammation is Associated with Brain Extracellular TAU-Protein Release after Spontaneous Subarachnoid Hemorrhage. *Curr. Drug Targets* 2016.

59. Yamada, K.; Cirrito, J. R.; Stewart, F. R.; Jiang, H.; Finn, M. B.; Holmes, B. B.; Binder, L. I.; Mandelkow, E.-M.; Diamond, M. I.; Lee, V. M. Y.; Holtzman, D. M., In Vivo Microdialysis Reveals Age-Dependent Decrease of Brain Interstitial Fluid Tau Levels in P301S Human Tau Transgenic Mice. *J. Neurosci.* 2011, *31* (37), 13110-13117.

60. Förster, Y.; Schmidt, J. R.; Wissenbach, D. K.; Pfeiffer, S. E. M.; Baumann, S.; Hofbauer, L. C.; von Bergen, M.; Kalkhof, S.; Rammelt, S., Microdialysis Sampling from Wound Fluids Enables Quantitative Assessment of Cytokines, Proteins, and Metabolites Reveals Bone Defect-Specific Molecular Profiles. *PLOS ONE* 2016, *11* (7), e0159580.

61. Christidis, N.; Ghafouri, B.; Larsson, A.; Palstam, A.; Mannerkorpi, K.; Bileviciute-Ljungar, I.; Lofgren, M.; Bjersing, J.; Kosek, E.; Gerdle, B.; Ernberg, M., Comparison of the Levels of Pro-Inflammatory Cytokines Released in the Vastus Lateralis Muscle of Patients with Fibromyalgia and Healthy Controls during Contractions of the Quadriceps Muscle--A Microdialysis Study. *PLoS One* 2015, *10* (12), e0143856.

62. Thelin, E. P.; Carpenter, K. L. H.; Hutchinson, P. J.; Helmy, A., Microdialysis Monitoring in Clinical Traumatic Brain Injury and Its Role in Neuroprotective Drug Development. *AAPS J.* 2017, 1-10.

63. Hammarlund-Udenaes, M., Intracerebral microdialysis in blood–brain barrier drug research with focus on nanodelivery. *Drug Discovery Today: Technol.* 2016, *20*, 13-18.

64. Quist, S. R.; Wiswedel, I.; Quist, J.; Gollnick, H. P., Kinetic Profile of Inflammation Markers in Human Skin In vivo Following Exposure to Ultraviolet B Indicates Synchronic Release of Cytokines and Prostanoids. *Acta Derm Venereol* 2016, *96* (7), 910-916.

65. Portnow, J.; Badie, B.; Liu, X.; Frankel, P.; Mi, S.; Chen, M.; Synold, T. W., A pilot microdialysis study in brain tumor patients to assess changes in intracerebral cytokine levels after craniotomy and in response to treatment with a targeted anti-cancer agent. *J Neurooncol* 2014, *118* (1), 169-77.

66. Bungay, P. M.; Morrison, P. F.; Dedrick, R. L., Steady-state theory for quantitative microdialysis of solutes and water in vivo and in vitro. *Life Sci* 1990, *46* (2), 105-19.

67. Kendrick, K. M.; De La Riva, C.; Hinton, M.; Baldwin, B. A., Microdialysis measurement of monoamine and amino acid release from the medial preoptic region of the sheep in response to heat exposure. *Brain Res. Bull.* 1989, *22* (3), 541-544.

68. Schutte, R. J.; Oshodi, S. A.; Reichert, W. M., In vitro characterization of microdialysis sampling of macromolecules. *Anal Chem* 2004, *76* (20), 6058-63.

69. Kjellström, S.; Appels, N.; Ohlrogge, M.; Laurell, T.; Marko-Varga, G., Microdialysis—a membrane based sampling technique for quantitative determination of proteins. *Chromatographia* 1999, *50* (9), 539-546.

70. Wang, Q.; Li, N.; Wang, W., Electrocatalytic Response of Dopamine at a Metallothioneins Self-Assembled Gold Electrode. *Anal. Sci.* 2002, *18* (6), 635-639.

71. Meechai, N.; Jamieson, A. M.; Blackwell, J., Translational Diffusion Coefficients of Bovine Serum Albumin in Aqueous Solution at High Ionic Strength. *J. Colloid Interface Sci.* 1999, *218* (1), 167-175.

72. Ao, X.; Stenken, J. A., Microdialysis sampling of cytokines. *Methods* 2006, *38* (4), 331-41.

73. Trickler, W. J.; Miller, D. W., Use of osmotic agents in microdialysis studies to improve the recovery of macromolecules. *J Pharm Sci* 2003, *92* (7), 1419-27.

74. Dahlin, A. P.; Purins, K.; Clausen, F.; Chu, J.; Sedigh, A.; Lorant, T.; Enblad, P.; Lewén, A.; Hillered, L., Refined Microdialysis Method for Protein Biomarker Sampling in Acute Brain Injury in the Neurointensive Care Setting. *Anal. Chem.* 2014, *86* (17), 8671-8679.

75. Chu, J.; Undin, T.; Lind, S. B.; Hjort, K.; Dahlin, A. P., Influence of surface modification and static pressure on microdialysis protein extraction efficiency. *Biomed. Microdevices* 2015, *17* (5), 96.

76. Ulrich, J. D.; Burchett, J. M.; Restivo, J. L.; Schuler, D. R.; Verghese, P. B.; Mahan, T. E.; Landreth, G. E.; Castellano, J. M.; Jiang, H.; Cirrito, J. R.; Holtzman, D. M., In vivo measurement of apolipoprotein E from the brain interstitial fluid using microdialysis. *Mol Neurodegener* 2013, *8*, 13.

77. Takeda, S.; Sato, N.; Ikimura, K.; Nishino, H.; Rakugi, H.; Morishita, R., Novel microdialysis method to assess neuropeptides and large molecules in free-moving mouse. *Neuroscience* 2011, *186*, 110-9.

78. Ao, X.; Sellati, T. J.; Stenken, J. A., Enhanced microdialysis relative recovery of inflammatory cytokines using antibody-coated microspheres analyzed by flow cytometry. *Anal Chem* 2004, *76* (13), 3777-84.

79. Cussler; L., E., *Diffusion:Mass Transfer in Fluid Systems*. Cambridge

University Press: Cambridge, 1984; p 395-408.

80. Zhuo, R.; Liu, H.; Liu, N.; Wang, Y., Ligand Fishing: A Remarkable Strategy for Discovering Bioactive Compounds from Complex Mixture of Natural Products. *Molecules* 2016, *21* (11).

81. Khramov, A. N.; Stenken, J. A., Enhanced Microdialysis Extraction Efficiency of Ibuprofen in Vitro by Facilitated Transport with β-Cyclodextrin. *Anal. Chem.* 1999, *71* (7), 1257-1264.

82. Mogopodi, D.; Torto, N., Enhancing microdialysis recovery of metal ions by incorporating poly-l-aspartic acid and poly-l-histidine in the perfusion liquid. *Analytica Chimica Acta* 2003, *482* (1), 91-97.

83. Kurosaki, Y.; Nakamura, S.; Shiojiri, Y.; Kawasaki, H., LIPO-MICRODIALYSIS : A NEW MICRODIALYSIS METHOD FOR STUDYING THE PHARMACOKINETICS OF LIPOPHILIC SUBSTANCES. *Biol. Pharm. Bull.* 1998, *21* (2), 194-196.

84. Sun, L.; Stenken, J. A., Improving microdialysis extraction efficiency of lipophilic eicosanoids. *J. Pharm. Biomed. Anal.* 2003, *33* (5), 1059-1071.

85. Ward, K. W.; Medina, S. J.; Portelli, S. T.; Mahar Doan, K. M.; Spengler, M. D.; Ben, M. M.; Lundberg, D.; Levy, M. A.; Chen, E. P., Enhancement of in vitro and in vivo microdialysis recovery of SB-265123 using Intralipid and Encapsin as perfusates. *Biopharm Drug Dispos* 2003, *24* (1), 17-25.

86. Khramov, A. N.; Stenken, J. A., Enhanced microdialysis recovery of some tricyclic antidepressants and structurally related drugs by cyclodextrin-mediated transport. *Analyst* 1999, *124* (7), 1027-33.

87. Ao, X.; Stenken, J. A., Water-soluble cyclodextrin polymers for enhanced relative recovery of hydrophobic analytes during microdialysis sampling. *Analyst* 2003, *128* (9), 1143-1149.

88. Fletcher, H. J.; Stenken, J. A., An in vitro comparison of microdialysis relative recovery of Met- and Leu-enkephalin using cyclodextrins and antibodies as affinity agents. *Anal Chim Acta* 2008, *620* (1-2), 170-5.

89. Herbaugh, A. W.; Stenken, J. A., Antibody-enhanced microdialysis collection of CCL2 from rat brain. *J Neurosci Methods* 2011, *202* (2), 124-7.

90. Wang, Y.; Stenken, J. A., Affinity-based microdialysis sampling using heparin for in vitro collection of human cytokines. *Anal Chim Acta* 2009, *651* (1), 105-11.

91. Ao, X.; Sellati, T. J.; Stenken, J. A., Enhanced Microdialysis Relative Recovery of Inflammatory Cytokines Using Antibody-Coated Microspheres Analyzed by Flow Cytometry. *Anal. Chem.* 2004, *76* (13), 3777-3784.

92. Schmerberg, C. M.; Li, L., Mass spectrometric detection of neuropeptides using affinity-enhanced microdialysis with antibody-coated magnetic nanoparticles. *Anal Chem* 2013, *85* (2), 915-22.

93. Duo, J.; Stenken, J. A., In vitro and in vivo affinity microdialysis sampling of cytokines using heparin-immobilized microspheres. *Anal Bioanal Chem* 2011, *399* (2), 783-93.

94. Larson, R. G., Structure and Rheology of Complex Fluids. Oxford University Press.

95. Lieberman, H. A.; Rieger, M. M.; Banker, G. S., *Pharmaceutical Dosage Forms--Disperse Systems*. M. Dekker: 1998.

96. Poehlein, G. W.; Ottewill, R. H.; Goodwin, J. W., *Science and Technology of Polymer Colloids: Preparation and reaction engineering*. Nijhoff: 1983.

97. Turkevich, J.; Stevenson, P. C.; Hillier, J., The Formation of Colloidal Gold. *J. Phys. Chem.* 1953, *57* (7), 670-673.

98. Patra, C. R.; Bhattacharya, R.; Wang, E.; Katarya, A.; Lau, J. S.; Dutta, S.; Muders, M.; Wang, S.; Buhrow, S. A.; Safgren, S. L.; Yaszemski, M. J.; Reid, J. M.; Ames, M. M.; Mukherjee, P.; Mukhopadhyay, D., Targeted delivery of gemcitabine to pancreatic adenocarcinoma using cetuximab as a targeting agent. *Cancer Res* 2008, *68* (6), 1970-8.

99. Murphy, C. J.; Gole, A. M.; Stone, J. W.; Sisco, P. N.; Alkilany, A. M.; Goldsmith, E. C.; Baxter, S. C., Gold Nanoparticles in Biology: Beyond Toxicity to Cellular Imaging. *Acc. Chem. Res.* 2008, *41* (12), 1721-1730.

100. Nicol, J. R.; Dixon, D.; Coulter, J. A., Gold nanoparticle surface functionalization: a necessary requirement in the development of novel nanotherapeutics. *Nanomedicine (Lond)* 2015, *10* (8), 1315-26.

101. Maji, S.; Cesur, B.; Zhang, Z.; De Geest, B. G.; Hoogenboom, R., Poly(N-isopropylacrylamide) coated gold nanoparticles as colourimetric temperature and salt sensors. *Polym. Chem.* 2016, *7* (9), 1705-1710.

102. Yeh, Y.-C.; Creran, B.; Rotello, V. M., Gold Nanoparticles: Preparation, Properties, and Applications in Bionanotechnology. *Nanoscale* 2012, *4* (6), 1871-1880.

103. Love, J. C.; Estroff, L. A.; Kriebel, J. K.; Nuzzo, R. G.; Whitesides, G. M., Self-assembled monolayers of thiolates on metals as a form of nanotechnology. *Chem Rev* 2005, *105* (4), 1103-69.

104. Zhang, J.; Liu, B.; Liu, H.; Zhang, X.; Tan, W., Aptamer-conjugated gold nanoparticles for bioanalysis. *Nanomedicine (Lond)* 2013, *8* (6), 983-93.

105. Omidfar, K.; Khorsand, F.; Darziani Azizi, M., New analytical applications of gold nanoparticles as label in antibody based sensors. *Biosens. Bioelectron.* 2013, *43*, 336-347.

106. Liu, R.; Wu, P.; Yang, L.; Hou, X.; Lv, Y., Inductively coupled plasma mass spectrometry-based immunoassay: a review. *Mass Spectrom Rev* 2014, *33* (5), 373-93.

107. Chiu, R. Y. T.; Thach, A. V.; Wu, C. M.; Wu, B. M.; Kamei, D. T., An Aqueous Two-Phase System for the Concentration and Extraction of Proteins from the Interface for Detection Using the Lateral-Flow Immunoassay. *PLOS ONE* 2015, *10* (11), e0142654.

108. Ye, H.; Yang, K.; Tao, J.; Liu, Y.; Zhang, Q.; Habibi, S.; Nie, Z.; Xia, X., An Enzyme-Free Signal Amplification Technique for Ultrasensitive Colorimetric Assay of Disease Biomarkers. *ACS Nano* 2017.

109. Lian, T.; Peng, M.; Vermorken, A. J.; Jin, Y.; Luo, Z.; Van de Ven, W. J.; Wan, Y.; Hou, P.; Cui, Y., Synthesis and Characterization of Curcumin-Functionalized HP-beta-CD-Modified GoldMag Nanoparticles as Drug Delivery Agents. *J Nanosci Nanotechnol* 2016, *16* (6), 6258-64.

110. Xue, Q.; Liu, Z.; Guo, Y.; Guo, S., Cyclodextrin functionalized graphene-gold nanoparticle hybrids with strong supramolecular capability for electrochemical thrombin aptasensor. *Biosens Bioelectron* 2015, *68*, 429-36.

111. Chen, Y.; Xianyu, Y.; Jiang, X., Surface Modification of Gold Nanoparticles with Small Molecules for Biochemical Analysis. *Acc. Chem. Res.* 2017.

112. Korgel, B. A.; Fitzmaurice, D., Condensation of Ordered Nanocrystal Thin Films. *Phys. Rev. Lett.* 1998, *80* (16), 3531-3534.

113. Biggs, S.; Mulvaney, P., Measurement of the forces between gold surfaces in water by atomic force microscopy. *J. Chem. Phys.* 1994, *100* (11), 8501-8505.

114. Hotze, E. M.; Phenrat, T.; Lowry, G. V., Nanoparticle aggregation: challenges to understanding transport and reactivity in the environment. *J Environ Qual* 2010, *39* (6), 1909-24.

115. Sun, M.; Liu, F.; Zhu, Y.; Wang, W.; Hu, J.; Liu, J.; Dai, Z.; Wang, K.; Wei, Y.; Bai, J.; Gao, W., Salt-induced aggregation of gold nanoparticles for photoacoustic imaging and photothermal therapy of cancer. *Nanoscale* 2016, *8* (8), 4452-4457.

116. Rezende, C. A.; Shan, J.; Lee, L. T.; Zalczer, G.; Tenhu, H., Tuning the structure of thermosensitive gold nanoparticle monolayers. *J Phys Chem B* 2009, *113* (29), 9786-94.

117. Shan, J.; Chen, J.; Nuopponen, M.; Tenhu, H., Two phase transitions of poly(N-isopropylacrylamide) brushes bound to gold nanoparticles. *Langmuir* 2004, *20* (11), 4671-6.

118. Shan, J.; Chen, J.; Nuopponen, M.; Viitala, T.; Jiang, H.; Peltonen, J.; Kauppinen, E.; Tenhu, H., Optical properties of thermally responsive amphiphilic gold nanoparticles protected with polymers. *Langmuir* 2006, *22* (2), 794-801.

119. Schmaljohann, D., Thermo- and pH-responsive polymers in drug delivery. *Adv. Drug Delivery Rev.* 2006, *58* (15), 1655-1670.

120. Gandhi, A.; Paul, A.; Sen, S. O.; Sen, K. K., Studies on thermoresponsive polymers: Phase behaviour, drug delivery and biomedical applications. *Asian J. Pharm. Sci.* 2015, *10* (2), 99-107.

121. Halperin, A.; Tirrell, M.; Lodge, T. P., Tethered chains in polymer microstructures. In *Macromolecules: Synthesis, Order and Advanced Properties*, Springer Berlin Heidelberg: Berlin, Heidelberg, 1992; pp 31-71.

122. Singh, N.; Cui, X.; Boland, T.; Husson, S. M., The role of independently variable grafting density and layer thickness of polymer nanolayers on peptide adsorption and cell adhesion. *Biomaterials* 2007, *28* (5), 763-771.

123. Wei, J.; Cai, J.; Li, Y.; Wu, B.; Gong, X.; Ngai, T., Investigation of cell behaviors on thermo-responsive PNIPAM microgel films. *Colloids Surf., B* 2015, *132*, 202-207.

124. Patel, N. G.; Zhang, G., Responsive systems for cell sheet detachment. *Organogenesis* 2013, *9* (2), 93-100.

125. Psarra, E.; Konig, U.; Ueda, Y.; Bellmann, C.; Janke, A.; Bittrich, E.; Eichhorn, K. J.; Uhlmann, P., Nanostructured Biointerfaces: Nanoarchitectonics of Thermoresponsive Polymer Brushes Impact Protein Adsorption and Cell Adhesion. *ACS Appl Mater Interfaces* 2015, *7* (23), 12516-29.

126. Trongsatitkul, T.; Budhlall, B. M., Temperature dependence of serum protein adsorption in PEGylated PNIPAm microgels. *Colloids Surf B Biointerfaces* 2013, *103*, 244-52.

127. Idota, N.; Kikuchi, A.; Kobayashi, J.; Sakai, K.; Okano, T., Modulation of graft architectures for enhancing hydrophobic interaction of biomolecules with thermoresponsive polymer-grafted surfaces. *Colloids Surf., B* 2012, *99*, 95-101.

128. Nolan, C. M.; Reyes, C. D.; Debord, J. D.; García, A. J.; Lyon, L. A., Phase Transition Behavior, Protein Adsorption, and Cell Adhesion Resistance of Poly(ethylene glycol) Cross-Linked Microgel Particles. *Biomacromolecules* 2005, *6* (4), 2032-2039.

129. Cole, M. A.; Jasieniak, M.; Thissen, H.; Voelcker, N. H.; Griesser, H. J., Time-of-flight-secondary ion mass spectrometry study of the temperature dependence of protein adsorption onto poly(N-isopropylacrylamide) graft coatings. *Anal Chem* 2009, *81* (16), 6905-12.

130. Silva, C. S.; Baptista, R. P.; Santos, A. M.; Martinho, J. M.; Cabral, J. M.; Taipa, M. A., Adsorption of human IgG on to poly(N-isopropylacrylamide)-based polymer particles. *Biotechnol Lett* 2006, *28* (24), 2019-25.

131. Choi, S.; Choi, B. C.; Xue, C.; Leckband, D., Protein adsorption mechanisms determine the efficiency of thermally controlled cell adhesion on poly(N-isopropyl acrylamide) brushes. *Biomacromolecules* 2013, *14* (1), 92-100.

132. Xue, C.; Yonet-Tanyeri, N.; Brouette, N.; Sferrazza, M.; Braun, P. V.; Leckband, D. E., Protein Adsorption on Poly(N-isopropylacrylamide) Brushes: Dependence on Grafting Density and Chain Collapse. *Langmuir* 2011, *27* (14), 8810-8818.

133. Pandiyarajan, C. K.; Genzer, J., Effect of Network Density in Surface-Anchored Poly(N-isopropylacrylamide) Hydrogels on Adsorption of Fibrinogen. *Langmuir* 2017, *33* (8), 1974-1983.

134. Yusa, S.; Fukuda, K.; Yamamoto, T.; Iwasaki, Y.; Watanabe, A.; Akiyoshi, K.; Morishima, Y., Salt effect on the heat-induced association behavior of gold nanoparticles coated with poly(N-isopropylacrylamide) prepared via reversible addition-fragmentation chain transfer (RAFT) radical polymerization. *Langmuir* 2007, *23* (26), 12842-8.

135. Zhang, Z.; Maji, S.; Antunes, A. B. d. F.; De Rycke, R.; Zhang, Q.; Hoogenboom, R.; De Geest, B. G., Salt Plays a Pivotal Role in the Temperature-Responsive Aggregation and Layer-by-Layer Assembly of Polymer-Decorated Gold Nanoparticles. *Chem. Mater.* 2013, *25* (21), 4297-4303.

136. Zyuzin, M. V.; Honold, T.; Carregal-Romero, S.; Kantner, K.; Karg, M.; Parak, W. J., Influence of Temperature on the Colloidal Stability of Polymer-Coated Gold Nanoparticles in Cell Culture Media. *Small* 2016, *12* (13), 1723-31.

137. Tomaszewska, E.; Soliwoda, K.; Kadziola, K.; Tkacz-Szczesna, B.; Celichowski, G.; Cichomski, M.; Szmaja, W.; Grobelny, J., Detection Limits of DLS and UV-Vis Spectroscopy in Characterization of Polydisperse Nanoparticles Colloids. *J. Nanomater.* 2013, *2013*, 10.

138. Hammond, L. J.; Bhalla, N.; Rafiee, D. S.; Estrela, P., Localized Surface Plasmon Resonance as a Biosensing Platform for Developing Countries. *Biosensors* 2014, *4* (2).

139. Ghosh, S. K.; Pal, T., Interparticle Coupling Effect on the Surface Plasmon Resonance of Gold Nanoparticles: From Theory to Applications. *Chem. Rev.* 2007, *107* (11), 4797-4862.

140. Boris Khlebtsov and Andrei Melnikov and Vladimir Zharov and Nikolai, K., Absorption and scattering of light by a dimer of metal nanospheres: comparison of dipole and multipole approaches. *Nanotechnology* 2006, *17* (5), 1437.

141. Shipway, A. N.; Lahav, M.; Gabai, R.; Willner, I., Investigations into the Electrostatically Induced Aggregation of Au Nanoparticles. *Langmuir* 2000, *16* (23), 8789-8795.

142. Gérardy, J. M.; Ausloos, M., Absorption spectrum of clusters of spheres from the general solution of Maxwell's equations. IV. Proximity, bulk, surface, and shadow effects (in binary clusters). *Phys. Rev. B* 1983, *27* (10), 6446-6463.

143. Jenkins, S. V.; Qu, H.; Mudalige, T.; Ingle, T. M.; Wang, R.; Wang, F.; Howard, P. C.; Chen, J.; Zhang, Y., Rapid determination of plasmonic nanoparticle agglomeration status in blood. *Biomaterials* 2015, *51*, 226-37.

144. Zook, J. M.; Rastogi, V.; Maccuspie, R. I.; Keene, A. M.; Fagan, J., Measuring agglomerate size distribution and dependence of localized surface plasmon resonance absorbance on gold nanoparticle agglomerate size using analytical ultracentrifugation. *ACS Nano* 2011, *5* (10), 8070-9.

145. Tscharnuter, W., Photon Correlation Spectroscopy in Particle Sizing. In *Encyclopedia of Analytical Chemistry*, John Wiley & Sons, Ltd: 2006.

146. Boyd, R. D.; Pichaimuthu, S. K.; Cuenat, A., New approach to inter-technique comparisons for nanoparticle size measurements; using atomic force microscopy, nanoparticle tracking analysis and dynamic light scattering. *Colloids Surf., A* 2011, *387* (1–3), 35-42.

147. Liu, H. H.; Surawanvijit, S.; Rallo, R.; Orkoulas, G.; Cohen, Y., Analysis of Nanoparticle Agglomeration in Aqueous Suspensions via Constant-Number Monte Carlo Simulation. *Environ. Sci. Technol.* 2011, *45* (21), 9284-9292.

148. Chekli, L.; Bayatsarmadi, B.; Sekine, R.; Sarkar, B.; Shen, A. M.; Scheckel, K. G.; Skinner, W.; Naidu, R.; Shon, H. K.; Lombi, E.; Donner, E., Analytical characterisation of nanoscale zero-valent iron: A methodological review. *Anal. Chim. Acta* 2016, *903*, 13-35.

149. Heo, K.; Miesch, C.; Emrick, T.; Hayward, R. C., Thermally reversible aggregation of Gold nanoparticles in polymer nanocomposites through hydrogen bonding. *Nano Lett* 2013, *13* (11), 5297-302.

150. Akiyama, E.; Morimoto, N.; Kujawa, P.; Ozawa, Y.; Winnik, F. M.; Akiyoshi, K., Self-Assembled Nanogels of Cholesteryl-Modified Polysaccharides: Effect of the Polysaccharide Structure on Their Association Characteristics in the Dilute and Semidilute Regimes. *Biomacromolecules* 2007, *8* (8), 2366-2373.

151. Neamtu, I.; Rusu, A. G.; Diaconu, A.; Nita, L. E.; Chiriac, A. P., Basic concepts and recent advances in nanogels as carriers for medical applications. *Drug Delivery* 2017, *24* (1), 539-557.

152. Soni, G.; Yadav, K. S., Nanogels as potential nanomedicine carrier for treatment of cancer: A mini review of the state of the art. *Saudi Pharm. J.* 2016, *24* (2), 133-139.

153. Chacko, R. T.; Ventura, J.; Zhuang, J.; Thayumanavan, S., Polymer nanogels: A versatile nanoscopic drug delivery platform. *Adv. Drug Delivery Rev.* 2012, *64* (9), 836-851.

154. Vinogradov, S. V.; Kohli, E.; Zeman, A. D., Comparison of Nanogel Drug Carriers and Their Formulations with Nucleoside 5′-Triphosphates. *Pharm. Res.* 2006, *23* (5), 920-930.

155. Vincent; B, *Surface Chemistry in Biomedical and Environmental Science*. IOS Press: 2006; Vol. 228.

156. Yallapu, M. M.; Jaggi, M.; Chauhan, S. C., Design and engineering of nanogels for cancer treatment. *Drug Discov Today* 2011, *16* (9-10), 457-63.

157. Aguirre, G.; Villar-Alvarez, E.; González, A.; Ramos, J.; Taboada, P.; Forcada, J., Biocompatible stimuli-responsive nanogels for controlled antitumor drug delivery. *J. Polym. Sci., Part A: Polym. Chem.* 2016, *54* (12), 1694-1705.

158. Molina, M.; Asadian-Birjand, M.; Balach, J.; Bergueiro, J.; Miceli, E.; Calderon, M., Stimuli-responsive nanogel composites and their application in nanomedicine. *Chem. Soc. Rev.* 2015, *44* (17), 6161-6186.

159. Pan, G.; Guo, Q.; Cao, C.; Yang, H.; Li, B., Thermo-responsive molecularly imprinted nanogels for specific recognition and controlled release of proteins. *Soft Matter* 2013, *9* (14), 3840-3850.

160. Xue, C.; Yonet-Tanyeri, N.; Brouette, N.; Sferrazza, M.; Braun, P. V.; Leckband, D. E., Protein adsorption on poly(N-isopropylacrylamide) brushes: dependence on grafting density and chain collapse. *Langmuir* 2011, *27* (14), 8810-8.

161. Rahme, K.; Chen, L.; Hobbs, R. G.; Morris, M. A.; O'Driscoll, C.; Holmes, J. D., PEGylated gold nanoparticles: polymer quantification as a function of PEG lengths and nanoparticle dimensions. *RSC Adv.* 2013, *3* (17), 6085-6094.

162. Jones, S. T.; Walsh-Korb, Z.; Barrow, S. J.; Henderson, S. L.; Del Barrio, J.; Scherman, O. A., The Importance of Excess Poly(N-isopropylacrylamide) for the Aggregation of Poly(N-isopropylacrylamide)-Coated Gold Nanoparticles. *ACS Nano* 2016.

163. Zabetakis, K.; Ghann, W. E.; Kumar, S.; Daniel, M.-C., Effect of high gold salt concentrations on the size and polydispersity of gold nanoparticles prepared by an extended Turkevich–Frens method. *Gold Bull.* 2012, *45* (4), 203-211.

164. Lo Verso, F.; Egorov, S. A.; Milchev, A.; Binder, K., Spherical polymer brushes under good solvent conditions: molecular dynamics results compared to density functional theory. *J Chem Phys* 2010, *133* (18), 184901.

165. Schulz, F.; Vossmeyer, T.; Bastús, N. G.; Weller, H., Effect of the Spacer Structure on the Stability of Gold Nanoparticles Functionalized with Monodentate Thiolated Poly(ethylene glycol) Ligands. *Langmuir* 2013, *29* (31), 9897-9908.

166. Zhang, Y.; Furyk, S.; Sagle, L. B.; Cho, Y.; Bergbreiter, D. E.; Cremer, P. S., Effects of Hofmeister Anions on the LCST of PNIPAM as a Function of Molecular Weight. *J. Phys. Chem. C* 2007, *111* (25), 8916-8924.

167. Humphreys, B. A.; Willott, J. D.; Murdoch, T. J.; Webber, G. B.; Wanless, E. J., Specific ion modulated thermoresponse of poly(N-isopropylacrylamide) brushes. *Phys. Chem. Chem. Phys.* 2016, *18* (8), 6037-6046.

168. Tagliazucchi, M.; Blaber, M. G.; Schatz, G. C.; Weiss, E. A.; Szleifer, I., Optical properties of responsive hybrid au@polymer nanoparticles. *ACS Nano* 2012, *6* (9), 8397-406.

169. Storhoff, J. J.; Lazarides, A. A.; Mucic, R. C.; Mirkin, C. A.; Letsinger, R. L.; Schatz, G. C., What Controls the Optical Properties of DNA-Linked Gold Nanoparticle Assemblies? *J. Am. Chem. Soc.* 2000, *122* (19), 4640-4650.

170. Korgel, B. A.; Fullam, S.; Connolly, S.; Fitzmaurice, D., Assembly and Self-Organization of Silver Nanocrystal Superlattices: Ordered "Soft Spheres". *J Phys Chem B* 1998, *102* (43), 8379-8388.

171. Huang, H. Y.; Chen, W. F.; Kuo, P. L., Self-assembly of gold nanoparticles induced by poly(oxypropylene)diamines. *J Phys Chem B* 2005, *109* (51), 24288-94.

172. Halperin, A.; Kroger, M., Collapse of Thermoresponsive Brushes and the Tuning of Protein Adsorption. *Macromolecules (Washington, DC, U. S.)* 2011, *44* (17), 6986-7005.

173. Schneck, E.; Berts, I.; Halperin, A.; Daillant, J.; Fragneto, G., Neutron reflectometry from poly (ethylene-glycol) brushes binding anti-PEG antibodies: evidence of ternary adsorption. *Biomaterials* 2015, *46*, 95-104.

174. Patanarut, A.; Luchini, A.; Botterell, P. J.; Mohan, A.; Longo, C.; Vorster, P.; Petricoin, E. F., 3rd; Liotta, L. A.; Bishop, B., Synthesis and characterization of hydrogel particles containing Cibacron Blue F3G-A. *Colloids Surf A Physicochem Eng Asp* 2010, *362* (1-3), 8-19.

175. Fänger, C.; Wack, H.; Ulbricht, M., Macroporous Poly(N-isopropylacrylamide) Hydrogels with Adjustable Size "Cut-off" for the Efficient and Reversible Immobilization of Biomacromolecules. *Macromol. Biosci.* 2006, *6* (6), 393-402.

176. Dionigi, C.; Lungaro, L.; Goranov, V.; Riminucci, A.; Pineiro-Redondo, Y.; Banobre-Lopez, M.; Rivas, J.; Dediu, V., Smart magnetic poly(N-isopropylacrylamide) to control the release of bio-active molecules. *J Mater Sci Mater Med* 2014, *25* (10), 2365-71.

177. Yoshizako, K.; Akiyama, Y.; Yamanaka, H.; Shinohara, Y.; Hasegawa, Y.; Carredano, E.; Kikuchi, A.; Okano, T., Regulation of Protein Binding toward a Ligand on Chromatographic Matrixes by Masking and Forced-Releasing Effects Using Thermoresponsive Polymer. *Anal. Chem.* 2002, *74* (16), 4160-4166.

178. Parikh, I.; Cuatrecasas, P., Affinity Chromatography, Principles and Applications. In *Methods Protein Sep.*, Catsimpoolas, N., Ed. Springer US: Boston, MA, 1975; pp 255-276.

179. Labrou, N. E.; Karagouni, A.; Clonis, Y. D., Biomimetic-dye affinity adsorbents for enzyme purification: Application to the one-step purification of Candida boidinii formate dehydrogenase. *Biotechnol. Bioeng.* 1995, *48* (3), 278-288.

180. Labrou, N. E., Dye-Ligand Affinity Chromatography for Protein Separation and Purification. In *Affinity Chromatography: Methods and Protocols*, Bailon, P.; Ehrlich, G. K.; Fung, W.-J.; Berthold, W., Eds. Humana Press: Totowa, NJ, 2000; pp 129-139.

181. Magni, R.; Espina, B. H.; Liotta, L. A.; Luchini, A.; Espina, V., Hydrogel nanoparticle harvesting of plasma or urine for detecting low abundance proteins. *J Vis Exp* 2014, (90), e51789.

182. Popova, T. G.; Teunis, A.; Magni, R.; Luchini, A.; Espina, V.; Liotta, L. A.; Popov, S. G., Chemokine-Releasing Nanoparticles for Manipulation of Lymph Node Microenvironment. *Nanomaterials (Basel)* 2015, *5* (1), 298-320.

183. Popova, T. G.; Teunis, A.; Espina, V.; Liotta, L. A.; Popov, S. G., Chemokine-Releasing Microparticles Improve Bacterial Clearance and Survival of Anthrax Spore-Challenged Mice. *PLoS One* 2016, *11* (9), e0163163.

184. Subramanian, S., Dye-ligand affinity chromatography: the interaction of Cibacron Blue F3GA with proteins and enzymes. *CRC Crit Rev Biochem* 1984, *16* (2), 169-205.

185. Sternberg, F.; Meyerhoff, C.; Mennel, F. J.; Bischof, F.; Pfeiffer, E. F., Subcutaneous glucose concentration in humans. Real estimation and continuous monitoring. *Diabetes Care* 1995, *18* (9), 1266-9.

186. Ishida, N.; Biggs, S., Salt-Induced Structural Behavior for Poly(N-isopropylacryamide) Grafted onto Solid Surface Observed Directly by AFM and QCM-D. *Macromolecules* 2007, *40* (25), 9045-9052.

187. McNay, E. C.; Sherwin, R. S., From artificial cerebro-spinal fluid (aCSF) to artificial extracellular fluid (aECF): microdialysis perfusate composition effects on in vivo brain ECF glucose measurements. *J Neurosci Methods* 2004, *132* (1), 35-43.

188. Paulus, A. S.; Heinzler, R.; Ooi, H. W.; Franzreb, M., Temperature-Switchable Agglomeration of Magnetic Particles Designed for Continuous Separation Processes in Biotechnology. *ACS Appl. Mater. Interfaces* 2015, *7* (26), 14279-14287.

189. Zhang, Y.; Furyk, S.; Bergbreiter, D. E.; Cremer, P. S., Specific Ion Effects on the Water Solubility of Macromolecules: PNIPAM and the Hofmeister Series. *J. Am. Chem. Soc.* 2005, *127* (41), 14505-14510.

190. Du, H.; Wickramasinghe, R.; Qian, X., Effects of Salt on the Lower Critical Solution Temperature of Poly (N-Isopropylacrylamide). *J. Phys. Chem. B* 2010, *114* (49), 16594-16604.

191. Currie, E. P. K.; Norde, W.; Cohen Stuart, M. A., Tethered polymer chains: surface chemistry and their impact on colloidal and surface properties. *Adv. Colloid Interface Sci.* 2003, *100–102*, 205-265.

192. Saunders, B. R., On the Structure of Poly(N-isopropylacrylamide) Microgel Particles. *Langmuir* 2004, *20* (10), 3925-3932.

193. Ramos, J.; Imaz, A.; Forcada, J., Temperature-sensitive nanogels: poly(N-vinylcaprolactam) versus poly(N-isopropylacrylamide). *Polym. Chem.* 2012, *3* (4), 852-856.

194. Bell, N. C.; Minelli, C.; Shard, A. G., Quantitation of IgG protein adsorption to gold nanoparticles using particle size measurement. *Anal. Methods* 2013, *5* (18), 4591-4601.

195. Cui, M.; Liu, R.; Deng, Z.; Ge, G.; Liu, Y.; Xie, L., Quantitative study of protein coronas on gold nanoparticles with different surface modifications. *Nano Res.* 2014, *7* (3), 345-352.

196. Sakulkhu, U.; Mahmoudi, M.; Maurizi, L.; Salaklang, J.; Hofmann, H., Protein Corona Composition of Superparamagnetic Iron Oxide Nanoparticles with Various Physico-Chemical Properties and Coatings. *Sci. Rep.* 2014, *4*, 5020.

197. Dominguez-Medina, S.; Blankenburg, J.; Olson, J.; Landes, C. F.; Link, S., Adsorption of a Protein Monolayer via Hydrophobic Interactions Prevents Nanoparticle Aggregation under Harsh Environmental Conditions. *ACS Sustainable Chem. Eng.* 2013, *1* (7), 833-842.

198. Koshkina, O.; Lang, T.; Thiermann, R.; Docter, D.; Stauber, R. H.; Secker, C.; Schlaad, H.; Weidner, S.; Mohr, B.; Maskos, M.; Bertin, A., Temperature-Triggered Protein Adsorption on Polymer-Coated Nanoparticles in Serum. *Langmuir* 2015, *31* (32), 8873-8881.

199. Borsos, A.; Gilanyi, T., Interaction of cetyl-trimethylammonium bromide with swollen and collapsed poly(N-isopropylacrylamide) nanogel particles. *Langmuir* 2011, *27* (7), 3461-7.

200. Tong, X. D.; Xue, B.; Sun, Y., A novel magnetic affinity support for protein adsorption and purification. *Biotechnol Prog* 2001, *17* (1), 134-9.

201. Zhang, J., *Protein-Protein Interactions - Computational and Experimental Tools*. InTech: 2012; p 484.

202. Annunziata, O.; Payne, A.; Wang, Y., Solubility of Lysozyme in the Presence of Aqueous Chloride Salts: Common-Ion Effect and Its Role on Solubility and Crystal Thermodynamics. *J. Am. Chem. Soc.* 2008, *130* (40), 13347-13352.

203. del Pilar Ferraris, M.; Barrera, G. I.; Padilla, A. P.; Rodríguez, J. A., Affinity adsorption of lysozyme on a macroligand prepared with Cibacron Blue 3GA attached to yeast cells. *J. Chromatogr. B: Biomed. Sci. Appl.* 2011, *879* (26), 2741-2745.

204. Odabaşı, M.; Denizli, A., Cibacron Blue F3GA incorporated magnetic poly(2-hydroxyethyl methacrylate) beads for lysozyme adsorption. *J. Appl. Polym. Sci.* 2004, *93* (2), 719-725.

205. Salih, B.; Zenobi, R., MALDI mass spectrometry of dye-peptide and dye-protein complexes. *Anal Chem* 1998, *70* (8), 1536-43.

206. Carneheim, C.; Stahle, L., Microdialysis of lipophilic compounds: a methodological study. *Pharmacol Toxicol* 1991, *69* (5), 378-80.

207. Jensen, S. M.; Hansen, H. S.; Johansen, T.; Malmlof, K., In vivo and in vitro microdialysis sampling of free fatty acids. *J Pharm Biomed Anal* 2007, *43* (5), 1751-6.

208. Ernberg, M. M.; Alstergren, P. J., Microdialysis of neuropeptide Y in human muscle tissue. *J Neurosci Methods* 2004, *132* (2), 185-90.

209. Helmy, A.; Carpenter, K. L.; Skepper, J. N.; Kirkpatrick, P. J.; Pickard, J. D.; Hutchinson, P. J., Microdialysis of cytokines: methodological considerations, scanning electron microscopy, and determination of relative recovery. *J Neurotrauma* 2009, *26* (4), 549-61.

210. Andac, M., Cibacron blue immobilized poly(glycidyl-methacrylate) nanobeads for albumin removal in proteome studies. *Artif Cells Nanomed Biotechnol* 2015, *43* (2), 133-9.

211. Antoni, G.; Casagli, M. C.; Bigio, M.; Borri, G.; Neri, P., Different interactions of human and bovine serum albumin with Cibacron Blue and Blue Dextran. *Ital J Biochem* 1982, *31* (2), 100-6.

212. Wolman, F. J.; Smolko, E. E.; Cascone, O.; Grasselli, M., Improved hollow-fibre membranes for dye-affinity chromatography. *J Sep Sci* 2005, *28* (1), 45-51.

213. Rao, S.; Zydney, A. L., Controlling protein transport in ultrafiltration using small charged ligands. *Biotechnol Bioeng* 2005, *91* (6), 733-42.

214. Tamburro, D.; Fredolini, C.; Espina, V.; Douglas, T. A.; Ranganathan, A.; Ilag, L.; Zhou, W.; Russo, P.; Espina, B. H.; Muto, G.; Petricoin, E. F., 3rd; Liotta, L. A.; Luchini, A., Multifunctional core-shell nanoparticles: discovery of previously invisible biomarkers. *J Am Chem Soc* 2011, *133* (47), 19178-88.

215. Longo, C.; Patanarut, A.; George, T.; Bishop, B.; Zhou, W.; Fredolini, C.; Ross, M. M.; Espina, V.; Pellacani, G.; Petricoin, E. F.; Liotta, L. A.; Luchini, A., Core-Shell Hydrogel Particles Harvest, Concentrate and Preserve Labile Low Abundance Biomarkers. *PLoS ONE* 2009, *4* (3), e4763.

216. Hogendoorn, E. A.; Dijkman, E.; Baumann, B.; Hidalgo, C.; Sancho, J.-V.; Hernandez, F., Strategies in Using Analytical Restricted Access Media Columns for the Removal of Humic Acid Interferences in the Trace Analysis of Acidic Herbicides in Water Samples by Coupled Column Liquid Chromatography with UV Detection. *Anal. Chem.* 1999, *71* (6), 1111-1118.

217. Sirgom da Silva, K. K. M.; Boralli, V. B.; Wisniewski, C.; Figueiredo, E. C., On-Line Restricted Access Molecularly Imprinted Solid-Phase Extraction of Selective Serotonin Reuptake Inhibitors Directly from Untreated Human Plasma Samples Followed by HPLC-UV Analysis. *J. Anal. Toxicol.* 2015.

218. Zhang, S.; Sun, Y., Study on protein adsorption kinetics to a dye-ligand adsorbent by the pore diffusion model. *J Chromatogr A* 2002, *964* (1-2), 35-46.

219. Thompson, S. T.; Stellwagen, E., Binding of Cibacron blue F3GA to proteins containing the dinucleotide fold. *Proc Natl Acad Sci U S A* 1976, *73* (2), 361-5.

220. Kopperschläger, G.; Böhme, H.-J.; Hofmann, E., Cibacron blue F3G-A and related dyes as ligands in affinity chromatography. In *Chromatography*, Fiechter, A., Ed. Springer Berlin Heidelberg: Berlin, Heidelberg, 1982; pp 101-138.

221. Hillman, J.; Aneman, O.; Anderson, C.; Sjogren, F.; Saberg, C.; Mellergard, P., A microdialysis technique for routine measurement of macromolecules in the injured human brain. *Neurosurgery* 2005, *56* (6), 1264-8; discussion 1268-70.

222. Sjögren, F.; Anderson, C. D., Are Cutaneous Microdialysis Cytokine Findings Supported by End Point Biopsy Immunohistochemistry Findings? *The AAPS Journal* 2010, *12* (4), 741-749.

223. Clough, G. F., Microdialysis of large molecules. *The AAPS Journal* 2005, *7* (3), E686-E692.

224. Hulme, E. C.; Trevethick, M. A., Ligand binding assays at equilibrium: validation and interpretation. *Br. J. Pharmacol.* 2010, *161* (6), 1219-1237.

225. Mathy, F. X.; Preat, V.; Verbeeck, R. K., Validation of subcutaneous microdialysis sampling for pharmacokinetic studies of flurbiprofen in the rat. *J Pharm Sci* 2001, *90* (11), 1897-906.

226. Wang, L.; Zhang, Y. Z.; Choquette, S.; Gaigalas, A. K., Measurement of Microsphere Concentration Using a Flow Cytometer with Volumetric Sample Delivery. *J Res Natl Inst Stand Technol* 2014, *119*, 629-43.

227. Rathod, V. P.; Sanjeevkumar, D., Peristaltic Flow of a Couple-Stress Fluid with Suspended Nanoparticles in an Asymmetric Channel with Flexible Walls. *IJMTT* 2016, *32* (2), 112-126.

228. Ebaid, A.; Aly, E. H., Exact Analytical Solution of the Peristaltic Nanofluids Flow in an Asymmetric Channel with Flexible Walls and Slip Condition: Application to the Cancer Treatment. *Computational and Mathematical Methods in Medicine* 2013, *2013*, 8.

229. Nadeem, S.; Riaz, A.; Ellahi, R.; Akbar, N. S., Mathematical model for the peristaltic flow of Jeffrey fluid with nanoparticles phenomenon through a rectangular duct. *Appl. Nanosci.* 2014, *4* (5), 613-624.

230. Chanphai, P.; Vesper, A. R.; Bariyanga, J.; Bérubé, G.; Tajmir-Riahi, H. A., Review on the delivery of steroids by carrier proteins. *J. Photochem. Photobiol., B* 2016, *161*, 184-191.

231. Luo, Q.; Wang, Y.; Yang, H.; Liu, C.; Ding, Y.; Xu, H.; Wang, Q.; Liu, Y.; Xie, Y., Modeling the interaction of interferon alpha-1b to bovine serum albumin as a drug delivery system. *J Phys Chem B* 2014, *118* (29), 8566-74.

232. Magrane, M.; Consortium, U., UniProt Knowledgebase: a hub of integrated protein data. *Database* 2011, *2011*, bar009-bar009.

233. Aziz, N.; Detels, R.; Quint, J. J.; Li, Q.; Gjertson, D.; Butch, A. W., Stability of cytokines, chemokines and soluble activation markers in unprocessed blood stored under different conditions. *Cytokine* 2016, *84*, 17-24.

234. Jing, M.; Bowser, M. T., A Review of Methods for Measuring Aptamer-ProteinEquilibria. *Anal. Chim. Acta* 2011, *686* (1-2), 9-18.

235. Chen, Z.; Weber, S. G., Determination of binding constants by affinity capillary electrophoresis, electrospray ionization mass spectrometry and phase-distribution methods. *Trends Anal. Chem.* 2008, *27* (9), 738-748.

236. Bungay, P. M.; Sumbria, R. K.; Bickel, U., Unifying the mathematical modeling of in vivo and in vitro microdialysis. *J Pharm Biomed Anal* 2011, *55* (1), 54-63.

237. Jia, D.; Cabrera, R. F. E.; Stenken, J. A., Comparison of heparin-immobilized vs. antibody-immobilized microspheres for the capture and detection of cytokines during microdialysis sampling. *2009 IEEE/NIH Life Science Systems and Applications Workshop (LiSSA 2009)* 2009, 112-15.

238. Edward Conrad, H., Chapter 11 - Heparin-Binding Proteins in Lipoprotein Metabolism. In *Heparin-Binding Proteins*, Academic Press: San Diego, 1998; pp 367-IV.

239. Edward Conrad, H., Chapter 6 - Heparinoid/Protein Interactions. In *Heparin-Binding Proteins*, Academic Press: San Diego, 1998; pp 183-202.

240. Edward Conrad, H., Chapter 7 - Antithrombin, the Prototypic Heparin-Binding Protein. In *Heparin-Binding Proteins*, Academic Press: San Diego, 1998; pp 203-238.

241. Edward Conrad, H., Chapter 8 - Heparin-Binding Proteins in Hemostasis. In *Heparin-Binding Proteins*, Academic Press: San Diego, 1998; pp 239-300.

242. Edward Conrad, H., Chapter 9 - Fibroblast Growth Factors. In *Heparin-Binding Proteins*, Academic Press: San Diego, 1998; pp 301-III.

243. Esko, J.; Linhardt, R., *Proteins that Bind Sulfated Glycosaminoglycans*. Cold Spring Harbor Laboratory Press: Cold Spring Harbor, 2009.

244. Pettersson, A.; Amirkhani, A.; Arvidsson, B.; Markides, K.; Bergquist, J., A Feasibility Study of Solid Supported Enhanced Microdialysis. *Anal. Chem.* 2004, *76* (6), 1678-1682.

245. Burdukova, E.; Li, H.; Ishida, N.; O'Shea, J. P.; Franks, G. V., Temperature controlled surface hydrophobicity and interaction forces induced by poly (N-isopropylacrylamide). *J Colloid Interface Sci* 2010, *342* (2), 586-92.